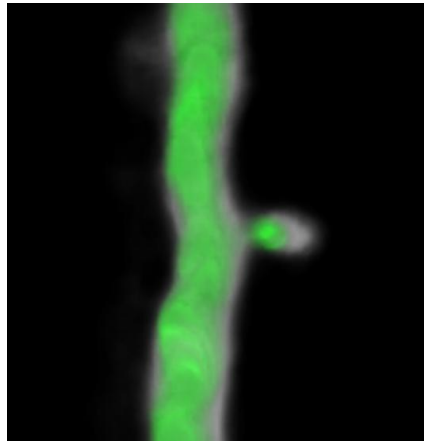


# **STRUCTURE – FUNCTION ANALYSIS ON THE LEVEL OF INDIVIDUAL SYNAPSES**



## **Inauguraldissertation**

zur

Erlangung der Würde eines Doktors der Philosophie

vorgelegt der

Philosophisch-Naturwissenschaftlichen Fakultät

der Universität Basel

von

**Niklaus Holbro**

aus Basel, Schweiz

Basel, 2010

Originaldokument gespeichert auf dem Dokumentenserver der Universität Basel  
**edoc.unibas.ch**



Dieses Werk ist unter dem Vertrag „Creative Commons Namensnennung-Keine kommerzielle  
Nutzung-Keine Bearbeitung 2.5 Schweiz“ lizenziert. Die vollständige Lizenz kann unter  
**[creativecommons.org/licences/by-nc-nd/2.5/ch](http://creativecommons.org/licences/by-nc-nd/2.5/ch)**  
eingesehen werden.

Genehmigt von der Philosophisch-Naturwissenschaftlichen Fakultät

auf Antrag von:

**Prof. Silvia Arber**

**Prof. Bernhard Bettler**

**Dr. Thomas Oertner**

Basel, den 9. Dezember 2008

Prof. Eberhard Parlow  
Dekan



## Namensnennung-Keine kommerzielle Nutzung-Keine Bearbeitung 2.5 Schweiz

---

### Sie dürfen:



das Werk vervielfältigen, verbreiten und öffentlich zugänglich machen

### Zu den folgenden Bedingungen:



**Namensnennung.** Sie müssen den Namen des Autors/Rechteinhabers in der von ihm festgelegten Weise nennen (wodurch aber nicht der Eindruck entstehen darf, Sie oder die Nutzung des Werkes durch Sie würden entlohnt).



**Keine kommerzielle Nutzung.** Dieses Werk darf nicht für kommerzielle Zwecke verwendet werden.



**Keine Bearbeitung.** Dieses Werk darf nicht bearbeitet oder in anderer Weise verändert werden.

- Im Falle einer Verbreitung müssen Sie anderen die Lizenzbedingungen, unter welche dieses Werk fällt, mitteilen. Am Einfachsten ist es, einen Link auf diese Seite einzubinden.
- Jede der vorgenannten Bedingungen kann aufgehoben werden, sofern Sie die Einwilligung des Rechteinhabers dazu erhalten.
- Diese Lizenz lässt die Urheberpersönlichkeitsrechte unberührt.

#### Die gesetzlichen Schranken des Urheberrechts bleiben hiervon unberührt.

Die Commons Deed ist eine Zusammenfassung des Lizenzvertrags in allgemeinverständlicher Sprache:  
<http://creativecommons.org/licenses/by-nc-nd/2.5/ch/legalcode.de>

#### Haftungsausschluss:

Die Commons Deed ist kein Lizenzvertrag. Sie ist lediglich ein Referenztext, der den zugrundeliegenden Lizenzvertrag übersichtlich und in allgemeinverständlicher Sprache wiedergibt. Die Deed selbst entfaltet keine juristische Wirkung und erscheint im eigentlichen Lizenzvertrag nicht. Creative Commons ist keine Rechtsanwaltsgesellschaft und leistet keine Rechtsberatung. Die Weitergabe und Verlinkung des Commons Deeds führt zu keinem Mandatsverhältnis.

# **TABLE OF CONTENTS**

<b><u>1. SUMMARY</u></b> .....	3
<b><u>2. INTRODUCTION</u></b> .....	7
<b>2.1 The hippocampus</b>	
<b>2.2 Pyramidal neurons</b>	
<b>2.3 Dendritic spines</b>	
2.3.1 The PSD and glutamate receptors	
2.3.2 Spine morphology	
2.3.3 Impact of spine morphology on synaptic function and plasticity	
2.3.4 Spine microanatomy and synaptic function	
Mitochondria	
Endosomes	
Ribosomes and polyribosomes	
Endoplasmic reticulum and the spine apparatus	
2.3.5 Spine calcium transients and synaptic plasticity of pyramidal neurons	
<b>2.4 LTP and LTD</b>	
<b>2.5 CaMKII and LTP</b>	
<b>2.6 Glutamate uncaging and single spine induction of synaptic plasticity</b>	
<b>2.7 Cooperativity between neighboring synapses</b>	
<b><u>3. AIM OF THE THESIS</u></b> .....	23
<b><u>4. PUBLICATIONS</u></b> .....	25
<b>4.A Synaptic depression at individual synapses is governed by spine microanatomy.</b>	
<b>4.B Spine neck plasticity controls postsynaptic calcium signals through electrical compartmentalization.</b>	
<b>4.C Optical induction of plasticity at single synapses reveals input-specific accumulation of alphaCaMKII.</b>	

<b><u>5. GENERAL CONCLUSIONS AND OUTLOOK</u></b>	<b>91</b>
<b>5.1 Microanatomy regulates synaptic function and plasticity</b>	
-Dynamic ER distribution as a major metaplasticity mechanism	
-mGluR dependent depression as a regulator for synaptic weight distribution	
-The ER as a general regulator of plasticity	
-Possible heterosynaptic spread of mGluR dependent LTD	
-ER calcium release as a homeostatic mechanism	
-Possible modulation of mGluR→IP3 pathway	
-Spine ER and protein handling	
<b>5.2 Impact of spine neck on synaptic signals</b>	
-Spines can be electrical compartments	
-Spine neck plasticity as a metaplasticity mechanism	
-Spine neck plasticity and implications for synaptic crosstalk	
<b>5.3 CaMKII accumulation is input specific</b>	
-New optical approach for the induction of LTP at identified synapses	
-CaMKII accumulation is input specific	
-The need for protein activity sensors	
<b>5.4 Concluding remarks</b>	
<b><u>6. APPENDIX: Two photon glutamate uncaging – practical consideration</u></b>	<b>100</b>
<b><u>7. REFERENCES</u></b>	<b>105</b>
<b><u>8. ABBREVIATIONS</u></b>	<b>117</b>
<b><u>9. AKNOWLEDGEMENTS</u></b>	<b>118</b>
<b><u>10. CURRICULUM VITAE</u></b>	<b>119</b>

## **1. SUMMARY**

Excitatory synapses in the mammalian brain are made on small protrusions of the postsynaptic cell called dendritic spines. Dendritic spines are highly variable in their morphology and in their microanatomy (e.g. presence of subsynaptic organelles). It is unclear whether and how variability in spine morphological and anatomical properties translates into differences in synaptic function. Using two photon imaging, we analyzed how spine properties can affect synaptic signals and the potential for synaptic plasticity at single identified spine synapses. We show that synaptic signals can be tightly regulated on the level of individual synapses and that differences in spine morphology and microanatomy regulate synaptic function. We also provide evidence for the existence of functionally distinct populations of synapses in regard to their potential for synaptic plasticity. The present thesis is subdivided into three main sections. The first section is dedicated to the analysis of the function of specialized subsynaptic organelles in regulating synaptic plasticity. In the second section we studied the impact of spine morphology on synaptic signals and in the third section we examined whether critical proteins can be tagged to individual synapses in response to plasticity inducing stimuli.

In pyramidal cells, only a subset of dendritic spines contains endoplasmic reticulum (ER). Spine ER often forms a 'spine apparatus', a specialized organelle with unknown function. It is unclear whether these specialized subsynaptic structures can affect the function of the synapse on the spine head. The possible involvement of spine ER in shaping spine calcium transients, a key trigger for synaptic plasticity, raises the possibility that spine ER could modulate the potential of a given synapse to undergo activity dependent modifications. Using a genetic approach to label the ER in living neurons, we find that the ER preferentially localizes to spines containing strong synapses. We demonstrate that spine ER represents a specialized calcium signaling machinery required for the induction of metabotropic glutamate receptor dependent long term depression at individual synapses. We demonstrate that different subsets of synapses exist in regard to their potential to undergo specific forms of plasticity. Spine ER represents the anatomical

correlate for a mechanism by which strong synapses can be retuned in an activity dependent manner.

Dendritic spines are separated from their parent dendrite by a thin spine neck. The spine neck slows down diffusion of molecules from the spine head to the parent dendrite, allowing spine-specific action of second messengers and activated enzymes. The resistance of the spine neck is crucial in determining whether spines can also be considered electrical compartments. Only a high enough spine neck resistance leads to electrical compartmentalization and activation of voltage gated channels in the spine in response to synaptic stimulation. We show that spine neck resistance can change in an activity dependent manner. Using single spine calcium imaging as a reporter of NMDA receptor activation and spine head depolarization, we show that spines can indeed act as electrical compartments. Using pharmacological experiments and modeling, we demonstrate that different voltage dependent channels cooperatively participate in shaping spine head depolarization and spine calcium transients. We also show that *in vivo* the spine neck resistance is higher compared to the situation in acutely sliced brain tissue, demonstrating that in the living animal a higher fraction of spines can be considered electrical compartments compared to the *in vitro* situation. We provide strong evidence that the spine neck can profoundly affect synaptic calcium signals. Biochemical and electrical compartmentalization is dynamically regulated in an activity dependent way.

Spine calcium signals can activate key signaling cascades responsible for the induction of synaptic plasticity. Long term potentiation (LTP) has been shown to require the activity of CaMKII, a serine/ threonine kinase. A chemical protocol leading to LTP has been shown to induce translocation of CaMKII to dendritic spines. It is however unclear whether this molecule acts at single synapses or whether it can spread and modulate neighboring synapses in response to more physiological protocols. Using a new optical approach to induce LTP at single visualized synapses, we show that LTP induction is accompanied by a long-lasting increase of CaMKII at the stimulated synapse. This increase was specific to the stimulated spine and did not spread to neighboring spines. We provide evidence that CaMKII acts locally, on the micrometer scale, to regulate

plasticity. We show that the concentration of proteins involved in regulating synaptic plasticity can be tightly regulated at the level of single synapses.





## **2. INTRODUCTION**

The brain is thought to be the most complex structure of an organism. The mammalian brain contains billions of interconnected cells which drive the organism's action. Currently, we are just starting to elucidate how processes happening on the level of single molecules, cells or entire networks can influence and drive behavior.

The human brain contains about  $10^{12}$  cells, 10% neurons and 90% glial cells. Glial cells are thought to support neurons, supply them with nutrients, insulate axons and regulate brain immune responses. In recent years it has been proposed that glial cells are also able to modulate synaptic function. Neurons, on the other hand, are thought to be the central cells for information processing and storage. The outcome of information flow and processing within neuronal networks is thought to drive behavior. Synapses are the sites where information flows from one neuron to the next. The regulation of synaptic strength has been proposed to underlie learning and memory processes and may therefore be crucial for driving adaptive behavior. Learning is thought to require plasticity among synaptic connections; the maintenance of specific memory traces, on the other hand, is thought to require stability at the level of individual synapses. At present it is unclear how conflicting requirements such as the regulation of plasticity and stability are regulated. It is also unclear whether all synapses have the same potential for plasticity or whether different subpopulations of synapses exist in this regard. It is plausible that the structure of synapses is strongly correlated with their functional properties and their potential for plasticity. The mammalian hippocampus represents a suitable brain area where factors regulating plasticity and stability can be studied on the molecular, synaptic, cellular and network levels.

### **2.1 The hippocampus**

The hippocampus is part of the forebrain, it is located in the medial temporal lobe and has been shown to play a central role in memory storage and spatial navigation (Rempel-Clower et al., 1996; Reed and Squire, 1997; Milani et al., 1998; Neves et al., 2008). The hippocampus consists of a highly organized network and is subdivided into the subregions CA1, CA2, CA3, dentate gyrus, subiculum, parasubiculum, perisubiculum and entorhinal

cortex. It receives inputs from many cortical and subcortical regions via subiculum and entorhinal cortex. Axons from the entorhinal cortex innervate cells in the dentate gyrus; from there the information flows to CA3 and CA1 neurons. Mossy fibers from dentate cells innervate CA3 pyramidal cells. CA3 cells innervate CA1 pyramidal cells through the Schaffer collateral or the commissural pathway. CA1 cells project outside the hippocampus, through subiculum and entorhinal cortex to several cortical and subcortical areas (Amaral and Witter, 1989). Due to its highly ordered structure, the hippocampus represents an optimal system to study synaptic physiology. The present dissertation focuses on analyzing the functional properties of individual synapses between CA3 and CA1 pyramidal neurons.

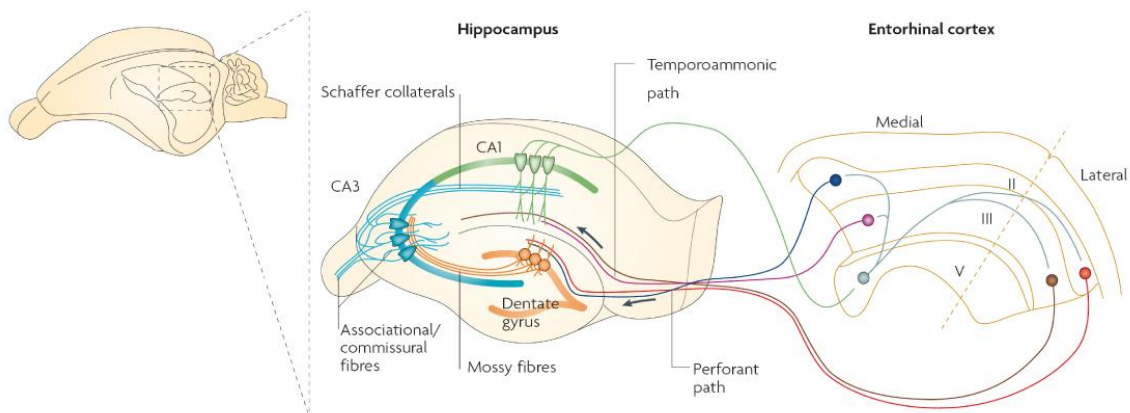


**Figure 1.1. The hippocampal formation.**

*Neurons in the entorhinal cortex project to the dentate gyrus via the perforant path. Mossy fibers of dentate gyrus cells project to the CA3 region. From CA3 neurons information flows to CA1 neurons through the Schaffer collaterals. CA1 neurons project back into entorhinal cortex. (Adapted from Neves et al., 2008)*

## 2.2 Pyramidal neurons

Pyramidal neurons are present in different forebrain areas such as the cerebral cortex, the amygdala and the hippocampus. These neurons consist of a soma, an axon and two distinct apical and basal dendritic trees. The basal and proximal apical dendrites of CA1 pyramidal neurons, mainly receive input from CA3 neurons via the Schaffer collateral pathway, whereas the distal apical dendrites mainly receive inputs from the entorhinal cortex via the perforant path and from thalamic nuclei (Spruston, 2008). Different

inhibitory interneurons target specific cellular domains of pyramidal neurons and are selective for the axon, soma or specific dendritic domains (Huang et al., 2007).

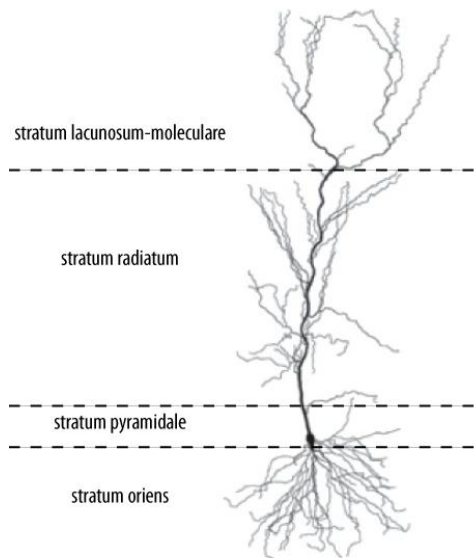


**Figure 1.2. CA1 pyramidal cell.**

*Pyramidal cells consist of a soma, an axon, basal and apical dendritic trees. Dendrites occupy different hippocampal strata and different afferents are thought to target different dendritic domains.*

*(Adapted from Spruston et al., 2008)*

### 2.3 Dendritic spines

The majority of excitatory synaptic connections in the mammalian brain are made on small protrusions of the dendrite called dendritic spines. Dendritic spines consist of a spine head and are separated from their parent dendrite by a thin spine neck (Gray, 1959a; Harris and Stevens, 1989). The spine head contains the postsynaptic density (PSD), an electron dense region where neurotransmitter receptors and many other proteins are integrated (Banker et al., 1974).

The function of dendritic spines is still debated (Spruston, 2008). Dendritic spines increase the surface of the postsynaptic cell, maximizing the possible number of synapses per cell. Spines also isolate the PSD from the dendrite and act as biochemical compartments, confining active second messengers and proteins close to the activated synapse (Svoboda et al., 1996; Sabatini et al., 2002; Bloodgood and Sabatini, 2005; Noguchi et al., 2005; Gray et al., 2006).

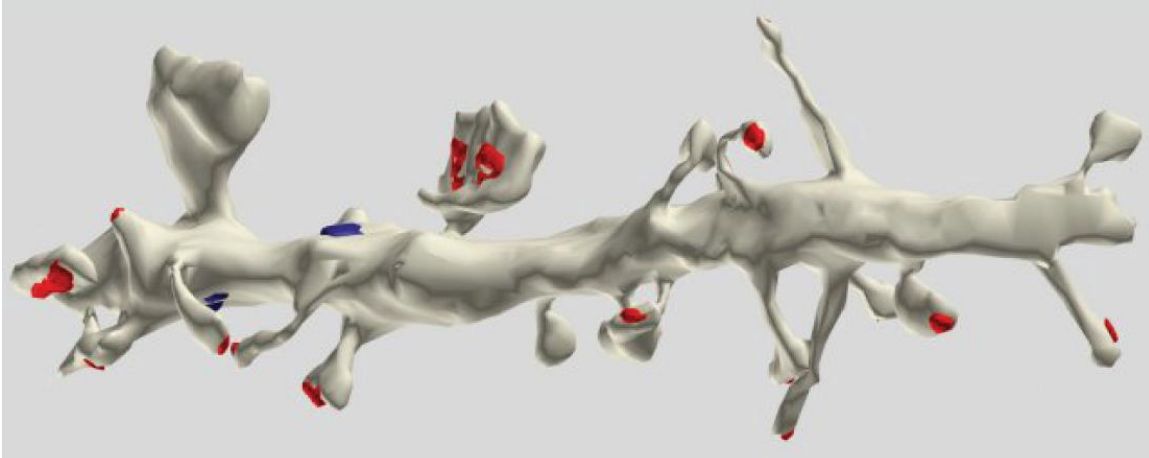


**Figure 1.3. Dendrite of CA1 pyramidal cell.**

3-D reconstruction from electron microscopy images of a CA1 pyramidal cell dendrite. Large variability in spine size and shape can be observed. Glutamatergic synapses are shown in red, GABAergic synapses in blue.

(Adapted from synapseweb.org)

Whether spines can also act as electrical compartments remains controversial. To act as electrical compartments and be able to amplify synaptic signals in a voltage dependent manner, the resistance of the spine neck needs to be high (Spruston, 2008). Although it has been shown that spine neck resistance can change in an activity dependent manner (Bloodgood and Sabatini, 2005), it is still debated whether voltage dependent channels can be activated in response to synaptic activity (Svoboda et al., 1996; Bloodgood and Sabatini, 2005; Araya et al., 2006b; Araya et al., 2007; Bloodgood and Sabatini, 2007a).

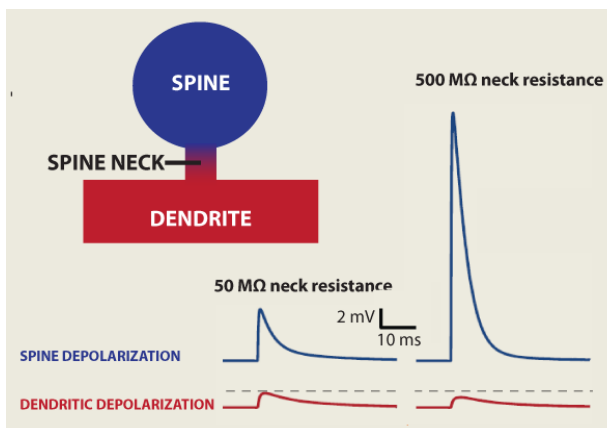


**Figure 1.4. Effect of neck resistance on synaptically evoked depolarization.**

In addition to regulating biochemical signaling, spine neck resistance determines the electrical function of dendritic spines. Spine depolarization (blue), in contrast to somatic or dendritic depolarization (red), is strongly dependent on the resistance between spine and parent dendrite. In response to synaptic stimulation, a neck resistance of 50 MΩ leads to weaker spine depolarization compared to a neck resistance of 500 MΩ.

(Adapted from Spruston et al., 2008)

### 2.3.1 The PSD and glutamate receptors

The postsynaptic density is composed of a large amount of different proteins including neurotransmitter receptors, voltage dependent channels, proteins involved in signaling cascades and scaffolding proteins. Important proteins such as the scaffolding proteins PSD-95 and Shank or glutamate receptors are thought to turn over at individual synapses on the timescale of minutes to hours (Adesnik et al., 2005; Gray et al., 2006; Tsuriei et al., 2006). At hippocampal Schaffer collateral synapses, the main neurotransmitter receptors are AMPA, NMDA and metabotropic glutamate receptors.

AMPA receptors are ionotropic receptors composed of GluR 1-4 subunits (Madden, 2002). Each functional receptor is composed of four subunits. AMPA receptors are permeable to potassium and sodium ions. AMPA receptors lacking the GluR2 subunit are also permeable to calcium (Burnashev et al., 1992). Most AMPA receptors in CA1 pyramidal cells contain the GluR2 subunit and are therefore impermeable to calcium ions (Geiger et al., 1995).

NMDA receptors are ionotropic receptors composed of NR1 and NR2A-D subunits (Madden, 2002). The subunit composition determines the calcium permeability of the receptor and is regulated during development. At early developmental stages, NMDA receptors are rich in NR2B subunits (high calcium permeability), later in development, these receptors are replaced by NR2A-subunit containing receptors (lower calcium permeability) (Sheng et al., 1994). The activity of NMDA receptors is highly voltage dependent: at resting membrane potential (around -70 mV), NMDA receptors are blocked by magnesium ions in the channel pore. Membrane depolarization relieves this block and the receptors become permeable to calcium, magnesium and potassium (Nowak et al., 1984). These receptors are thought to be the main pathway for calcium entry during synaptic activity (Mainen et al., 1999; Kovalchuk et al., 2000; Sabatini et al., 2002). Differences in the number and subtype of activated NMDA receptors are thought to be the major determinants regulating spine calcium signals during synaptic activity (Sabatini et al., 2001; Sobczyk et al., 2005).

Metabotropic glutamate receptors (mGluRs) are members of the G-protein coupled receptors and contain seven transmembrane domains. They are subdivided into groups I,

II and III (Bortolotto et al., 1999; Fagni et al., 2000). Receptors in the group I are coupled to the phospholipase C/ inositol-trisphosphate signaling cascade and their activation can result in calcium release from intracellular stores. Group II and group III mGluRs are negatively coupled to adenylyl cyclase and therefore prevent the formation of cAMP. mGluRs can affect different ionotropic receptors and other ion-channels and are thought to be involved in different forms of synaptic plasticity (Bortolotto et al., 1999; Nevian and Sakmann, 2006). In the hippocampus, Group I receptors (including mGluR1 and mGluR5) are thought to be mainly located on the postsynaptic side, whereas Group II and III receptors seem to be mostly presynaptic (Shigemoto et al., 1997).

### 2.3.2 Spine morphology

Spines have been shown to be highly variable in their morphology. Electron microscopy studies have shown that spine volume varies between 0.004 and 0.6  $\mu\text{m}^3$  and spine neck length can range from 0.1  $\mu\text{m}$  to 2  $\mu\text{m}$ , whereas neck diameter can range from 0.04 to 0.5  $\mu\text{m}$  (Harris and Stevens, 1989). Spine neck resistance, however, can not be directly measured. Electron microscopy data or optical measurements of spine-to-dendrite diffusional coupling (such as fluorescence recovery after photobleaching or photoactivation) have provided different estimates of spine neck resistance, with resistances between 4 and 1200  $\text{M}\Omega$  (Harris and Stevens, 1989; Svoboda et al., 1996; Bloodgood and Sabatini, 2005). Determining the actual spine neck resistance represents a key task in elucidating the possible electrical function of dendritic spines.

### 2.3.3 Impact of spine morphology on synaptic function and plasticity

Electron microscopy studies have shown that spine volume is correlated with the amount of AMPA receptors in the PSD, no correlation was found between spine volume and NMDA receptor content (Nusser et al., 1998). More recently, using optical stimulation of identified spines, it has been shown that synapses on big spines produce larger synaptic currents compared to synapses on small spines, demonstrating a tight correlation between spine volume and postsynaptic strength (Matsuzaki et al., 2001). Spine volume also seems to affect the ability of a synapse to undergo long term potentiation (LTP), a

specific form of synaptic plasticity: small spines seem to be more prone to undergo LTP compared to big spines (Matsuzaki et al., 2004).

Spine neck properties have been shown to regulate biochemical compartmentalization of second messengers and proteins (Svoboda et al., 1996; Noguchi et al., 2005). It is still a matter of debate, whether and under what conditions the spine neck can electrically isolate the synapse from its parent dendrite. Likely, spine neck properties, by regulating biochemical and electrical compartmentalization, can affect the potential for plasticity of a given synapse. However, experimental evidence supporting this hypothesis has never been provided.

#### 2.3.4 Spine microanatomy and synaptic function

Dendritic spines have been shown to contain different types of cellular organelles. The presence of these organelles is highly variable between spines. It is unclear whether these subsynaptic organelles can influence synaptic function and plasticity.

##### Mitochondria

Only a small percentage of spines has been shown to contain mitochondria (Bourne and Harris, 2008). The presence of mitochondria in dendritic spines can change in an activity dependent way: stimuli which induce LTP have been shown to increase the amount of spines containing mitochondria (Li et al., 2004). Whether spine-mitochondria primarily play a role in energy production or whether they also play other functions (such as calcium buffering during synaptic activity) remains unknown.

##### Endosomes

Endosomes are characterized as intracellular tubular compartments and are classified into several different types (clathrin-coated vesicles, uncoated vesicles, tubular compartments, multivesicular bodies) (Cooney et al., 2002). The exact function of these structures is not known, although they have been involved in endo- and exocytotic processes. A major function for endosomal compartments has been proposed to be the delivery and removal of receptors after synaptic plasticity (Park et al., 2006).



### Ribosomes and polyribosomes

Free or ER bound ribosomes are found in a subset of spines (Pierce et al., 2000). These structures could serve for synapse specific protein synthesis and therefore play an important role in protein synthesis dependent forms of synaptic plasticity. LTP has been proposed to redistribute polyribosomes from dendrites to spines, where they could play a central role for the long-term maintenance of synaptic modifications (Ostroff et al., 2002).

### Endoplasmic reticulum and the spine apparatus

Neuronal ER is thought to form a continuous membrane system of interconnected tubes and is present in the soma, axon, dendrites and in a subset of dendritic spines (Terasaki et al., 1994; Cooney et al., 2002; Choi et al., 2006). The ER in neurons is thought to be involved in protein synthesis and modification, lipid synthesis and calcium signaling (Berridge, 1998). Its role in modulating calcium signals has been proposed to affect many calcium dependent processes such as synaptic plasticity, gene expression or cell growth (Berridge, 1998; Verkhratsky, 2005). Neuronal ER contains calcium releasing channels such as the ryanodine receptors (RyRs) or the inositol-trisphosphate receptors (IP3Rs), in addition to specialized calcium ATPases (SERCA pumps). The ER has been proposed to act as a calcium source or as a calcium sink during neuronal activity (Sharp et al., 1993; Berridge, 1998; Sala et al., 2005). It is unknown, however, whether the ER in dendritic spines participates in regulating spine calcium dynamics and synaptic plasticity.

Different investigators, mainly using electrophysiological techniques and mutant animals for specific calcium release channels, have proposed a possible involvement of calcium release from the ER in regulating different forms of synaptic plasticity in cortical neurons (Svoboda and Mainen, 1999; Rose and Konnerth, 2001). These studies however, could not address the location of the required release channels (presynaptic/ postsynaptic; subcellular localization). In addition to that, studies using different strains of mutant animals often came to contradictory results, possibly reflecting differences in genetic compensation mechanisms (Balschun et al., 1999; Futatsugi et al., 1999; Nishiyama et al.,

2000; Shimuta et al., 2001). New calcium imaging techniques could address more precisely the possible involvement of the ER in regulating cellular calcium handling and the subcellular location of the involved channels. Using calcium imaging techniques, it has been shown that strong synaptic activation evokes a calcium release wave in the apical dendrite of pyramidal neurons of different brain areas (Nakamura et al., 1999; Power and Sah, 2002; Larkum et al., 2003). These calcium release events are dependent on mGluR and IP3R activation and could represent a powerful synapse-to-nucleus signaling machinery for the regulation of gene transcription in an activity dependent way (Berridge, 1998).

Whether and under what conditions the ER in dendritic spines participates in shaping spine calcium transients is highly debated. In cerebellar purkinje cells, where all spines contain a thin ER tube, calcium release from spine-ER is involved in the induction of synaptic depression in response to strong stimulation (Harris and Stevens, 1989; Finch and Augustine, 1998; Miyata et al., 2000). In cortical pyramidal cells, where only about 20% of dendritic spines contain ER, the possible involvement of the ER in shaping spine calcium transients is strongly debated (see next section) (Svoboda and Mainen, 1999; Cooney et al., 2002; Bloodgood and Sabatini, 2007c). In these cells, spine ER often differentiates into an electron dense structure called the ‘spine apparatus’ (Gray, 1959a). The spine apparatus consists of stacks of ER cisterns and is tightly associated with the actin binding protein synaptopodin (Deller et al., 2000). Animals lacking this protein have been shown to be devoid of spines containing a spine apparatus and to have deficits in synaptic plasticity (Deller et al., 2003). Although the role of the spine apparatus is not known, it could dramatically influence synaptic function and plasticity.

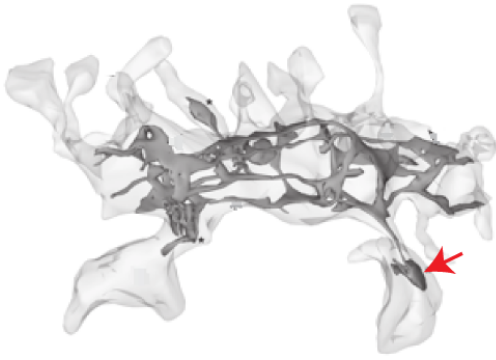


**Figure 1.5. Dendrite of CA1 pyramidal cell with endoplasmic reticulum.**

*3-D reconstruction from electron microscopy images of a CA1 pyramidal cell dendrite and intracellular endoplasmic reticulum (ER). Only a subset of spines contains ER (red arrow: example of ER-containing spine). (Adapted from Cooney et al. 2002)*

### 2.3.5 Spine calcium transients and synaptic plasticity of pyramidal neurons

Stimulation of presynaptic fibers leads to calcium transients which are restricted to the stimulated spine. Spine calcium signals are thought to be a key trigger for synaptic plasticity (Bloodgood and Sabatini, 2007c). Several studies in the hippocampus and other cortical areas have indicated NMDA receptors as the main pathway for fast calcium entry (Mainen et al., 1999; Kovalchuk et al., 2000; Sabatini et al., 2002). NMDA receptors, mainly blocked near resting membrane potential, get unblocked by AMPA receptor activation and spine head depolarization (Nevian and Sakmann, 2004; Bloodgood and Sabatini, 2007b). In recent studies it has been suggested that other voltage gated channels such as calcium, sodium or potassium channels can play a major role in modulating spine head depolarization and spine calcium influx (Ngo-Anh et al., 2005; Araya et al., 2007; Bloodgood and Sabatini, 2007b, 2007a).

The possible involvement of spine ER in shaping spine calcium transients during synaptic activity remains controversial (Bloodgood and Sabatini, 2007c). Two recent studies showed that blockade of ER calcium release had no effect on the amplitude of synaptically evoked spine calcium transients (Kovalchuk et al., 2000; Sabatini et al., 2002). In contrast to these studies, another study showed that RyRs represent the main source for spine-calcium during synaptic activity (Emptage et al., 1999). These conflicting results could be explained by differences in the preparation used, differences in recording/ stimulation technique or by a bias in the spines selected for the experiment (ER-containing versus ER-lacking spines). A more established concept, is that spine ER

can regulate calcium buffering during neuronal activity (Emptage et al., 1999; Sabatini et al., 2001; Noguchi et al., 2005). The fact that only a minority of spines in pyramidal neurons contains ER complicates the attempt to define a clear role for these structures. It is conceivable that major functional differences exist between spines containing ER and spines lacking ER.

Spine calcium signals are thought to be the main trigger regulating different forms of synaptic plasticity such as long term potentiation (LTP) and long term depression (LTD) (see next section) (Bear et al., 1987; Nevian and Sakmann, 2004). The calcium sources regulating the occurrence, magnitude and direction of change in synaptic strength are still unclear. Although calcium influx through NMDA receptors is known to play an important role in regulating different forms of plasticity, other calcium sources could participate in shaping spine calcium signals and regulating plasticity (Bloodgood and Sabatini, 2007c).

Spine ER structures could significantly modulate spine calcium signals required for the induction of synaptic plasticity. The differential distribution of ER in spines of pyramidal cells could therefore be an important aspect for the regulation of functional properties at individual synapses.

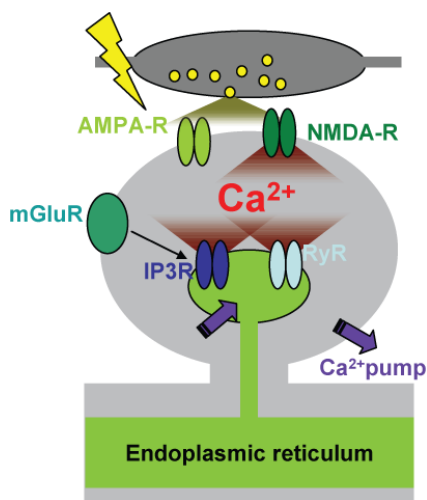


**Figure 1.6. Spine calcium signaling.**

Synaptic stimulation leads to activation of glutamate receptors in the PSD. NMDA receptors (NMDA-R) are thought to be the main pathway for calcium influx. Spine ER could strongly contribute to spine calcium signals through ryanodine receptor (RyR) or IP3 receptor (IP3R) mediated calcium release. Calcium pumps or calcium exchangers in the plasma membrane are responsible for calcium extrusion, ER calcium pumps could potentially participate in calcium sequestration.

## 2.4 LTP and LTD

Long term changes in synaptic strength, such as LTP and LTD, are thought to be cellular correlates for learning and memory (Bliss and Collingridge, 1993).

In the CA1 region of the hippocampus, LTP can be induced using different induction protocols which elicit strong postsynaptic depolarization and large, NMDA receptor dependent postsynaptic calcium transients. These calcium signals are thought to be the necessary trigger for plasticity. However, it remains elusive whether other calcium sources participate in shaping the triggering signal and which calcium microdomains are involved in regulating plasticity (Malenka and Nicoll, 1999; Malenka and Bear, 2004).

The site of LTP expression at Schaffer collateral synapses is still highly debated. Many reports demonstrated a strong postsynaptic component in being responsible for the increase in synaptic strength (change in AMPA receptor number and subtype, as well as single channel conductance and recruitment of silent synapses). Other reports also observed changes in presynaptic properties (increase in release probability) following LTP inducing stimuli (Bear and Malenka, 1994; Mainen et al., 1998; Malenka and Nicoll, 1999; Emptage et al., 2003; Ward et al., 2006).

At least two forms of LTD have been shown to coexist at CA3 to CA1 synapses: one form is dependent on mGluR activation and the other on the activation of NMDA receptors (Oliet et al., 1997). LTD at these synapses can be induced using prolonged low frequency stimulation or by negative pairing of pre- and postsynaptic cell firing (Bear and Malenka, 1994; Nishiyama et al., 2000). mGluR dependent LTD seems to require postsynaptic group 1 mGluR receptors and rapid local protein synthesis (Huber et al., 2000; Snyder et al., 2001). Its site of expression is thought to be presynaptic in young animals (change in release probability) and mainly postsynaptic in older animals (change in AMPA receptor number, subtype and channel conductance) (Bear and Malenka, 1994; Snyder et al., 2001; Nosyreva and Huber, 2005). Although several studies reported that NMDA receptor dependent LTD requires a rise in postsynaptic calcium (Bear and Malenka, 1994), a recent study suggests that spike timing dependent LTD depends on presynaptically located NMDA receptors (Rodriguez-Moreno and Paulsen, 2008).

NMDA receptor dependent LTD leads to changes in AMPA receptor number and properties but has also a strong presynaptic component, leading to changes in release probability (Bear and Malenka, 1994; Zhang et al., 2006).

Recent studies have addressed the structural correlates of LTP at the level of individual synapses (see later), it is however unknown whether LTD can be induced at single synapses and what the structural correlates for this form of plasticity are.

## 2.5 CaMKII and LTP

Spine calcium transients can activate various calcium dependent second messenger cascades and ultimately lead to the induction of synaptic plasticity. A major protein which has been involved in the induction of LTP is Calcium/calmodulin-dependent protein kinase II (CaMKII) (Lisman and Zhabotinsky, 2001). This protein is highly expressed in the nervous system and is enriched in the PSD (Erondy and Kennedy, 1985; Miller and Kennedy, 1985). Blockade of CaMKII activity blocks the induction of LTP (Malinow et al., 1989). Imaging experiments have shown that CaMKII translocates to dendritic spines in response to chemical LTP induction. It has been suggested that CaMKII translocation to the spine could be the key step in the induction of LTP (Otmakhov et al., 2004). Activated CaMKII could phosphorylate important target proteins in the PSD and lead to synaptic potentiation. It is however unclear, whether CaMKII translocates to stimulated spines in response to more physiological stimuli and whether CaMKII is tagged to the stimulated spine only or whether it can spread to neighboring spines.

## 2.6 Glutamate uncaging and single spine induction of synaptic plasticity

New advances in technology have enabled the analysis of synaptic function and plasticity at individual synapses. Two-photon uncaging of glutamate has become a major technique to study synaptic signals on the level of single spines or short dendritic branches (Matsuzaki et al., 2001; Carter and Sabatini, 2004; Sobczyk et al., 2005; Gasparini and Magee, 2006). This technique consists of the focal release of glutamate from an inactive precursor compound (caged glutamate) using a brief and focused laser pulse. The

uncaged glutamate mimics the glutamate released by presynaptic afferents and activates receptors on the postsynaptic membrane (Matsuzaki et al., 2001). Glutamate uncaging has the advantage over conventional electrical stimulation of presynaptic fibers in that it allows stimulation of any identified synapse. The observed effects are purely postsynaptic, allowing precise analysis of postsynaptic processes. However, care must be taken in calibrating the intensity and duration of the laser pulse used for uncaging, the evoked responses have to lie within a physiological regime (Bloodgood and Sabatini, 2007b, 2007c).

Two-photon uncaging of glutamate has been used to characterize AMPA receptor mediated synaptic currents at single spines. It has been shown that the content of functional AMPA receptors is correlated with spine volume: big spines contain a larger amount of AMPA receptors compared to small spines (Matsuzaki et al., 2001). Using a similar approach it has been demonstrated that such a correlation does not exist for NMDA receptors. NMDA receptor number and subunit composition seems to be regulated on the single synapse level, it is not correlated with spine volume and can rapidly change in an activity dependent manner (Sobczyk et al., 2005; Sobczyk and Svoboda, 2007).

Glutamate uncaging has also been used to induce LTP on single visualized spine synapses (Matsuzaki et al., 2004; Harvey and Svoboda, 2007). It has been shown that LTP stimuli lead to an increase in the uncaging evoked excitatory postsynaptic current (uEPSC) specifically at the synapse receiving the stimulus, with no change in uEPSC amplitude at neighboring synapses. The increase in synaptic current is accompanied by an increase in the volume of the spine containing the potentiated synapse. The amount of potentiation seems to be inversely correlated with spine volume (Matsuzaki et al., 2004), a finding which is, however, still debated and inconsistent with another study (Kopec et al., 2006). In this study the authors show that chemical induction of LTP leads to exocytosis of AMPA receptors at the spine surface. Although the authors found an inverse correlation between spine volume and fractional increase in receptor content (increase normalized to spine volume), no correlation was observed between absolute

amount of exocytosed receptors and spine volume. This finding, which contrasts to the Matsuzaki et al. study, provides evidence that both, small and big spines can undergo potentiation.

Although the link between spine volume and potential for plasticity is debated and remains to be confirmed, the studies performed by the groups of Kasai and Svoboda (Matsuzaki et al., 2004; Harvey and Svoboda, 2007) demonstrate that synaptic strength can be modulated at individual synapses, that there is a structural correlate for LTP and that spines can be considered as the potential smallest memory units. Since synapses on big spines appear to be less prone to undergo potentiation (but see Kopec et al., 2006), it has been proposed that the plastic synapses on smaller spines are capable of rapid storage of new information, whereas synapses on big spines are responsible for storage of previously acquired information (Bourne and Harris, 2007). A recent study, using a similar approach, showed that the increases in synaptic strength and spine volume have been shown to have a fast and a slow component, with the slower component speculated to be dependent on new protein synthesis and BDNF signaling (Tanaka et al., 2008).

## 2.7 Cooperativity between neighboring synapses

Several studies reported that LTP induction caused structural (increase in spine volume) and functional (increase in synaptic currents) changes at the stimulated spines with no obvious changes at neighboring spines (Matsuzaki et al., 2004; Harvey and Svoboda, 2007; Tanaka et al., 2008). A recent study asked whether LTP induction alters the ability of neighboring spines to undergo this form of plasticity. The authors found that after LTP induction, the threshold for the induction of plasticity on neighboring spines was drastically reduced. This form of synaptic crosstalk was found to act over short dendritic stretches ( $\sim 10 \mu\text{m}$ ) (Harvey and Svoboda, 2007). This study demonstrates the existence of spatially clustered groups of synapses acting in a cooperative and reciprocally reinforcing manner. Ras, a small GTPase, has been proposed to be the responsible molecule for this form of synaptic crosstalk. Activated Ras has been shown to diffuse from the potentiated spine to neighboring spines, blockade of its activity inhibits synaptic crosstalk (Harvey et al., 2008).



Recent work from the laboratory of Jeffrey Magee shows that when neighboring synapses get simultaneously activated, a dendritic spike can be generated, leading to a supralinear summation of synaptic responses (Gasparini and Magee, 2006; Losonczy and Magee, 2006). These studies demonstrate that synapses on the same branch can actively cooperate to increase synaptic signals by generating local spikes. More recently, the authors show that repeated generation of dendritic spikes can even lead to potentiation of the responses (Losonczy et al., 2008).

In summary, these recent studies show that, although single synapses are capable of important computational processes, short dendritic branches can act as cooperative computational units and could play major roles in information processing and storage. The understanding of the function and plasticity of single synapses, the relationship between synapse structure and function and the processes involved in cooperativity between neighboring synapses is key for understanding brain function.

### **3. AIM OF THE THESIS**

Synapses in the brain undergo activity dependent modifications in their strength; these processes are thought to underlie learning. However, in order to keep stable memory traces, synapses also need to maintain stability. How these conflicting requirements are regulated at individual synapses is unknown. It is plausible that different subpopulations of synapses exist in regard to their potential for plasticity and stability and that these processes are dynamically regulated at individual synaptic connections. The morphology and microanatomy (e.g. presence of subsynaptic organelles) of dendritic spines has been demonstrated to be highly variable. It is conceivable that the differential regulation of spine morphology and microanatomy dramatically affects synaptic function and plasticity.

The aim of my thesis was to elucidate how plasticity and stability can be regulated at single spine synapses and how differences in spine structure influence synaptic function. The dynamic regulation of spine properties could be the structural basis for regulating the potential of individual synapses in processes underlying learning and memory.

In the first part of my thesis I focused on the possible impact of specialized microanatomical structures on synaptic function and plasticity. In the mammalian forebrain, only a small subset of dendritic spines contains endoplasmic reticulum (ER), which often forms a specialized structure of unknown function called ‘spine apparatus’. Using a genetic approach to visualize the ER in living neurons, in combination with two-photon imaging and uncaging, we show that subsynaptic ER strongly influences synaptic plasticity. In ER containing spines we observed a new form of synaptically triggered calcium release event and we provide strong evidence that this response triggers synaptic depression. We show that only synapses on spines containing ER can undergo a specific form of long term depression. In summary, we show how spine microanatomy can influence synaptic function and plasticity.

In the second part of my thesis, we analyzed how morphological properties of dendritic spines can influence synaptic signals. A key function of dendritic spines is to biochemically isolate neighboring synapses. It is unclear whether spines also act as electrical compartments and amplify synaptic signals. Electrical compartmentalization can only be achieved if the resistance of the spine neck, the thin tube connecting the spine head to its parent dendrite, is high enough. We demonstrate that the spine neck resistance is highly plastic and changes in an activity dependent way. Using single spine calcium imaging as a reporter for spine head depolarization, we demonstrate that spines are capable of electrical compartmentalization. We identify different channels to be responsible for the amplitude of spine head depolarization and spine calcium transients.

Spine calcium signals can activate key signaling cascades leading to synaptic plasticity. In the last part of my thesis we studied whether key plasticity-inducing proteins, such as CaMKII, can be tagged to single synapses. Using a new, all optical LTP induction protocol on the single synapse level, we demonstrate that LTP induces a long lasting volume increase of the stimulated spine. We observed that CaMKII translocates to the activated spine, but not to neighboring spines. Our study provides evidence for a role of CaMKII in regulating plasticity on the level of single synapses and shows that important second messenger proteins can be compartmentalized and tagged to individual synapses.

The work described herein sheds light on the function of dendritic spines and shows how the modulation of spine properties can regulate biochemical and electrical signals on a micrometer scale. We provide evidence that synapses can work as the minimal computational units and that spine morphology and microanatomy can regulate the potential for plasticity or stability of individual synapses.

## **4. PUBLICATIONS**

### **Part 4.A:**

#### **Synaptic depression at individual synapses is governed by spine microanatomy**

**Niklaus Holbro, Åsa Grunditz, Thomas G. Oertner**

*Submitted Nature Neuroscience*

#### **ABSTRACT**

To maintain balance between learning and stable memory traces, the brain has to regulate plasticity and stability on the level of single synapses. How this is achieved and whether all synapses have the same potential for plasticity is unknown. Here we combine two-photon imaging and glutamate uncaging to investigate how the presence of endoplasmic reticulum (ER) affects synaptic function and plasticity in individual spines of CA1 pyramidal cells. ER was frequently found in large spines that contained strong synapses, but rarely in small spines. Low frequency stimulation of synapses on ER containing spines produced delayed calcium release events and mGluR-dependent synaptic depression. Both phenomena were dependent on mGluR activation and IP<sub>3</sub> signaling and were never observed in spines without ER. We conclude that in pyramidal cells, spine ER controls the potential for synaptic depression on the single synapse level.

## INTRODUCTION

Excitatory connections between pyramidal cells vary greatly in strength due to differences in transmitter release and due to the variable number of glutamate receptors in the postsynaptic terminal (Schikorski and Stevens, 1997; Koester and Johnston, 2005). This heterogeneity of the synaptic population at any given time is thought to reflect a large degree of use-dependent plasticity at individual excitatory synapses. Synaptic plasticity itself is also subject to regulation, the most prominent example being the developmental switch from NR2B to NR2A-containing NMDA receptors that modulates long term potentiation (LTP), critical periods and associative learning abilities in many vertebrate species (Dumas, 2005). It is less clear whether plasticity can also be regulated on the level of *individual* synapses. Conceptually, this would seem to be an attractive feature: Reducing plasticity of a specific set of synapses could be used to protect an established neuronal circuit from further changes while the rest of the synaptic population would still be available for use-dependent modification (Abraham, 2008). However, few studies have addressed the activity-dependent regulation of plasticity or ‘metaplasticity’ with single synapse resolution (Matsuzaki et al., 2004; Harvey and Svoboda, 2007). There is a general consensus that strong synapses have a reduced ability to undergo further potentiation (Debanne et al., 1999; Matsuzaki et al., 2004; Zhang and Oertner, 2007) and that they can get locked in a state of high strength (O'Connor et al., 2005), but the underlying regulatory mechanisms remain poorly understood.

The morphology of dendritic spines is highly variable and has been shown to be correlated with synaptic strength (Matsuzaki et al., 2001). From ultrastructural studies, we know that spines also possess a rich internal structure (Gray, 1959a; Cooney et al., 2002). Spine microanatomy, e.g. the presence of subsynaptic organelles, could potentially influence both synaptic function and synaptic plasticity. An organelle that could play a major regulatory role is the endoplasmic reticulum (ER). Interestingly, in cortical pyramidal cells, only a subset of dendritic spines contains ER, often in the form of a specialized structure known as the spine apparatus (Gray, 1959b, 1959a; Cooney et al., 2002). The number of spines containing a spine apparatus is regulated in an activity-dependent manner, as shown by *in vivo* lesion experiments (Deller et al., 2006). The function of these ER structures in spines is unknown at present, although they have been

proposed to act as a sink or source for calcium ions during synaptic activity (Emptage et al., 1999; Kovalchuk et al., 2000; Sabatini et al., 2002). Here we combine two-photon imaging and two-photon glutamate uncaging to compare functional and morphological properties of spines with and without ER. We show that spine ER affects electrical and biochemical signaling and controls plasticity on the single synapse level.

## RESULTS

### A genetic approach to identify ER containing spines in CA1 pyramidal cells

To visualize the ER in intact hippocampal tissue, we constructed a green ER label by fusing EGFP with ER-targeting and ER-retention sequences (**Fig. A1a**). Organotypic hippocampal slice cultures were biolistically co-transfected with the ER label and a cytoplasmic red fluorescent protein to visualize cell morphology (**Fig. A1a**). Two-photon microscopy allowed us to image transfected CA1 pyramidal cells at high resolution (**Fig. A1b**) and to identify ER containing (ER+) and other (ER-) spines on oblique dendrites (**Fig. A1c**). Analysis of several transfected CA1 cells showed that  $18.7\% \pm 2.3\%$  of spines were positive for the ER label ( $n = 318$  spines, 8 cells; **Fig. A1d**). A similar fraction of ER containing spines has been reported in CA1 cells of perfusion fixed hippocampus and in dissociated hippocampal cell culture (Cooney et al., 2002; Toresson and Grant, 2005).

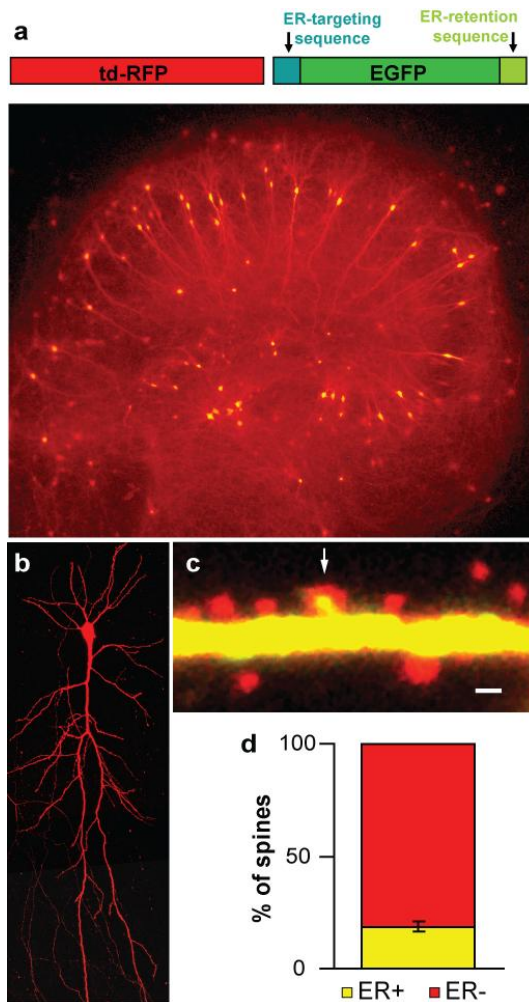


**Figure A1. ER labeling in living neurons.**

(a) Organotypic hippocampal cultures were biolistically transfected with a cytoplasmic RFP (red) and an ER-targeted EGFP (GFP-ER, green).

(b) 2-photon image of a transfected CA1 pyramidal cell (RFP fluorescence).

(c) Dendrite of a transfected CA1 pyramidal cell with one large ER-containing spine (arrow). Overlay of red (RFP) and green (GFP-ER) fluorescence results in yellow color. Scale bar: 1  $\mu\text{m}$ .

(d) Fraction of ER-containing spines ( $n=318$  spines, 8 cells). Values represent mean  $\pm$  SEM.

### ER-containing spines have large heads and often contain a spine apparatus

Quantification of spine morphology showed that ER<sup>+</sup> spines had significantly ( $P < 0.001$ ) larger cytoplasmic volumes ( $0.058 \mu\text{m}^3 \pm 0.005 \mu\text{m}^3$ ,  $n = 49$ ) than the rest of the population ( $0.028 \mu\text{m}^3 \pm 0.002 \mu\text{m}^3$ ,  $n = 91$ , **Fig. A2a**). Since we used the fluorescence intensity of a cytoplasmic marker to estimate spine volume (see methods), the volume of the ER itself was excluded. Including the ER volume would have made the volume difference between the populations even larger. From ultrastructural studies, it is known that the ER in the spine head is connected to the dendritic ER by a thin tube passing through the spine neck. Therefore, ER could affect the diffusional coupling between spine head and parent dendrite by physically obstructing the spine neck (Bloodgood and Sabatini, 2005). To address this issue, we measured time constants ( $\tau$ ) of fluorescence recovery after photobleaching (FRAP) in ER containing and other spines by bleaching

the cytoplasmic RFP. The recovery time constants of the two groups of spines were not significantly different ( $\tau_{ER+} = 235 \text{ ms} \pm 40 \text{ ms}$ ,  $n = 26$ ;  $\tau_{ER-} = 218 \text{ ms} \pm 20 \text{ ms}$ ,  $n = 35$ , **Fig. A2b**), demonstrating that the ER did not block diffusion between spine head and dendrite. In fact, due to the larger head volumes of ER+ spines (**Fig. A2a**), these would be expected to have longer time constants assuming identical neck properties (Bloodgood and Sabatini, 2005; Biess et al., 2007). The similar time constants therefore suggest that the necks of ER+ spines provided an even weaker diffusional barrier compared to spines lacking ER.

In spines of pyramidal cells, ER often forms a specialized organelle consisting of stacked membrane discs, the spine apparatus (Gray, 1959b; Cooney et al., 2002). To assess which fraction of ER+ spines in our sample contained this organelle, we combined live ER imaging with post-hoc immunohistochemistry against synaptopodin, a protein associated with the spine apparatus (Deller et al., 2000) (**Fig. A2c**). We found that the majority (78%) of ER+ spines were also positive for synaptopodin (**Fig. A2d**) and thus very likely contained a spine apparatus.

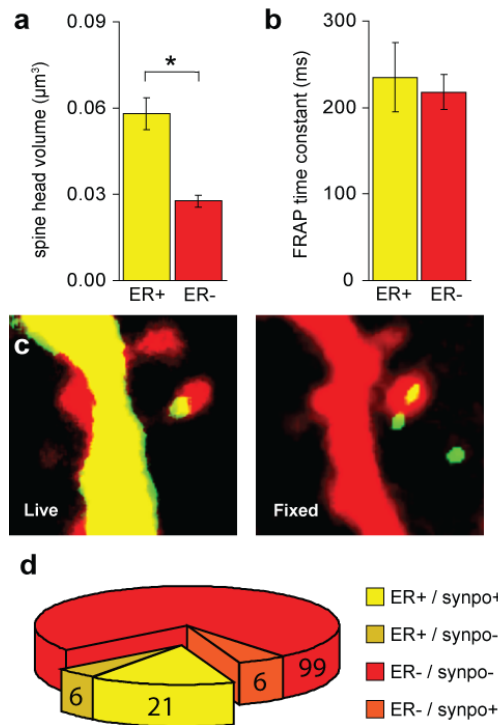


**Figure A2. Morphology of ER-containing spines.**

(a) Spine head volume of ER+ spines was significantly larger compared to ER- spines (ER+:  $n = 49$ ; ER-:  $n = 91$ ;  $P < 0.001$ , Mann-Whitney rank sum test).

(b) FRAP time constant was not different in ER+ spines (ER+:  $n = 26$ ; ER-:  $n = 35$ ).

(c) Post-hoc immunostaining against the spine apparatus associated protein synaptopodin (synpo); example of a spine that contained ER (left panel) and was immunopositive for synpo (right panel). In the right panel yellow color indicates synaptopodin immunoreactivity (green) in a cell of interest stained with Alexa Fluor 594 conjugated streptavidin (red).

(d) Correspondence between ER identification in live tissue (ER+) and anti-synaptopodin immunoreactivity (synpo). Number of spines in each group indicated on pie chart. Values in (a) and (b) represent mean  $\pm$  SEM.



### Synapses on ER-containing spines are strong

To assess the functional properties of spine synapses, we stimulated individual spines by two-photon glutamate uncaging. First, we identified ER<sup>+</sup> spines on oblique dendrites (**Fig. A3a**). After spine pre-selection, cells were patch-clamped and uncaging evoked currents (uEPSCs) were measured. On average, uEPSCs had amplitudes of  $11.4 \text{ pA} \pm 0.7 \text{ pA}$  ( $n = 74$  spines, 23 cells), similar to the amplitude of miniature EPSCs in these cells. Stimulation of ER<sup>+</sup> spines evoked significantly ( $P < 0.001$ ) larger uEPSCs ( $17.1 \text{ pA} \pm 1.9 \text{ pA}$ ,  $n = 30$ ) than stimulation of other spines ( $7.5 \text{ pA} \pm 0.5 \text{ pA}$ ,  $n = 44$ ; **Fig. A3b, c**). To exclude systematic differences in stimulation intensity, we consistently stimulated 1-2 ER<sup>+</sup> and control spines on the same dendrite. Furthermore, we compared the amount of Alexa Fluor 594 bleaching by the uncaging laser pulse (Bloodgood and Sabatini, 2007b), which was identical in ER containing and other spines (see **Supplementary Fig. A1**). This control verified that both groups of spines were stimulated by equal amounts of photoactivated glutamate. In our sample of spine synapses, uEPSC amplitude was positively correlated with spine volume ( $R^2 = 0.46$ ,  $n = 62$ ; **Fig. A3d**), which is in line with previous studies (Matsuzaki et al., 2001). Thus, ER containing spines are not only morphologically distinct by their larger volume, but also carry stronger synapses (**Fig. A3d**).

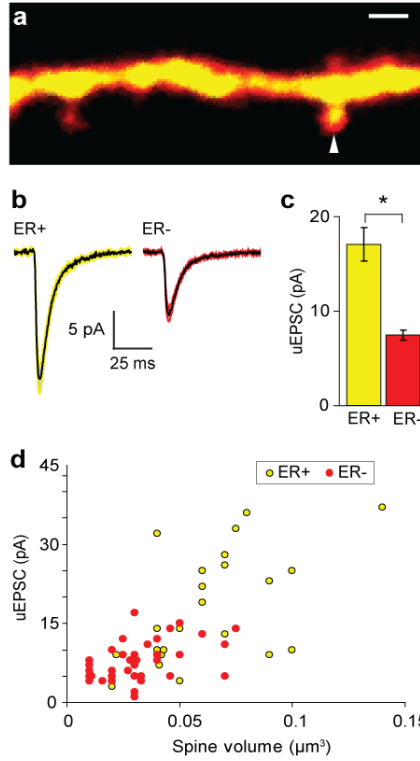
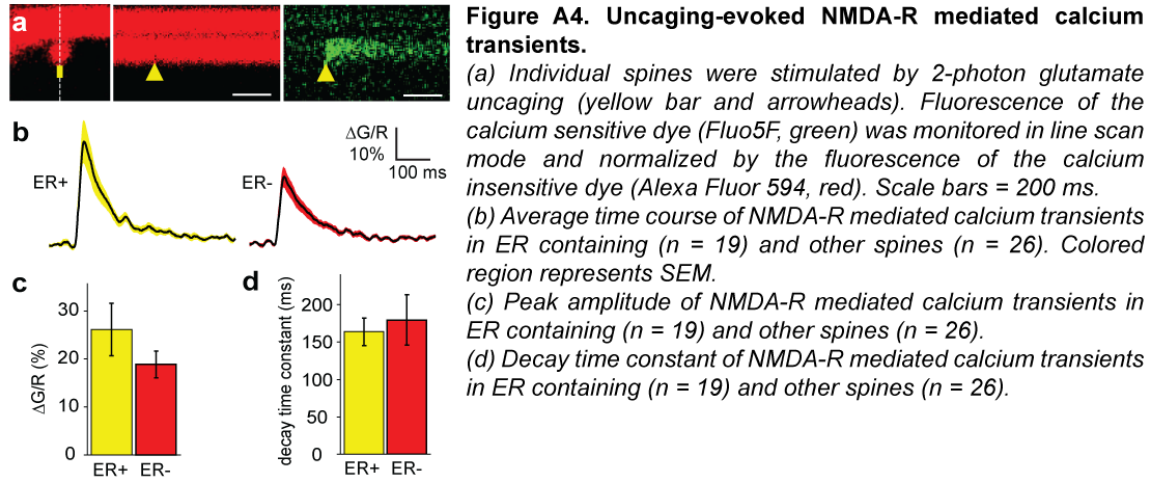


**Figure A3. ER-containing spines bear strong synapses.** (a) Stimulation of ER containing spine by two-photon glutamate uncaging (arrowhead). Scale bar: 1 μm. (b) Average uEPSC (black) for ER containing ( $n = 30$ ) and other spines ( $n = 44$ ). Colored region represents SEM. (c) Peak amplitude of uEPSC was significantly larger in ER+ spines ( $n = 30$ ) compared to ER- spines ( $n = 44$ ;  $P < 0.001$ , Mann-Whitney rank sum test). (d) Relationship between spine volume and uEPSC amplitude ( $n = 62$ ). Values in (C) represent mean  $\pm$  SEM.

### NMDA receptor mediated calcium transients are similar in ER+ and ER- spines

The ER could potentially modulate the time course of postsynaptic calcium transients, which are an important trigger for synaptic plasticity (Brocher et al., 1992; Nevian and Sakmann, 2006). To compare calcium transients in spines with and without ER, we filled transfected CA1 pyramidal cells with a mixture of a green calcium-sensitive dye (Fluo5F) and a red calcium-insensitive dye (Alexa Fluor 594). At the excitation wavelength used in the calcium imaging experiments (810 nm), GFP and RFP fluorescence was negligible. Glutamate uncaging evoked spine calcium transients with short latencies (CaTs; **Fig. A4a**). These CaTs were blocked by 10 μM dCPP (22.8% of control amplitude,  $n = 4$ ), confirming that NMDA receptors were the main pathway for fast calcium entry (Bloodgood and Sabatini, 2007c). When we compared peak amplitudes in different spines (**Fig. A4b, c**), we found a small but not significant difference between ER containing spines ( $\Delta G/R = 26\% \pm 6\%$ ) and other spines ( $\Delta G/R = 19\% \pm 3\%$ ). The decay time constants ( $\tau_{\text{decay}}$ , **Fig. A4d**) were also very similar (ER+  $\tau_{\text{decay}} = 164 \text{ ms} \pm 19 \text{ ms}$ ; ER-  $\tau_{\text{decay}} = 179 \text{ ms} \pm 34 \text{ ms}$ ). How the amplitude of these rapid calcium transients is regulated is still an open question, although differential activation of NMDA receptors and other

voltage-sensitive channels are known to play a major role (Sabatini et al., 2002; Bloodgood and Sabatini, 2007c; Sobczyk and Svoboda, 2007). Our data suggest that spine ER is not a major modulator of NMDA receptor mediated calcium transients during the EPSP.



### ER containing spines actively release calcium

In all spines tested, glutamate uncaging triggered fast rising calcium transients (average time to peak: 47 ms) with a slow decay ( $\tau_{\text{decay}} = 173 \text{ ms} \pm 21 \text{ ms}$ ). In addition, in some spines, we observed a second, delayed rise in calcium concentration (average delay: 470 ms  $\pm$  41 ms; **Fig. A5a**). This second calcium transient (CaT2) reached much higher amplitudes than the fast, NMDA-R mediated transient (CaT1:  $\Delta G/R = 22\% \pm 3\%$ , CaT2:  $\Delta G/R = 141\% \pm 26\%$ ; **Fig. A5b**). Delayed CaTs were observed in 7 out of 19 ER+ spines, but never in ER- spines ( $n = 26$ ; **Fig. A5e**). Our best estimate for the frequency of spines with delayed CaTs is 0.368, so assuming a binomial distribution, the probability of observing no delayed CaTs in ER- spines is  $6.6 \times 10^{-6}$ . Therefore, ER+ and ER- spines represent two distinct populations with respect to their calcium signaling.

Delayed CaTs never preceded uncaging stimulation (**Fig. A5c**), but appeared to be triggered by the stimulation in a stochastic fashion (**Fig. A5a**). In the spines that showed delayed CaTs, they occurred in ~20% of the individual stimulations (range 6% - 43%). Simultaneous voltage clamp recordings revealed that delayed CaTs had no electrical correlate, ruling out the possibility that they were caused by voltage-gated calcium influx

(**Fig. A5c**). In many cases, delayed CaTs were also detected in the dendrite (**Fig. A5c**), but the higher amplitude and fast kinetics of spine calcium transients argues for a trigger inside the spine rather than diffusion of calcium from the dendrite into the spine. Blocking group I metabotropic glutamate receptors (mGluRs) with a cocktail of mGluR1 and mGluR5 antagonists (LY367385 and MPEP,  $n = 9$ ; **Fig. A5d, e**) or blocking IP<sub>3</sub> receptors with intracellular heparin (4 mg/ml,  $n = 12$ ; **Fig. A5e**) abolished delayed CaTs in ER<sup>+</sup> spines. Whole cell perfusion with 100  $\mu$ M IP<sub>3</sub>, on the other hand, increased the fraction of ER<sup>+</sup> spines showing delayed CaTs ( $n = 5$ ; **Fig. A5e**). The amplitude of uEPSCs was not affected by these pharmacological manipulations (see **Supplementary Fig. A2**). In summary, our data suggest that delayed CaTs are IP<sub>3</sub> receptor mediated calcium release events, triggered by mGluR activation and restricted to ER<sup>+</sup> spines.

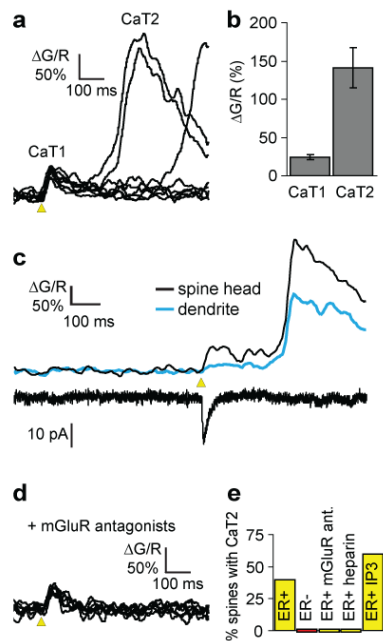


**Figure A5. mGluR dependent calcium release in ER-containing spines.**

(a) Delayed calcium transients (CaT2) in an ER containing spine (single traces).

(b) Amplitude of delayed calcium transient (CaT2) was large compared to NMDA-R mediated transient (CaT1) ( $n = 7$  ER<sup>+</sup> spines). Values represent mean  $\pm$  SEM

(c) Delayed calcium transients were evoked by the uncaging pulse, had higher amplitude in the spine compared to dendrite and had no electrical correlate.

(d) Group I mGluR block completely abolished delayed calcium transients.

(e) Pharmacological profile of delayed calcium transients ( $n = 19, 26, 9, 12, 5$ ).

### Synapses on ER-containing spines express mGluR-dependent depression

Using electrophysiological approaches, it has been suggested that IP<sub>3</sub> mediated calcium release is involved in the induction of LTD in several cortical areas (Reyes and Stanton, 1996; Nishiyama et al., 2000; Bender et al., 2006). However, it is unclear whether this form of plasticity is restricted to specialized synapses or whether all synapses have the potential to undergo LTD. At Schaffer collateral to CA1 synapses, at least two different

forms of LTD have been described, one dependent on NMDA receptors and one dependent on mGluR activation (Oliet et al., 1997). mGluR dependent LTD has been shown to have a strong postsynaptic component (Zhang et al., 2006). The specificity of mGluR  $\rightarrow$  IP<sub>3</sub> mediated spine calcium signals (**Fig. A5**) raised the possibility that synapses on ER+ spines are preferential sites for this form of synaptic depression. We tested this possibility by comparing the effects of low frequency stimulation, a classical LTD induction protocol, on ER+ spines. To isolate mGluR dependent effects, NMDA receptors were blocked with dCPP. In a series of control experiments, we verified that delayed CaTs were still present under NMDA receptor block. The strength of synapses on spines of interest was measured before and after low frequency uncaging stimulation (LFU, 0.2 Hz, 15 min; **Fig. A6a**). Indeed, low frequency glutamate uncaging induced depression of the uEPSC in ER+ spines (average depression:  $27.6\% \pm 4\%$ ,  $n = 20$ ,  $P < 0.001$ ; **Fig. A6b, c**). This depression was long-lasting ( $n = 3$ , **Fig. A6a**) and could not be evoked in spines lacking ER ( $n = 11$ , **Fig. A6b, c**). The depression of uEPSCs at ER+ spines was completely blocked by group I mGluR antagonists ( $n = 7$ ; **Fig. A6c**) and by the IP<sub>3</sub> receptor antagonist heparin (4 mg/ml,  $n = 9$ ; **Fig. A6c**). The identical pharmacology of synaptic depression and delayed CaTs in ER+ spines (**Fig. A5e**) suggests that calcium release from the spine apparatus is a key trigger for the induction of depression at these synapses.

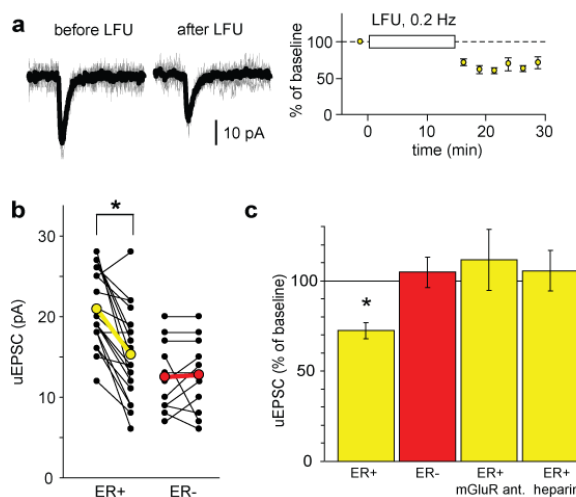


**Figure A6. Optical induction of synaptic depression.**

(a) uEPSCs before and after 15 min of low frequency glutamate uncaging (LFU, 0.2 Hz) on ER+ spine. Thick trace: Average of 5 uEPSCs. Right: Time course of LFU-induced depression ( $n = 3$  ER+ spines).

(b) LFU induced depression in ER containing spines ( $n = 20$ ;  $P < 0.001$ , Wilcoxon signed-rank test), but not in other spines ( $n = 11$ ).

(c) Pharmacological profile of LFU-induced depression (mGluR antagonists:  $n = 7$ ; heparin:  $n = 9$ ). Values in (a) and (c) represent mean  $\pm$  SEM.

## DISCUSSION

Our results show that ER containing spines on CA1 pyramidal cells are preferential sites for mGluR-mediated LTD. For the first time, we demonstrate the existence of defined subpopulations of spines with regard to their potential for synaptic plasticity. Furthermore, we show that ER containing spines frequently generate large mGluR dependent calcium transients, which we interpret as calcium release from intracellular stores (**Fig. A5**). It is highly likely that these calcium release events act as a trigger for synaptic depression, since pharmacological manipulations that prevented the occurrence of calcium release events also blocked synaptic depression after low-frequency stimulation (**Fig. A6**). In addition to its function in calcium signaling, it is very possible that ER contributes in additional ways to synaptic function and plasticity, e.g. by providing a substrate for local protein synthesis and modification (Huber et al., 2000). The complete absence of mGluR-dependent LTD in spines lacking ER highlights a level of functional diversity that was impossible to discover by electrophysiological methods alone.

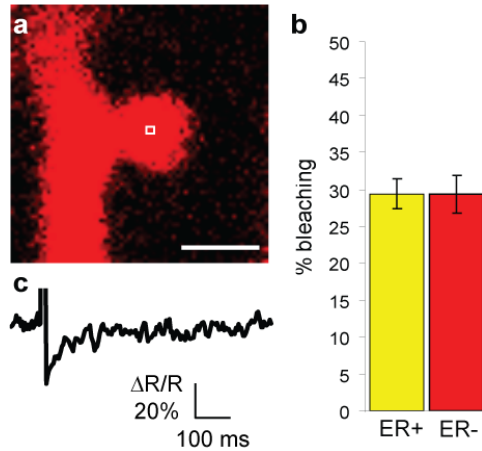
At least 78% of the ER containing spines in our sample contained a fully developed spine apparatus, which we identified by its immunoreactivity against synaptopodin (**Fig. A2**). The spine apparatus has been implicated in calcium homeostasis and synaptic plasticity on the basis of synaptopodin<sup>-/-</sup> mice, which develop no spine apparatus and show reduced LTP. Here we show that in CA1 pyramidal cells, the spine apparatus governs the potential for synaptic depression with single spine specificity. In Purkinje cells of the cerebellum, IP<sub>3</sub> signaling has been shown to be involved in LTD of parallel fiber synapses (Finch and Augustine, 1998; Miyata et al., 2000). In these cells, however, there is no indication of a regulation of plasticity on the single synapse level, a functional uniformity that is reflected in the homogenous morphology of Purkinje cell spines. Furthermore, much stronger stimulation was needed to elicit calcium release events in Purkinje cell spines, possibly connected to the simpler, tube-like morphology of ER in these spines. In our experiments, a single quantum-like stimulation of a single synapse could trigger calcium release events (**Fig. A5**). Therefore, although the general mechanism of mGluR→IP<sub>3</sub> mediated depression seems to be conserved in different cell

types and brain areas, the selective targeting of the ER to strong synapses (**Fig. A3**) and the low activation threshold might be a specific feature of pyramidal cells.

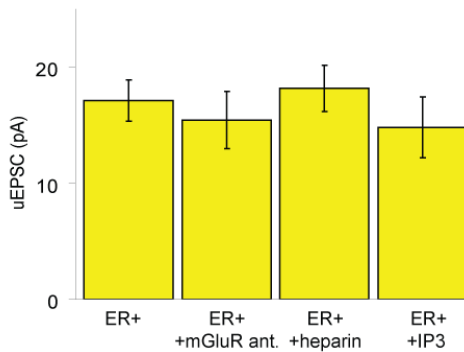
Our results have important implications for the distribution of synaptic weights in populations of synapses. Several theoretical studies have pointed out a central problem of Hebbian and spike-timing dependent plasticity: Strong synapses contribute more often to postsynaptic spiking and thus will get even more potentiated over time (Song et al., 2000; van Rossum et al., 2000; Sjostrom et al., 2008). This positive feedback mechanism would result in a bimodal distribution of synaptic weights, which is not what has been observed experimentally (van Rossum et al., 2000). Various homeostatic mechanisms have been postulated to prevent runaway excitation and to keep synapses in a state of dynamic equilibrium (Kepecs et al., 2002). Here we show that large spines with strong synapses contain specialized machinery for synaptic depression. Is it possible that the ER is actively moving into large spines? Dynamic movements of the ER in and out of spines have been demonstrated using sequential imaging (Toresson and Grant, 2005). Overexpression of the postsynaptic adaptor proteins Shank and Homer leads to spine enlargement and also recruits ER and IP<sub>3</sub> receptors into spines (Sala et al., 2001; Sala et al., 2005). Thus, regulated ER motility could be the structural basis of a metaplasticity mechanism that allows strong synapses to become depressed in an activity-dependent way. In this context, it is interesting to note that in the intact animal, spines that are stable over days and weeks often contain a spine apparatus (Knott et al., 2006). Altered sensory experience, for example sensory deprivation, can lead to destabilization and removal of these stable spines (Holtmaat et al., 2006). The mechanism we describe here might be critical for the weakening and the eventual disappearance of initially stable synaptic connections.

In summary, we show that not only the outside shape of spines (Matsuzaki et al., 2001), but also their organelle content has to be considered to understand the relation between structure and function of synaptic connections. Differences in spine microanatomy, which have been noted already in the very first ultrastructural studies of synapses half a century ago (Gray, 1959b, 1959a), play a crucial role in determining the competence of individual synapses for long-term plasticity.

## SUPPLEMENTARY FIGURES



**Supplementary Figure A1. Properties of uncaging pulse**  
*(a)* To test for the strength of the uncaging laser beam, after the experiment, we directed a laser pulse to the center of the spine and monitored the amount of bleaching of the red fluorophore (Alexa Fluor 594). Scale bar: 1  $\mu$ m.  
*(b)* Fluorescence recovery after photobleaching (FRAP) of Alexa Fluor 594 in spine shown in (a).  
*(c)* Amount of Alexa Fluor 594 bleaching was similar in ER+ and ER- spines indicating identical stimulation strength.



## METHODS

### Slice preparation and plasmid construction

Organotypic hippocampal slices were prepared from Wistar rats at postnatal day 5 as described (Stoppini et al., 1991). After 3-5 days in vitro, cultures were transfected with synapsin-GFP-ER and synapsin-RFP (tdimer2, R. Y. Tsien), using a Helios Gene Gun (BioRad). GFP-ER was constructed by fusing EGFP to the ER targeting sequence of calreticulin and the ER retention sequence KDEL.



## **Two-photon imaging and uncaging**

Imaging experiments were performed between 1 and 2 weeks after transfection. We used a custom built two-photon imaging and uncaging setup based on an Olympus BX51WI microscope equipped with a LUMFL 60x 1.1 NA objective controlled by ScanImage (Pologruto et al., 2003). Two ultrafast IR lasers (Chameleon-Ultra, Coherent) controlled by Pockel's cells (350-80, Conoptics) were combined by polarizing optics (Thorlabs) for 2-photon imaging (930 nm for GFP / RFP imaging, 810 nm for Alexa Fluor 594 / Fluo5F imaging) and uncaging of MNI-glutamate (725 nm). Fluorescence was detected in epi- and transfluorescence modes using 4 photomultiplier tubes (R3896, Hamamatsu). To measure calcium signals, green and red fluorescence was collected during 250 Hz line scans across the spine head and parent dendrite (7-15 trials/ spine). Fluorescence changes were quantified as increases in green fluorescence from baseline normalized to the red fluorescence ( $\Delta G/R$ ). For each imaging trial, photomultiplier dark noise was measured before shutter opening and subtracted from the dataset. Fluorescence was monitored 640 ms before the stimulus and 640 ms after the stimulus.

Glutamate uncaging was achieved using a 0.5 ms laser pulse for experiments analyzing synaptic properties and a 1 ms pulse for experiments looking at synaptic depression. Mushroom-shaped spines well separated from neighboring spines were used for the experiments. Standard uncaging location was  $\sim 0.5 \mu\text{m}$  from the spine center, in direction away from the parent dendrite. These uncaging parameters minimized the possibility of activation of dendritic channels. Laser intensity was  $\sim 50 \text{ mW}$  for 0.5 ms pulses and  $\sim 40 \text{ mW}$  for 1.0 ms pulses, measured in the back focal plane of the objective. The same laser pulse, if directed to the center of the spine, bleached 30% of the Alexa Fluor 594 fluorescence. We used this control to ensure equal stimulation strength for ER+ and ER-spines.

## **Analysis of calcium transients**

We wrote analysis software in MATLAB to extract amplitude and decay time constant of NMDA-R mediated calcium signals by fitting the difference of two exponentials to the average fluorescence transient ( $\Delta G/R$ ) for each spine. Traces with non-monotonous

fluorescence decay (i.e. delayed calcium transients) were excluded from the average. A delayed calcium transient was defined as a response with a second peak larger than 10 times the standard deviation of the baseline. Calcium signal delay was defined as the difference between the peak of the fluorescence transient and the onset of stimulation.

### **Spine volume measurements**

To determine absolute spine volume, we measured the integrated fluorescence intensity of the spine in the red channel, which is proportional to its cytoplasmic volume (Svoboda, 2004; Zhang et al., 2008). For each cell, a calibration measurement was taken by focusing the laser into the proximal apical dendrite, a cellular compartment large enough to contain the entire point-spread function (PSF) of our microscope, to get the maximum fluorescence intensity ( $f_{\max}$ ). The volume of the PFS ( $V_{\text{PSF}} = 0.30 \mu\text{m}^3$ ) was determined using fluorescent beads ( $0.1 \mu\text{m}$ , Molecular Probes).

### **Measurement of diffusional coupling**

Fluorescence Recovery after Photobleaching (FRAP) experiments were performed on spines of transfected cells. A brief laser pulse was used to bleach ~30% of RFP (5 trials per spine). Fluorescence recovery was fit by a single exponential function. The average recovery time constant for each spine was taken as a measure of diffusional coupling between spine and parent dendrite.

### **Electrophysiology**

Slice cultures were superfused with artificial cerebrospinal fluid (ACSF) at 30-32° C containing (in mM): 127 NaCl, 25 NaHCO<sub>3</sub>, 25 D-glucose, 2.5 KCl, 1 MgCl<sub>2</sub>, 2 CaCl<sub>2</sub>, 1.25 NaH<sub>2</sub>PO<sub>4</sub>, 0.05 chloroadenosine, 0.01 serine. For uncaging experiments, 5 MNI-Glutamate (Tocris) was added to the ACSF. For plasticity experiments, serine was replaced by 0.01 dCPP in the ACSF. To block mGluR1 and mGluR5 receptors, we added LY367385 (0.1) and MPEP (0.01). Whole-cell recordings were made with an Axopatch 200B amplifier (Axon Instruments), using 4-6 M $\Omega$  electrodes filled with (in mM): 135 K-gluconate, 10 HEPES, 10 sodium phosphocreatine, 3 sodium ascorbate, 4 MgCl<sub>2</sub>, 4 Na<sub>2</sub>-ATP, 0.4 Na-GTP and 0.015 Alexa Fluor 594 (pH 7.2). For calcium imaging

experiments, 0.3 Fluo5F (Molecular Probes) was added. Calcium imaging experiments were performed under current clamp conditions, measurements of postsynaptic currents in voltage clamp. uEPSC peak amplitude was extracted by fitting the difference of two exponentials to the average electrical response for each spine (5 trials / spine). To allow for dye and drug diffusion, we started the stimulation 15-20 min after break-in.

### **Induction of synaptic depression at single spines**

We attempted to mimic a conventional low frequency LTD stimulation protocol (15 min, 1 Hz, 900 pulses). Since in contrast to the reliable uncaging stimulus, the average release probability of Schaffer collateral synapses is only  $\sim 0.2$ , we used a 5 times lower frequency for the low frequency uncaging stimulation (LFU: 15 min, 0.2 Hz, 180 pulses). To optimize signal to noise ratio of the electrical recording only spines with an average uEPSC  $> 7$  pA were selected for the experiment. To quantify synaptic response amplitude, spines were stimulated before and after LFU with 5 test pulses spaced 30 s apart. To quantify depression, the average response after LFU was divided by the average response before LFU. For long term recordings after LFU, spines were stimulated with test pulses at 0.03 Hz. Cells were held in voltage clamp at -65 mV.

### **Immunohistochemistry**

Transfected cells were imaged and subsequently patched with an intracellular solution containing neurobiotin (1mg/ ml). Slices were then fixed in 4% paraformaldehyde and incubated with PBS containing 0.3% Triton X-100, 10  $\mu$ g/ml Alexa Fluor 594 conjugated streptavidin, 4% horse serum for 3h at room temperature (RT). The fixed slices were incubated in blocking solution (20% horse serum in PBS) at RT for 4 h and then incubated with anti-Synaptopodin antibody (1:2000, Sigma-Aldrich) in PBS overnight at 4°C. Next, the slices were incubated in Alexa Fluor 488 goat anti-rat secondary antibody (1:200, Invitrogen) for 3 h at RT. The stained slices were mounted in Aquatex media (Merck) and imaged using a two-photon laser-scanning microscope tuned to 780 nm.

**Statistical analysis**

Data are reported as mean  $\pm$  SEM. To test for significance we used the Mann-Whitney rank sum test (unpaired data) or the Wilcoxon signed-rank test (paired data).



## **Part 4.B:**

### **Spine neck plasticity controls postsynaptic calcium signals through electrical compartmentalization**

**Åsa Grunditz<sup>\*</sup>, Niklaus Holbro<sup>\*</sup>, Lei Tian, Yi Zuo, Thomas G. Oertner**

**\*contributed equally**

*Journal of Neuroscience, in press*

#### **ABSTRACT**

Dendritic spines have been proposed to function as electrical compartments for the active processing of local synaptic signals. However, estimates of the resistance between the spine head and the parent dendrite suggest that compartmentalization is not tight enough to electrically de-couple the synapse. Here we show in acute hippocampal slices that spine compartmentalization is initially very weak, but increases dramatically upon postsynaptic depolarization. Using NMDA receptors as voltage sensors, we provide evidence that spine necks not only regulate diffusional coupling between spines and dendrites, but also control local depolarization of the spine head. In spines with high resistance necks, presynaptic activity alone was sufficient to trigger calcium influx through NMDA receptors and R-type calcium channels. We conclude that calcium influx into spines, a key trigger for synaptic plasticity, is dynamically regulated by spine neck plasticity through a process of electrical compartmentalization.

## INTRODUCTION

In hippocampal pyramidal cells, the induction of synaptic long-term plasticity is associated with changes in shape and size of dendritic spines (Toni et al., 1999; Matsuzaki et al., 2004; Zhou et al., 2004; Harvey and Svoboda, 2007). How spine morphology affects synaptic function, on the other hand, is less clear. The narrow necks of mushroom-shaped spines form diffusional barriers that slow down the exchange of second messengers between spine heads and dendrites (Muller and Connor, 1991). As a consequence of the partial biochemical isolation of synapses on neighboring spines, changes in synaptic strength can be induced with single-synapse specificity (Matsuzaki et al., 2004; Harvey and Svoboda, 2007; Zhang et al., 2008). A second potential function of dendritic spines is more controversial: Since spines are equipped with different types of voltage-gated channels (Bloodgood and Sabatini, 2007b), they could in principle serve as active electrical amplifiers (Segev and Rall, 1988). According to this theory, active spines could locally boost synaptic currents at minimal metabolic cost, providing a substrate for information storage as well as information processing (Koch and Poggio, 1985; Koch, 1999). Whether or not electrical amplification plays a role in synaptic transmission depends critically on the amplitude of the excitatory postsynaptic potential (EPSP) inside the spine (Koch and Zador, 1993). Unfortunately, it is not yet possible to measure spine EPSPs or the electrical resistance of individual spine necks directly. What can be assessed in live neurons is the diffusional coupling between spine head and dendrite, using photoactivation or fluorescence recovery after photobleaching (FRAP). Diffusion time constants can in principle be used to estimate spine neck resistance, since current propagation in neurons is mediated by electrodiffusion. Estimates from different preparations, however, did not reach agreement about the typical resistance of a spine neck (Harris and Stevens, 1989; Svoboda et al., 1996; Bloodgood and Sabatini, 2005). In brain slice cultures, it has been demonstrated that spine neck properties change dynamically, dependent on the level of activity (Bloodgood and Sabatini, 2005). This is an alarming finding, since the level of spontaneous activity in the most popular model system for synaptic physiology, the acute brain slice, is very low. Low spontaneous activity provides a conveniently quiet baseline for electrophysiological studies, but might have unexpected effects on synaptic function.

In this study, we revisit the question of electrical compartmentalization using two-photon calcium imaging of synaptically triggered calcium transients (CaTs) in spines. The strong voltage dependence and high calcium permeability of synaptic NMDA receptors (NMDARs) provided us with a natural sensor for spine head depolarization during the EPSP. However, the relationship between calcium current and depolarization is not linear, and in addition, depolarizing currents through NMDARs and other voltage-dependent channels provide positive feedback. To estimate spine head depolarization from the amplitude of synaptically evoked CaTs, we therefore simulated the interplay of different ion channels using an active compartmental model of a CA1 pyramidal cell. We show that the spine neck resistance tightly controls NMDAR unblocking and spine calcium transients, but has little effect on the amplitude of somatic EPSPs. This might explain how the dramatic neck resistance changes we demonstrate here could go unnoticed in many years of electrophysiological experiments.

## RESULTS

Prompted by a study reporting changes in spine neck resistance after pharmacological modulation of activity (Bloodgood and Sabatini, 2005), we set out to test whether depolarization of a single cell affects the diffusional coupling between its spines and dendrites. To measure FRAP time constants ( $\tau_{\text{FRAP}}$ ) of individual spines, we filled CA1 pyramidal cells with Alexa Fluor 594 (**Fig. B1a**) and bleached spine heads on oblique dendrites by two-photon excitation at 810 nm. To our surprise, shortly after a 4 min depolarizing pulse to 0 mV,  $\tau_{\text{FRAP}}$  was increased by a factor of 10, on average (**Fig. B1b, c**). The increase in  $\tau_{\text{FRAP}}$  built up gradually during the depolarizing pulse, as shorter pulses induced smaller changes. The diffusional coupling also changed in response to bursts of backpropagating action potentials. A theta-burst protocol (three trains (0.1 Hz) of ten bursts (5 Hz) of five bAPs at 100 Hz) induced a 5.4-fold increase, on average (before stimulation: median  $\tau_{\text{FRAP}}$  = 30 ms, range, 8-130 ms; after theta-burst: median  $\tau_{\text{FRAP}}$  = 162 ms, range, 82-475 ms,  $n = 16$ ). To exclude possible damage to the spine by the first bleach pulse, we also compared spines on step-depolarized and unstimulated cells in the same slice (**Fig. B1d**). The difference in  $\tau_{\text{FRAP}}$  between the two groups was



12-fold, indicating that the changes were not induced by spine photodamage during the bleaching pulse (before depolarization: median  $\tau_{\text{FRAP}}$  = 43 ms, range, 16-159 ms,  $n$  = 23; 5-10 min after depolarization: median  $\tau_{\text{FRAP}}$  = 524 ms, range, 177-778 ms,  $n$  = 22). One hour after step depolarization, spine neck resistances were still significantly increased (median  $\tau_{\text{FRAP}}$  = 500 ms, range, 250-650,  $n$  = 7). Switching to nominally  $\text{Ca}^{2+}$ -free saline prior to depolarization completely prevented the increase in  $\tau_{\text{FRAP}}$ , indicating that  $\text{Ca}^{2+}$  influx during the step depolarization triggered the change in diffusional coupling (Fig. B1d). The time a dye molecule stays inside a spine depends on spine neck diameter and length, but also on the volume of the spine head (Bloodgood and Sabatini, 2005; Biess et al., 2007). However, we did not detect significant changes in spine head volume after step depolarization (Fig. B1e). Therefore, rapid calcium-induced remodeling of the spine neck seems to be responsible for the dramatic changes in diffusional coupling.

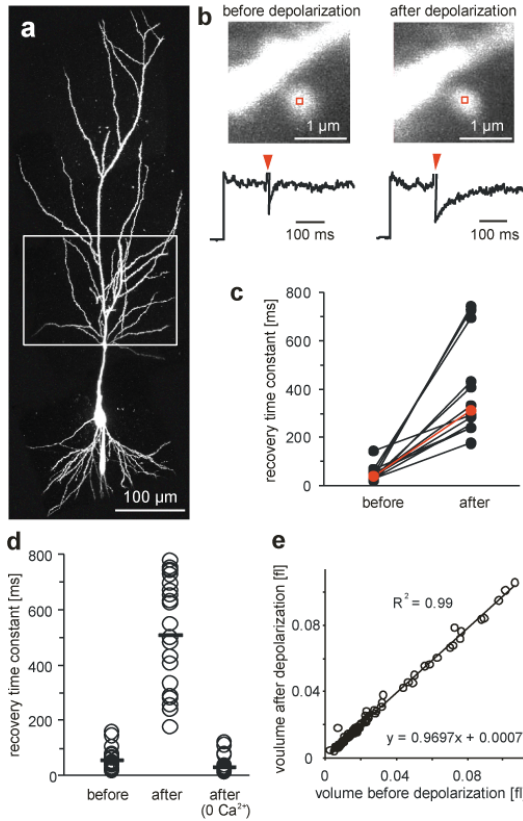


**Figure B1. Postsynaptic depolarization reduces diffusional coupling between spine head and dendrite.**

(a) CA1 pyramidal cell filled with Alexa Fluor 594 through a somatic patch pipette. Box indicates oblique dendrites used for FRAP experiments.

(b) Example of a repeated FRAP experiment before and after a 4 min step depolarization to 0 mV. Line scans across the spine head were used to measure fluorescence recovery. Red arrow heads indicate time of bleaching.

(c) In individual spines,  $\tau_{\text{FRAP}}$  increased by a factor of 10, on average. The median value of  $\tau_{\text{FRAP}}$  increased by a factor of 7.8 (before depolarization: median  $\tau_{\text{FRAP}}$  = 40 ms, range, 22-146 ms; after depol: median  $\tau_{\text{FRAP}}$  = 312 ms, range, 177-743 ms,  $n$  = 12).

(d) Group comparison of  $\tau_{\text{FRAP}}$  of CA1 spines in naïve slices (median  $\tau_{\text{FRAP}}$  = 43 ms, range, 16-159 ms,  $n$  = 23), after step depolarization (median  $\tau_{\text{FRAP}}$  = 524 ms, range, 177-778 ms,  $n$  = 22), and after step depolarization in nominally  $\text{Ca}^{2+}$ -free saline (median  $\tau_{\text{FRAP}}$  = 29 ms, range, 14-120 ms,  $n$  = 15).

(e) Step depolarization did not induce changes in spine head volume.

After step depolarization,  $\tau_{\text{FRAP}}$  in individual spines ranged from 177 to 778 ms (**Fig. B1d**). We wanted to test whether the corresponding variability in the electrical resistance of the spine necks had measurable effects on spine head depolarization during the EPSP. To measure spine head depolarization, we made use of the fact that postsynaptic NMDA receptors (NMDARs) are blocked by  $\text{Mg}^{2+}$  ions in a strongly voltage-dependent fashion (Jahr and Stevens, 1990). NMDARs are highly permeable for  $\text{Ca}^{2+}$  and we could monitor NMDAR activation in individual spines by two-photon calcium imaging (**Fig. B2a, Supplementary Fig. B1**). However, there is no simple relation between spine depolarization and spine calcium levels: Number and subunit composition of NMDARs, as well as spine head volume, are heterogeneous, leading to differences in absolute calcium concentrations in individual spines even for identical EPSP amplitudes (Sobczyk et al., 2005). We developed an experimental protocol to compensate for this variability: Synaptically evoked  $\text{Ca}^{2+}$  transients (CaTs) were measured under two conditions: Depolarized to the synaptic reversal potential in voltage clamp (here denoted as ‘0 mV’) and free running (current clamp, denoted as ‘CC’) (**Fig. B2b**). The ratio between the calcium signal amplitude in CC and at 0 mV we call the fractional  $\text{Ca}^{2+}$  transient (fCaT). The stronger the spine depolarizes during the EPSP, the larger the fCaT will be. In control experiments at 0 mV, we verified that calcium influx was indeed mediated by NMDARs (97% block of CaTs by 10  $\mu\text{M}$  dCPP,  $n = 3$ , data not shown). In a sample of 33 synaptically stimulated spines, the amplitude of fCaTs ranged from 0.02 – 0.51, pointing to large differences in spine head depolarization. These differences were not reflected by the somatic EPSP ( $R^2 = 0.12$ ,  $n = 21$ , **Supplementary Fig. B2**). Since we used extracellular stimulation and typically activated more than one synaptic connection, the compound EPSP could not be used as a reporter of depolarization of the spine under scrutiny. If spine depolarization were controlled by the spine neck, we would expect the spines with the largest fCaTs to have the highest neck resistances and the longest diffusion time constants. As a measure of spine neck diffusional resistance, we used the decay time constant of the calcium signal at 0 mV ( $\tau_{\text{decay}}$ , **Fig. B2b**). This measure was highly correlated to the FRAP time constant (**Fig. 2C**) and was used as a proxy to avoid the additional photodamage caused by FRAP experiments. Indeed, we found a positive correlation between spine head depolarization and diffusional resistance ( $R^2 = 0.42$ , **Fig.**

**B2d**). Spines with fast time constants generated small fCaTs, indicating weak depolarization of the spine head. As discussed in the previous section, diffusion time constants depend both on the geometry of the spine neck and on the volume of the spine head. Spine volumes, however, were not different in fast and slow spines (**Supplementary Fig. B2**). Together, these findings point to the spine neck as the main variable controlling diffusion speed and electrical coupling of spines.

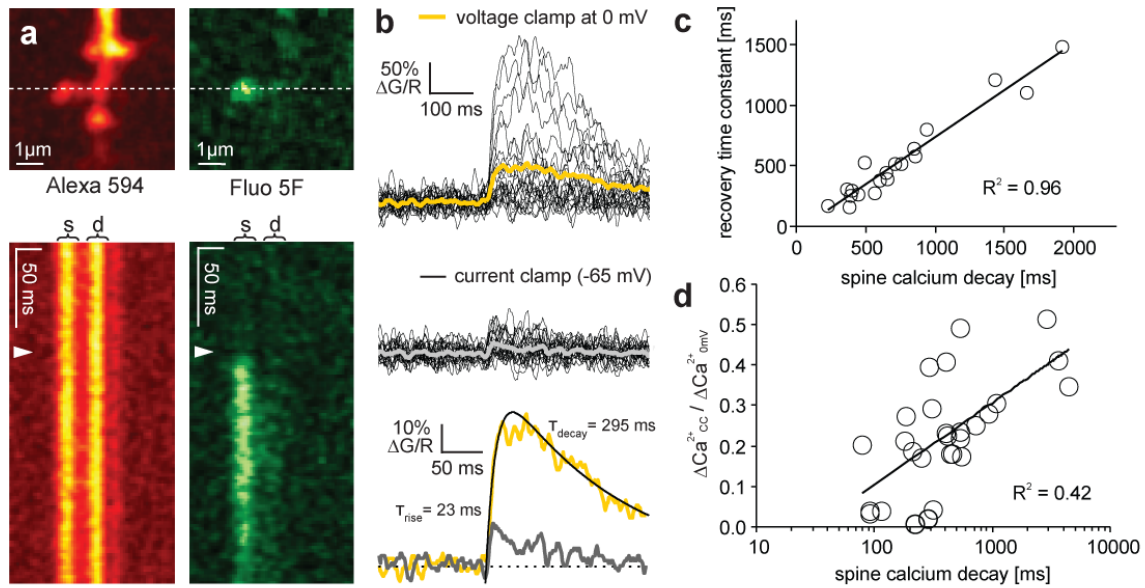


**Figure B2. Spine neck resistance controls NMDA receptor activation during the EPSP.**

(a) Synaptically evoked spine calcium transients. For ratio measurements, cells were filled with a green calcium-sensitive dye (fluo-5F) and a red dye (Alexa-Fluor 594). Calcium signals were measured in line-scan mode.

(b) Synaptically evoked calcium transients were measured first under depolarized conditions (voltage clamp at synaptic reversal potential, yellow trace), then in current clamp (black trace).  $\tau_{decay}$  was extracted by fitting the difference of 2 exponentials to the average response under depolarized conditions (yellow trace).

(c) Decay time constant of the calcium transient at the synaptic reversal potential was correlated with FRAP recovery time constant, indicating diffusion of calcium-bound dye molecules through the spine neck.

(d) Fractional calcium transient amplitude was correlated with spine neck properties (decay time constant of the calcium transient at the synaptic reversal potential). Coefficient of determination  $R^2 = 0.42$ ,  $p < 0.01$  (two-tailed test),  $n = 28$  spines.

Next, we tested the electrical interactions between different channels pharmacologically. For these experiments, we used synaptically stimulated spines that were identified under depolarized conditions and, in addition, produced sizable CaTs in current clamp. Spines that did not show CaTs in current clamp (Ca<sup>2+</sup>-silent spines, see **Fig. B2d**) were not further investigated. As expected, blocking NMDARs strongly reduced the spine CaTs in

current clamp to 9% of the control amplitude (**Fig. B3a**). Blocking AMPARs also had a very strong effect on CaTs, reducing them to 16% of the control amplitude, on average. Clearly, AMPAR-mediated depolarization was needed to enable NMDAR-mediated  $\text{Ca}^{2+}$  influx. Voltage-gated  $\text{Ca}^{2+}$  channels of the R-type have been identified as the main spine  $\text{Ca}^{2+}$  source triggered by back-propagating action potentials (Yasuda et al., 2003). We found that blocking R-type channels by SNX-482 reduced CaTs to 44% (**Fig. B3b**), indicating that EPSP amplitude in most spines was sufficiently high to open these high-voltage activated channels. SNX-482 application did not affect the probability of observing CaTs ( $p_{\text{CaT}}$ ) after presynaptic stimulation (control:  $p_{\text{CaT}} = 0.45 \pm 0.19$ ; SNX:  $p_{\text{CaT}} = 0.45 \pm 0.21$ ,  $n = x$ ), indicating that R-type channels are not involved in the regulation of glutamate release at these synapses. Another commonly used R-type antagonist,  $\text{Ni}^{2+}$  ions at low concentration, did affect  $p_{\text{CaT}}$  in some experiments. Therefore, we did not use wash-in of  $\text{Ni}^{2+}$ , but compared fCaT amplitudes of spines recorded in ACSF containing  $10 \mu\text{M}$   $\text{Ni}^{2+}$  to fCaTs recorded in standard solution. The group comparison indicated that  $\text{Ni}^{2+}$  reduced the amplitude of CaTs to 58% of control (**Fig. B3d**). Compared to wash-in of SNX-482, this was a slightly weaker effect, but  $10 \mu\text{M}$   $\text{Ni}^{2+}$  is a sub-saturating concentration for R-type channel block (Foehring et al., 2000). We used the same group comparison strategy to test for the activation of fast  $\text{Na}^+$  channels during the EPSP. Blocking  $\text{Na}^+$  channels in the postsynaptic cell by intracellular loading with QX-314 did not lead to significant suppression of spine  $\text{Ca}^{2+}$  signals (**Fig. B3d**). Sodium channels are known to be present in spines on basal dendrites of mouse neocortical pyramidal cells (Araya et al., 2007), but are either absent or were not activated during the EPSP in the spines we investigated. In summary, we concluded that at least three types of channels contributed to the depolarization of the spine head: AMPARs, NMDARs, and R-type calcium channels.

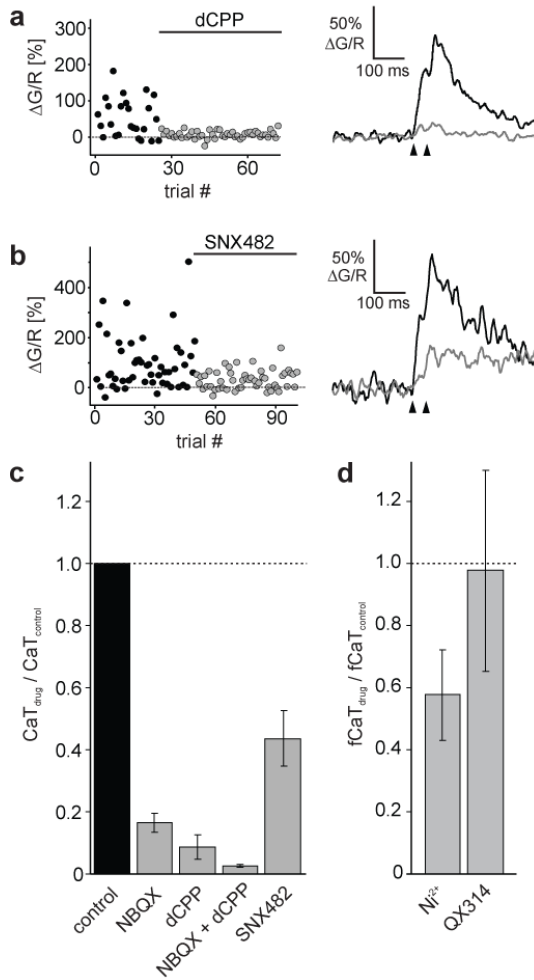


**Figure B3. Pharmacology of synaptically evoked spine calcium transients.**

(a) Example of NMDAR blocking experiment using dCPP (10  $\mu$ M). Paired pulse stimulation was used to increase release probability.

(b) Example of R-type calcium channel blocking experiment using SNX-482 (0.1  $\mu$ M).

(c) Summary of bath application experiments. The calcium transient amplitudes were normalized to the responses in current clamp before drug application. NBQX (10  $\mu$ M),  $0.166 \pm 0.029$ ,  $n = 6$ ; dCPP (10  $\mu$ M),  $0.087 \pm 0.040$ ,  $n = 3$ ; NBQX+dCPP,  $0.025 \pm 0.003$ ,  $n = 2$ ; SNX-482 (0.1  $\mu$ M),  $0.437 \pm 0.089$ ,  $n = 4$  (mean  $\pm$  SEM).

(d) To compensate for potential presynaptic effects of  $Ni^{2+}$ , we recorded trials at 0 mV and in current clamp in  $Ni^{2+}$  (10  $\mu$ M), calculated the fCaT and compared it to the average fCaT in standard ACSF ( $0.576 \pm 0.145$ ,  $n = 6$ ). The same strategy was used for the intracellular  $Na^+$  channel blocker QX-314 (5 mM,  $0.976 \pm 0.324$ ,  $n = 4$ ).

In current clamp experiments, blocking a single type of channel will affect depolarization and thus change the amplitude of all other currents. The best way to dissect the relative contributions of different channels to spine depolarization and spine calcium is biophysical modeling. We used the NEURON simulation environment to set up a model spine equipped with AMPA, NMDA and R-type channels and connected it to the oblique dendrite of a passive CA1 pyramidal cell model (Hines and Carnevale, 1997; Golding et al., 2001) (**Fig. B4b**). The voltage-dependent blocking function of synaptic NMDARs was experimentally determined (**Supplementary Fig. B1**) and implemented in the NEURON mechanism. Channel densities and spine neck resistance ( $R_{neck}$ ) were adjusted to reproduce the relative amplitude of fluorescence transients measured in our pharmacological experiments (**Fig. B4a**, **Supplementary Fig. B3**, and **Supplementary Table B1**). The strong effect of AMPA receptor block on calcium signal amplitude was

only reproduced in simulations with  $R_{\text{neck}} > 1 \text{ G}\Omega$ . We were pleased to see that not only the amplitude, but also the time course of the calcium transients under various pharmacological conditions was faithfully reproduced in our simulated spine (**Fig. B4c**), indicating that the simple model captured the essential mechanism of spine calcium transient generation. From the simulation, we could extract the individual currents (**Fig. B4d**) and the typical EPSP in the spine head (**Fig. B4e**), which had an amplitude of 55 mV and lasted ~10 ms (full width at half maximum). Depolarization was actively amplified and prolonged by the joint activation of NMDARs and R-type calcium channels. At the soma, the EPSP was attenuated to ~1 mV (**Fig. B4e, insert, Supplementary Table B2**).

In a second set of simulations, we run the same model with a 10-fold lower spine neck resistance ( $R_n = 120 \text{ M}\Omega$ ), to simulate spine neck properties before step depolarization (see **Fig. B1**). The EPSP in the spine decreased by ~20 % in peak amplitude and was also much briefer (**Fig. B4e, dotted line**). As a consequence, only a small fraction of NMDAR became unblocked and no R-type channels were activated in the 120 M $\Omega$  spine, leading to a 82% reduction in the simulated CaT (**Fig. B4f, dotted line**). Expressed as fractional calcium transient, the simulated 120 M $\Omega$  spine produced in current clamp only 4.5% of its maximum calcium signal at 0 mV and would have been classified as a ‘Ca<sup>2+</sup> silent’ spine in our imaging experiments (see **Fig. B2d**). In summary, our simulation suggested that an increase in spine neck resistance from 120 M $\Omega$  to 1.2 G $\Omega$  would lead to a slight reduction (~20%) of somatic EPSP amplitude (**Fig. B4e, insert**), but would strongly enhance voltage-gated calcium influx into the spine head, boosting spine calcium transients by a factor of 5.6.

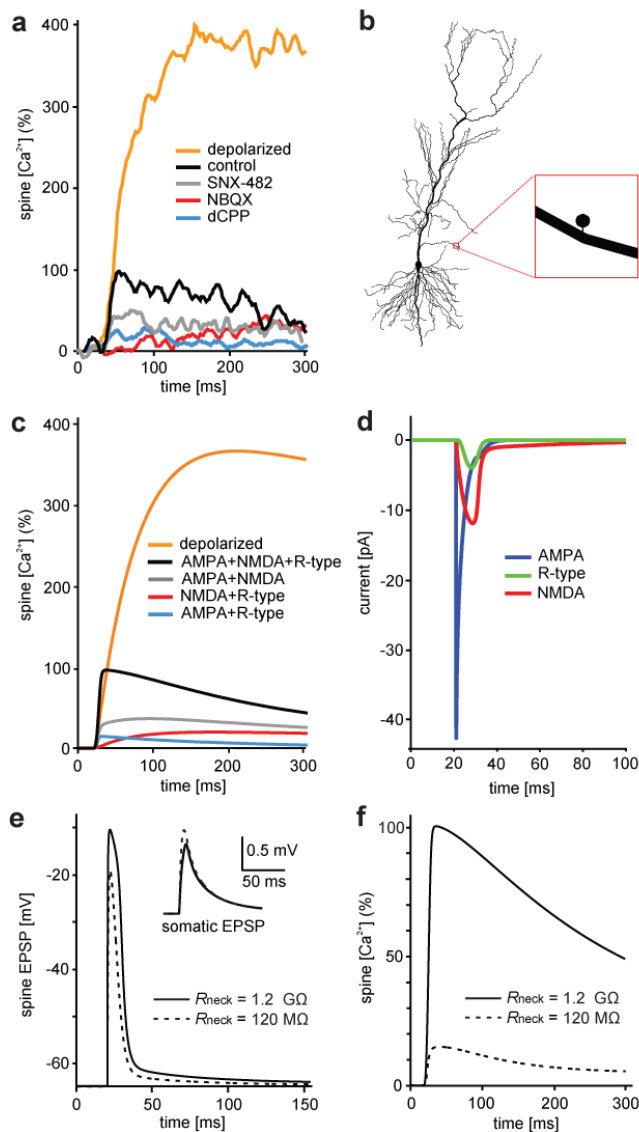


**Figure B4. Assessing the functional impact of spine neck resistance by compartmental modeling.**

(a) Experimental data: Pharmacological block of R-type calcium channels (gray curve), AMPA receptors (red curve), or NMDA receptors (blue curve) partially blocked spine calcium signals. Traces from three different experiments (average of 40-54 responses each) were normalized to the control response in current clamp (100%; black trace). For comparison, the average response in voltage clamp (0 mV) is also shown (yellow trace).

(b) NEURON model: Single spine attached to oblique dendrite of CA1 pyramidal cell.

(c) Model simulation with  $R_{neck} = 1.2 \text{ G}\Omega$  reproduced amplitude and time course of the fluorescence transients under all conditions tested.

(d) The model reveals the sequence of currents during the EPSP: NMDA and R-type currents lead to a substantial prolongation of the depolarization.

(e) EPSP in the spine head reached 55 mV in amplitude and lasted ~10 ms, while somatic depolarization was only ~1 mV (insert). With  $R_{neck} = 120 \text{ M}\Omega$ , spine EPSP was smaller and shorter while somatic EPSP was slightly larger (dashed lines).

(f) With  $R_{neck} = 120 \text{ M}\Omega$ , CaT was reduced to 18% (dashed line).

We tested the predictions of our model by measuring EPSPs in CA1 cells evoked by Schaffer collateral stimulation (**Fig. B5a**). The same step depolarization protocol that induced 10-12 fold changes in spine neck resistance had no consistent effect on the EPSP amplitude measured at the soma. This was no surprise given the large body of literature about pairing protocols: Postsynaptic depolarization of CA1 pyramidal cells alone has not been reported to induce lasting changes in EPSP amplitude. Thus, spine neck resistance controls local postsynaptic signaling independent of electrical signaling to the soma.



Our spine model suggested that even in a spine with  $R_n = 1.2 \text{ G}\Omega$ , synaptic activation will not trigger runaway depolarization, i.e. activation of *all* voltage-gated channels. Increasing the AMPAR current, however, could lead to such a ‘spine spike’ (**Supplementary Fig. B3**). Cyclothiazide is known to increase both amplitude and duration of synaptic AMPA currents. Using the  $1.2 \text{ G}\Omega$  spine model and published measurements of cyclothiazide modulation of AMPA currents (Rammes et al., 1996), we predicted a 4.1 fold increase of CaT amplitude. When we applied cyclothiazide ( $40 \mu\text{M}$ ) during synaptic stimulation in current clamp, we indeed observed a dramatic increase in the amplitude of spine calcium signals (**Fig. B5b**). In several spines, calcium transients under cyclothiazide reached or even exceeded the amplitude of transients recorded at the reversal potential, possibly due to the generation of calcium spikes in the spine head. On average, CaT amplitude increased by a factor of 4.2 (**Fig. B5b**). These experiments also suggest that additional dendritic depolarization, e.g. by coincident backpropagating APs or by simultaneously active neighboring synapses, would strongly boost spine depolarization. The previously reported linear summation of uncaging-evoked potentials on spines (Araya et al., 2006a) can be explained by such an active amplification process (**Supplementary Fig. B3**). A third insight from the model was that in low neck resistance spines, EPSPs in the spine head are relatively brief (**Fig. B4e**). In such spines, AMPAR block should have a weaker effect on postsynaptic calcium transients, since much of the calcium influx is due to the ‘leakiness’ of the NMDA receptor at the resting potential. To test this prediction, we sorted our AMPAR block experiments into two groups: Spine that had a fast decaying calcium signal ( $\tau_{\text{decay}} < 1 \text{ s}$ ) at  $0 \text{ mV}$ , indicating low resistance necks, and spines with  $\tau_{\text{decay}} > 1 \text{ s}$ . In diffusionally isolated spines ( $\tau_{\text{decay}} > 1 \text{ s}$ ), AMPAR block reduced the calcium signal to 8% of the control amplitude, on average, indicating that 92% of the control calcium transient was dependent on AMPAR-mediated depolarization (**Fig. B5c**). In spines with faster decay of the calcium signal, AMPAR block reduced the calcium signal to 43% of the control amplitude, on average, indicating that 57% of the original calcium signal amplitude was due to AMPAR activity. The remaining  $\text{Ca}^{2+}$  influx after AMPAR block was abolished after wash-in of dCPP, consistent with a leak current through NMDARs (**Fig. B5c**).



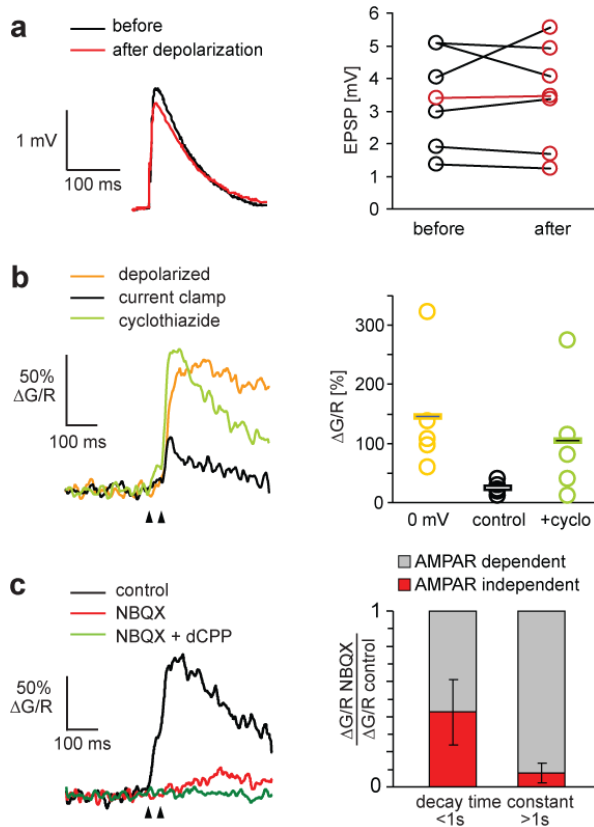


**Figure B5. Testing predictions of the model.**

(a) As predicted by the model, EPSP amplitude at the soma was not significantly affected by step depolarization ( $n = 6$ ).

(b) Increasing AMPAR affinity by cyclothiazide ( $40 \mu\text{M}$ ) led to a dramatic boosting of the spine calcium signals in current clamp (green curve). Current clamp recordings were preceded by recordings at the reversal potential ( $0 \text{ mV}$ , yellow trace).

(c) AMPAR antagonist NBQX ( $10 \mu\text{M}$ ) reduced amplitude and changed the time course of spine calcium transients. Remaining calcium transient was NMDAR-dependent ( $10 \mu\text{M}$  dCPP). Traces are averages over all trials (failures and successes). Paired-pulse stimulation was used to increase the number of successful synaptic transmission events. Sorting NBQX experiments according to spine neck properties ( $n = 7$ ). Effect of AMPAR block on calcium transients was weaker in spines with low resistance necks ( $\tau$  decay  $< 1 \text{ s}$ , residual CaT:  $0.43 \pm 0.18$ ) than in spines with high resistance necks (residual CaT:  $0.08 \pm 0.05$ ).

Our calcium imaging experiments demonstrate the complex interactions between ligand- and voltage-gated channels in the spine head. However, all functional imaging was preceded by a depolarized period of at least 4 min, which, as we show in **Fig. B1**, alters spine neck properties. To find out how the results of our slice study would compare to the *in vivo* situation, we performed spine FRAP experiments through the thinned skull of a thy1-YFP mouse (**Fig. B6**). We found a large range of diffusional time constants (range,  $0.27 - 2.42 \text{ s}$ ; median,  $0.62 \text{ s}$ ). In acute cortical slices cut from the same transgenic line, we measured much faster time constants in layer I spines (range,  $0.01 - 0.54 \text{ s}$ ; median,  $0.23 \text{ s}$ ), suggesting lower spine neck resistances. Since the different imaging conditions *in vivo* and in slices could have introduced a selection bias, we also compared the fluorescence intensity of layer I spines relative to the parent dendrites *in vivo* and in perfusion fixed slices of thy1-YFP mice. Relative spine head intensity was  $1.05 \pm 0.04$  ( $n = 124$  spines) *in vivo* and  $1.07 \pm 0.06$  ( $n = 138$  spines) in perfusion fixed slices. Therefore, we can exclude a systematic bias towards larger spines as a reason for the longer time constants measured *in vivo*.

The activity-dependence of spine-dendrite coupling seems to be conserved in mouse neocortical and rat hippocampal pyramidal cells. For a quantitative comparison between YFP and Alexa FRAP experiments, we determined a conversion factor by filling YFP-expressing cells with Alexa Fluor 594 and measuring  $\tau_{\text{FRAP}}$  of both fluorophores simultaneously (conversion factor = 4.85). After this correction for fluorophore size, spine neck time constants were comparable in acute slices from rat hippocampus and from mouse cortex, indicating similar compartmentalization properties (**Fig. B6c**). Interestingly, the broad distribution of FRAP time constants we found *in vivo* partially overlapped with the distributions from both naïve and depolarized cells in acute slices. This indicates that a subset of spines *in vivo* is in a state of high neck resistance, possibly reflecting the history of synaptic activity.

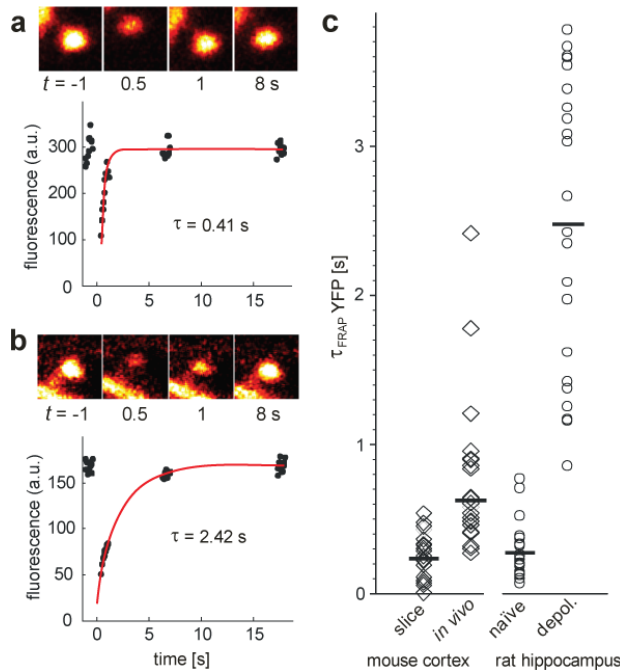


**Figure B6. In vivo FRAP experiments.**

(a) Bleaching of single spine in frame scan mode (13 Hz frame rate, 64x64 pixels). To extract the fluorescence time course and compensate for heart beat induced movements, a region of interest (ROI) of fixed size was manually centered on the spine head in every frame. Red line: Mono-exponential fit.

(b) Example of spine with high diffusional resistance. Note that visibility of spine neck can not be used to predict diffusional resistance.

(c) Recovery time constants of spines in neocortical slices (median  $\tau_{\text{FRAP}} = 0.23$  s, range, 0.01-0.54 s,  $n = 21$ ) and *in vivo* of thy1-YFPH mice (median  $\tau_{\text{FRAP}} = 0.62$  s, range, 0.27 -2.42 s,  $n = 24$  spines, 3 animals). To facilitate direct comparison with Alexa-FRAP experiments in acute rat hippocampal slices (naïve/depol.), we replotted the data from Fig. B1d scaled by the experimentally determined conversion factor 4.85.

## DISCUSSION

In this study, we show that the amplitude of postsynaptic calcium transients during the EPSP is correlated with the diffusional resistance of the spine neck. In addition, we

demonstrate dramatic changes in spine neck resistance following step depolarization of the postsynaptic cell. For the first time, we integrated the information gained from calcium imaging experiments under various pharmacological conditions in a quantitative biophysical model. The modeling study suggests that after postsynaptic depolarization, spine neck resistance typically exceeds 1 G $\Omega$ . Estimates of the Ohmic resistance of spine necks have been previously derived from diffusion measurements (Svoboda et al., 1996). However, these estimates depend critically on assumptions about specific resistivity ( $R_i$ ) and viscosity of the cytoplasm, parameters that are not well known and might even be different inside the thin spine neck and elsewhere in a cell. Here, we used a different approach, relying on voltage-gated calcium influx as a measure of spine head depolarization. In cells that were depolarized for several minutes, a large fraction of NMDARs became activated during the EPSP in the majority of spines (**Fig. B2d**). Compartmental modeling of depolarization and diffusion of Ca<sup>2+</sup>-bound dye pointed to surprisingly high EPSP amplitudes and electrical amplification in spines (**Fig. B4**).

We provide six lines of evidence for an electrical function of the spine neck. First, we show that spine head depolarization is strongest in spines that are well isolated from the dendrite (**Fig. B2d**). Second, calcium influx was localized to the spine head, and no fast rising calcium signals were seen in the parent dendrite (**Fig. B2a**). Since the dendrites of CA1 pyramidal cells are equipped with a variety of voltage-gated calcium channels (Magee et al., 1998; Bloodgood and Sabatini, 2007b), the strict localization of the calcium signal can only be explained by a steep voltage drop along the spine neck. Third, in addition to NMDARs, we could detect the activation of high-threshold voltage-gated calcium channels the spine head during the EPSP (**Fig. B3**). Forth, we directly measured the voltage-dependence of synaptic NMDARs following the calcium imaging strategy pioneered by (Kovalchuk et al., 2000). In these experiments, we blocked K<sup>+</sup> channels and AMPARs to improve voltage clamp (**Supplementary Fig. B1**). The steep voltage dependence we found indicated that significant unblocking of synaptic NMDARs requires a strong and long-lasting depolarization of the spine head (**Fig. B4e**). Experiments with AMPA receptor antagonists provided a fifth line of evidence for the electrical function of spine necks: NBQX blocked spine calcium transients more

effectively in spines with high resistance necks (**Fig. B5c**). This is consistent with the idea that spines with a low neck resistance cannot efficiently unblock their NMDARs. In these spines, a large fraction of the calcium influx during the EPSP is due to the imperfect  $Mg^{2+}$  block of NMDARs at rest and is thus less affected by AMPAR block. Finally, the long diffusion time constants we measured after step depolarization are consistent with an electrical neck resistance of  $1.2\text{ G}\Omega$ , on average.

Individual Schaffer collateral synapses have been documented to produce up to 40 pA of current (Conti and Lisman, 2003), but the number of active AMPARs in our model spine (Supplemental Table 1) is still higher than most previous estimates (Matsuzaki et al., 2001; Nimchinsky et al., 2004). When we tuned our model, we used only data from spines that *did* produce sizable calcium transients in current clamp. The ‘ $Ca^{2+}$  silent’ spines that we also frequently encountered in our calcium imaging experiments (**Fig. B2d**) are likely to have fewer AMPARs. Furthermore, an important difference between our experimental measurements and our single spine model is the frequent stimulation of additional synapses outside the field of view of our imaging experiments, reflected in somatic EPSPs of 4.7 mV, on average (**Supplementary Fig. B2**). Simultaneous activation of multiple synapses leads to local dendritic depolarization, which in turn reduces the number of AMPARs per spine head needed to explain our experimental results. A dendritic EPSP of 10 mV generated by other stimulated synapses, for example, reduced the number of AMPARs needed to generate sufficient depolarization in the spine of interest by a factor of 3. Thus, the absolute number of AMPARs in the spine head can not be derived from our experiments which were not performed under conditions of minimal stimulation. The interaction of multiple inputs we have only started to explore (**Supplementary Fig. B3**), and it remains a challenge to design experiments to address the complex nonlinear effects resulting from the synchronous activation of multiple synapses (Schiller et al., 2000; Gasparini and Magee, 2006).

In terms of ion channel types, our spine model is intentionally minimalist. Reality is likely to be both more complex and more diverse, with other types of voltage-gated channels contributing to the EPSP in many spines. To aid further refinement of the model

as more information becomes available, we have deposited it in the NEURON database. In its current form, the model allowed us to explore functional consequences of the fast and dramatic changes in spine neck resistance we observed experimentally after postsynaptic depolarization (**Fig. B1**). We show that spine neck resistance controls calcium influx at the spine head, but has little effect on somatic EPSPs, which might explain why this form of structural plasticity has been overlooked for many years.

Understanding the functional impact of activity-induced changes in spine neck resistance might help to resolve several long-standing controversies in the field of synaptic physiology. First, the voltage-dependence of postsynaptic calcium signals has been tested in several studies by AMPAR blocking experiments, abolishing the fast component of the EPSP. However, while some laboratories reported a weak effect of AMPAR block on postsynaptic calcium signals (Koester and Sakmann, 1998; Kovalchuk et al., 2000), others studies demonstrated nearly complete block of calcium transients after AMPAR block (Emptage et al., 1999; Yuste et al., 1999; Nevian and Sakmann, 2004). To understand this discrepancy, it is important to point out that in calcium imaging experiments using synaptic stimulation, the search for responsive spines is greatly facilitated by clamping the membrane potential of the postsynaptic cell to 0 mV (Yasuda et al., 2004). This procedure will, as we show here, dramatically alter spine neck properties. Thus, subtle differences in the experimental strategy used by different laboratories could have considerably altered the outcome of AMPAR blocking experiments (**Fig. B5c**) and thus changed the estimate of NMDAR conductance at the resting potential.

Second, very different diffusion time constants have been reported in different preparations, leading to a debate about the typical electrical resistance of the spine neck (Harris and Stevens, 1989; Svoboda et al., 1996; Majewska et al., 2000; Bloodgood and Sabatini, 2005). Here we show that in non-stimulated acute brain slices, diffusional coupling between spines and dendrites is significantly stronger than *in vivo* (**Fig. B6c**). Potential reasons are the formation of novel spines during the incubation period (Kirov et al., 1999) and the absence of spontaneous activity in acute slices. Furthermore, we

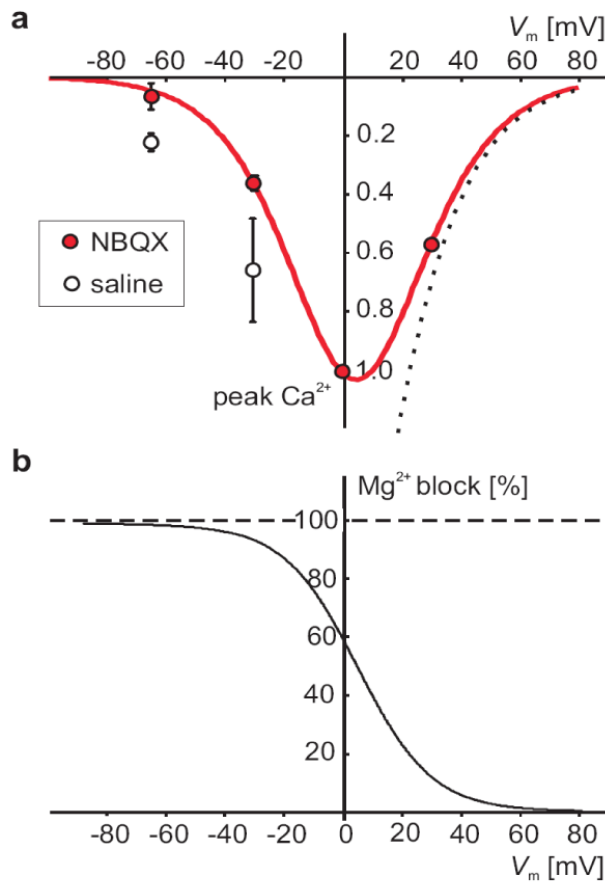
demonstrate the strong activity-dependence of spine neck resistance in acute slices (Fig. 1), consistent with previous reports from organotypic slice cultures (Bloodgood and Sabatini, 2005). From the broad range of spine neck time constants found *in vivo* (**Fig. B6c**), we conclude that EPSP amplitude and duration are likely to be highly variable between individual spines, although we studied only 2 examples from this broad spectrum in detailed simulations ( $R_{\text{neck}} = 120 \text{ M}\Omega$  and  $1.2 \text{ G}\Omega$ , **Fig. B4e**). Nevertheless, it became clear that the biophysical properties of spines reflect the history of neuronal activity and are thus expected to be different in different preparations.

Third, for the activation of multiple inputs on the same dendrite, different modes of integration have been reported: sublinear, linear, and supralinear (Polsky et al., 2004; Araya et al., 2006a; Gasparini and Magee, 2006; Sjostrom et al., 2008). Integration has been shown to depend on the activation of voltage-gated channels and NMDA receptors and is therefore an active process (Cash and Yuste, 1999; Carter et al., 2007). In simulations of two simultaneously active spine synapses, we could readily reproduce different integration modes just by changing the resistance of the spine necks (**Supplementary Fig. B3**). When we removed NMDARs and R-type channels from the model to simulate ‘passive’ spines, integration of neighboring inputs became sublinear (**Supplementary Fig. B3**). Apparently, dendritic integration of EPSPs depends on the gain of the spine amplifier, which is regulated by the electrical resistance of the spine neck. Taking into account the dynamic changes in spine neck resistance (**Fig. B1**), this suggests a novel mechanism by which local dendritic calcium spikes could change the dendritic integration mode in a branch-specific manner.

As a fourth point we would like to discuss the potential impact of spine compartmentalization on long-term potentiation (LTP). LTP is classically induced by pairing of presynaptic activity with postsynaptic depolarization. It has been noted, however, that pairing is only effective at the end of a long depolarizing pulse, but not at its beginning (Chen et al., 1999). This finding points to a slow,  $\text{Ca}^{2+}$ -dependent process in the postsynaptic neuron that is triggered by depolarization and enables functional plasticity. Other stimuli that induce high postsynaptic calcium levels, e.g. dendritic

calcium spikes, have also been shown to facilitate LTP induction (Kampa et al., 2006). Could spine neck changes be an essential first step in the process of LTP induction? The 10-fold change in diffusional resistance we report here leads to increased  $\text{Ca}^{2+}$  influx during the EPSP, but will in addition prolong the residence time of  $\text{Ca}^{2+}$ -activated second messengers, e.g.  $\alpha\text{CaMKII}$ , in the active spine. We suggest that electrical and chemical isolation induced by high spine neck resistance cooperate to facilitate the induction of long-term plasticity at spine synapses. Therefore, although spine neck changes have little direct impact on EPSP amplitudes at the soma, they could be a key mechanism for synaptic metaplasticity.

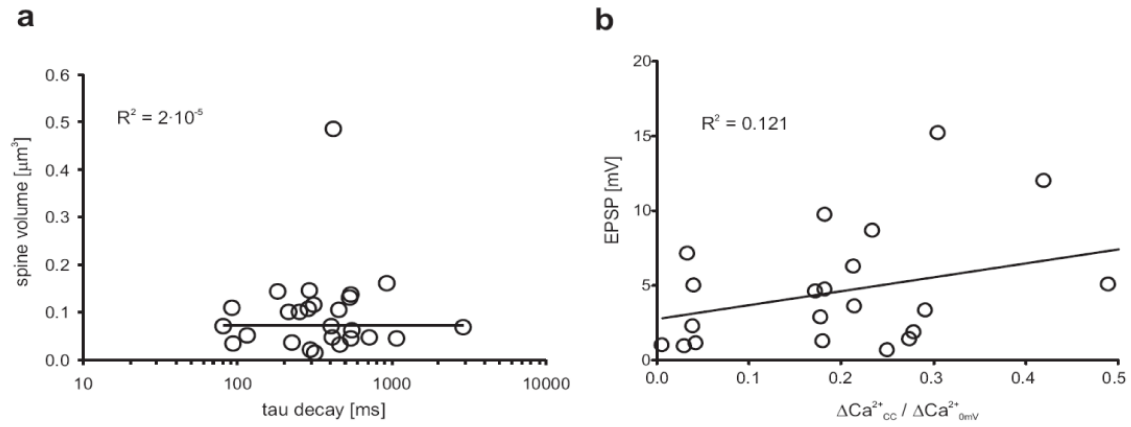
## SUPPLEMENTARY FIGURES



**Supplementary Figure B1. Voltage-dependence of synaptically evoked spine calcium transients.**

(a) Red circles: Amplitude of spine calcium transients at different holding potentials normalized to the amplitude at the synaptic reversal potential (0 mV). To improve space clamp, Cs<sup>+</sup>-based intracellular solution was used and AMPA currents were blocked by NBQX (10  $\mu\text{M}$ ). The voltage-dependence of the current is well fit by combining the Goldman-Hodgkin-Katz current equation for  $\text{Ca}^{2+}$  (dotted line) with the voltage-dependent gating function of the NMDA receptor (red curve). In experiments without AMPAR block (white circles), spines escaped the somatic voltage clamp and depolarized, resulting in larger calcium transients.

(b) Voltage-dependent gating function of synaptic NMDARs, extracted from fit in (a).  $g(V_m) = 1/[1 + \exp(-0.08V_m)(C/0.69)]$ , where  $V_m$  is the membrane potential and  $C$  is the extracellular  $\text{Mg}^{2+}$  concentration in mM.

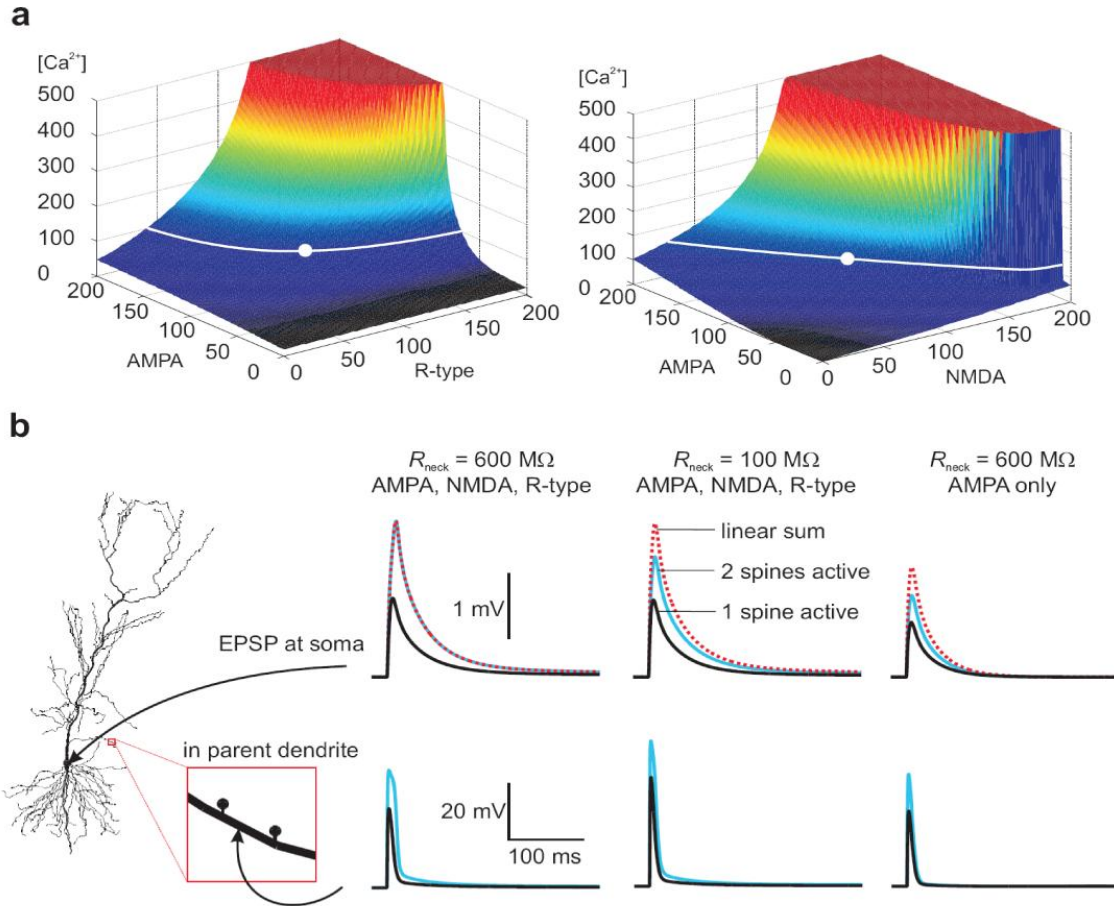


### Supplementary Figure B2. Correlations

(a) Spine head volumes were not correlated with diffusional time constants (decay time constants of the spine calcium transients at 0 mV).

(b) Average EPSP amplitudes at the soma were not correlated with fractional calcium transients. Large somatic EPSPs indicate the activation of several synapses.





### Supplementary Figure B3. Receptor number and input summation

(a) Parameter space of NEURON model. The amplitude of simulated spine calcium transients was dependent on AMPA receptor and R-type calcium channel densities (left) and NMDA receptor density (right). White dot indicates channel densities used in (b) and in Fig. B4. White line indicates other channel density combinations consistent with our experimental data. All axes scaled in % of best fit, absolute channel numbers are given in Supplementary Table 1. Black area:  $\text{Ca}^{2+}$  silent spines. Truncated red area: Spine spike caused by runaway depolarization.

(b) Electrical amplification leads to linear summation of simultaneously active inputs. Simulated EPSPs are shown at the soma (top row) and in the thin dendrite between the two active spines (bottom row). Black traces: single input; Blue trace: both inputs active; Red dotted trace: linear prediction. If spine neck resistance is low (center column) or the spines lack voltage-activated conductances (right column), summation becomes sublinear due to the reduction in driving force.

## SUPPLEMENTAL TABLES

**Supplementary Table B1:** Number of channels used in simulation

	AMPA receptor	NMDA receptor	R-type VGCC
# of channels present in spine	240	110	230
maximum # of channels open during EPSP	240	18	9

**Supplementary Table B2:** Electrotonic attenuation of EPSC and EPSP (1.2 G $\Omega$  spine neck)

	EPSC amplitude (Voltage clamp)	EPSP amplitude (Current clamp)
spine head	41 pA	54.8 mV
spine base	n/a	22.2 mV
soma	24 pA	1.1 mV

## METHODS

### Slice preparation

Acute hippocampal brain slices were prepared from Sprague Dawley rats (postnatal day 16-20) in accordance with the animal care and use guidelines of the Veterinary Department Basel-Stadt. Horizontal slices (350  $\mu$ m) were cut on a vibroslicer (Leica) in ice-cold solution containing (in mM): 110 choline chloride, 25 NaHCO<sub>3</sub>, 25 D-glucose, 11.6 sodium ascorbate, 7 MgSO<sub>4</sub>, 2.5 KCl, 1.25 NaH<sub>2</sub>PO<sub>4</sub> and 0.5 CaCl<sub>2</sub>. Slices were incubated at 34°C for 30-45 min in oxygenated artificial CSF (ACSF), containing (in mM) 127 NaCl, 25 NaHCO<sub>3</sub>, 25 D-glucose, 2.5 KCl, 1 MgCl<sub>2</sub>, 2 CaCl<sub>2</sub>, 1.25 NaH<sub>2</sub>PO<sub>4</sub> and then stored at room temperature until used. Experiments were performed at 32° C in ACSF containing 10  $\mu$ M bicuculline, 30  $\mu$ M serine and 2  $\mu$ M thapsigargin to block

GABA<sub>A</sub> receptors, glycine-dependent desensitization of NMDARs, and intracellular Ca<sup>2+</sup> stores.

### **Electrophysiology**

Whole-cell recordings from CA1 pyramidal cells were made with a Multiclamp 700B amplifier (Axon Instruments), using 3-6 M $\Omega$  pipettes filled with (in mM): 130 K-methylsulfonate (or 135 cesium methanesulfonate), 10 HEPES, 10 sodium phosphocreatine, 3 sodium ascorbate, 4 MgCl<sub>2</sub>, 4 Na<sub>2</sub>-ATP, 0.4 Na-GTP, 0.6 fluo-5F and 0.03 Alexa Fluor 594 (pH 7.2). Schaffer collaterals were stimulated with a monopolar glass electrode filled with 1M NaCl, positioned 15-25  $\mu$ m from an oblique dendrite, using short hyperpolarizing pulses (0.2 ms, -3 to -5 V) delivered by a stimulus isolator (NPI Electronics). The synaptic reversal potential was determined by first depolarizing the cell at the soma until the synaptic currents reversed, then slowly repolarizing until synaptic stimulation evoked zero current. This procedure provided precise compensation for unavoidable space clamp errors. In K<sup>+</sup> based internal solution, current reversal was typically achieved with the soma clamped between +25 and +30 mV. If the synaptic currents could not be reversed, the experiment was aborted.

### **Two-photon imaging and data analysis**

Two-photon imaging was performed as previously described. For FRAP experiments, we bleached Alexa Fluor 594 (Molecular Probes) with a 0.5 ms laser pulse at 810 nm. The fluorescence recovery was fit with a single exponential function. For calcium imaging experiments, we used a mixture of fluo-5F and Alexa Fluor 594. Responsive spines on oblique dendrites 100-200  $\mu$ m (average 170  $\mu$ m) from the soma were identified using frame scans (4 Hz). For quantitative measurements, line scans (500 Hz) were used. We subtracted the PMT dark current and evaluated the ratio of green/red fluorescence intensity (*G/R*) (Yasuda et al., 2004). To quantify the amplitude of spine calcium transients, we first generated a response template for each spine by fitting the difference of two exponentials to the average response. This response template was scaled in amplitude to fit each individual response (scaling factor \* template amplitude = response amplitude).

### **Using calcium signal decay to estimate spine diffusional coupling**

Under our experimental conditions, removal of free calcium ions from the cytoplasm was compromised for the following reasons: i) the membrane potential was always above the calculated reversal potential of the sodium/calcium exchanger  $E_{\text{NCX}} = 3E_{\text{Na}} - 2E_{\text{Ca}} = -103$  mV (Torok, 2007), ii) SERCA pumps were blocked by thapsigargin, iii) plasma membrane  $\text{Ca}^{2+}$  pumps had to compete for free  $\text{Ca}^{2+}$  ions with the high added buffer capacity of 600  $\mu\text{M}$  fluo-5F ( $K_d \sim 0.8 \mu\text{M}$ ). Under these conditions, the decay of the fluorescence signal in the spine was mainly due to diffusion of calcium-bound dye molecules into the dendrite, which we verified by combining two-photon uncaging of MNI-glutamate and FRAP experiments.

### **Spine volume measurements**

Spine volume measurements were performed as previously described (section 4.A).

### **In vivo FRAP measurements**

Transgenic mice expressing yellow fluorescent protein (B6.Cg-Tg(Thy1-YFPH)2Jrs/J, Jackson Laboratory) were anesthetized by IP injection (17 mg/ml ketamine, 1.7 mg/ml xylazine). The skull was exposed and thinned with a dental drill as described (Grutzendler et al., 2002). For imaging and photobleaching, an Ultima 2-photon microscope (Prairie Technologies) with a 60x/1.1NA Objective (Olympus) was used at 920 nm excitation wavelength (Mai Tai HP, Spectra Physics). Of each spine, 40 images (64x64 pixels) were taken at 13 Hz according to the following protocol: 10 frames baseline, bleach pulse (0.5 s), 10 frames, 5 s wait, 10 frames, 10 s wait, 10 frames (Fig. 6). Laser power was adjusted to bleach the spine to 30-40% of its baseline intensity. Custom-written software (Matlab) was used to measure the spine fluorescence intensity, compensating for small movements by centering the region of interest (ROI) on the spine in every frame.

### Estimation of spine neck resistance

In our simulations, the strong effect of AMPA receptor block on calcium signal amplitude was only reproduced with  $R_{\text{neck}} \sim 1.2 \text{ G}\Omega$ . Is such a high neck resistance consistent with the decay time constants measured in the calcium imaging experiments? The average fluorescence decay time constant of all spines with a clear calcium response at resting membrane potential (excluding ‘calcium-silent’ spines) was  $\tau = 0.9 \text{ s}$  (**Fig. B2d**). Based on these measurements, we calculated the spine neck length to cross section ratio ( $L/A$ ) according to the equation (Bloodgood and Sabatini, 2005)

$$L/A = \tau \cdot D / V = 900 [\text{ms}] \cdot 0.1 [\mu\text{m}^2/\text{ms}] / 0.11 [\mu\text{m}^3] = 818 [\mu\text{m}^{-1}] ,$$

where  $D$  is the diffusion coefficient of fluo-5F in cytoplasm ( $100 \mu\text{m}^2/\text{s}$ ) (Michailova et al., 2002) and  $V$  is the average spine volume of our sample ( $0.11 \mu\text{m}^3$ ).

We estimated the resistance of the spine neck according to the cable equation

$$R_{\text{neck}} = R_i \cdot L / A = 150 \cdot 10^4 [\Omega \mu\text{m}] \cdot 818 [\mu\text{m}^{-1}] = 1.2 \cdot 10^9 [\Omega]$$

assuming an internal resistivity  $R_i = 150 \Omega\text{cm}$ .

Thus, the spine neck resistance that produced realistic interactions between AMPA, NMDA and R-Type channels in the NEURON simulation ( $1.2 \text{ G}\Omega$ , **Fig. B4c**) is also consistent with the decay time constants we found experimentally (**Fig. B2d**).

## **Part 4.C:**

### **Optical induction of plasticity at single synapses reveals input-specific accumulation of $\alpha$ CaMKII**

Yan-Ping Zhang, Niklaus Holbro and Thomas G. Oertner

*Proc Natl Acad Sci U S A. 2008 Aug 19;105(33):12039-44.*

#### **ABSTRACT**

Long-term potentiation (LTP), a form of synaptic plasticity, is a primary experimental model for understanding learning and memory formation. Here we use light-activated channelrhodopsin-2 (ChR2) as a tool to study the molecular events that occur in dendritic spines of CA1 pyramidal cells during LTP induction. Two-photon uncaging of MNI-glutamate allowed us to selectively activate excitatory synapses on optically identified spines while ChR2 provided independent control of postsynaptic depolarization by blue light. Pairing of these optical stimuli induced lasting increase of spine volume and triggered translocation of  $\alpha$ CaMKII to the stimulated spines. No changes in  $\alpha$ CaMKII concentration or cytoplasmic volume were observed in neighboring spines on the same dendrite, providing evidence that  $\alpha$ CaMKII accumulation at postsynaptic sites is a synapse-specific memory trace of coincident activity.

## INTRODUCTION

Activity-dependent changes in synaptic strength are generally considered to be the cellular basis of learning and memory (Bliss and Collingridge, 1993). Long-term potentiation (LTP), the most extensively studied form of such synaptic plasticity, can be triggered within seconds by coincident activity in pre- and postsynaptic cells. The possible structural modifications that occur at synapses where LTP has been induced are poorly known due to the difficulty of simultaneously measuring functional and morphological parameters at individual synapses. Furthermore, it is controversial whether neighboring synapses can be modified independently (Engert and Bonhoeffer, 1997; Bi and Poo, 2001; Matsuzaki et al., 2004). In a recent report, it has been shown that spatially clustered synapses can cooperate in the induction of plasticity, and that cytoplasmic factors are responsible for this functional crosstalk (Harvey and Svoboda, 2007). The identity of these diffusible factors, however, has not been clarified.

A key player in the LTP signaling cascade is  $\alpha$ CaMKII, which is thought to function as a molecular switch: Following activation by  $\text{Ca}^{2+}$ -calmodulin, it can stay active for prolonged periods of time via autophosphorylation (Giese et al., 1998; Lisman and Zhabotinsky, 2001). Reports that brief application of glutamate or NMDA to cultured hippocampal neurons induces CaMKII accumulation in spines (Shen and Meyer, 1999; Shen et al., 2000; Merrill et al., 2005) have created much interest because  $\alpha$ CaMKII activation is both necessary and sufficient to induce synaptic plasticity (Lledo et al., 1995; Giese et al., 1998). It has been suggested that postsynaptic accumulation of  $\alpha$ CaMKII could be responsible for the synapse-specificity of LTP, because it localizes

the putative activated kinase close to its substrates, e.g. AMPA receptors (Soderling and Derkach, 2000; Lisman and Zhabotinsky, 2001), and protects it from dephosphorylation (Mullasseril et al., 2007). However, a crucial prediction of this hypothesis, namely that  $\alpha$ CaMKII accumulates specifically and exclusively at synapses that undergo LTP, has never been tested experimentally.

To address whether  $\alpha$ CaMKII accumulates specifically in spines experiencing coincident activity, we developed an all-optical pairing protocol to induce synaptic plasticity at identified spines, combining two-photon uncaging of MNI-glutamate (Matsuzaki et al., 2001) with postsynaptic channelrhodopsin-2 (ChR2) activation. Thus, we could avoid the wash-out problems typically associated with whole-cell patch clamp (**see supplementary Fig. C1**) while maintaining precise temporal control over the postsynaptic depolarization. Spine morphology and  $\alpha$ CaMKII concentration were monitored by two-photon ratiometric measurements. We show that paired stimulation of a single synapse can induce long-lasting  $\alpha$ CaMKII accumulation at that synapse, but not at neighboring spines that were not exposed to glutamate.

## **RESULTS**

### **A novel strategy for non-invasive LTP induction**

In the classical electrophysiological pairing protocol, presynaptic action potentials are paired with postsynaptic depolarization that is provided by current injection via a somatic patch electrode (Chen et al., 1999). Using this technique, plasticity has to be induced within 5-10 min after break-in, because important signaling molecules, e.g. CaMKII, are



rapidly washed out (**supplementary Fig. C1**). Since our goal was to optically monitor the concentration of fluorescently labeled  $\alpha$ CaMKII during the induction of plasticity, it was essential not to disturb the cytoplasm during the experiment. We therefore used the light-gated cation channel Channelrhodopsin-2 (ChR2) (Boyden et al., 2005) to depolarize individual postsynaptic cells in a non-invasive fashion.

Comparing protein concentrations in dendrites and spines presented a second challenge. Most dendritic spines were substantially smaller than the point spread function of our microscope. As a result, the fluorescence intensity of labeled  $\alpha$ CaMKII in individual spines was determined by two unknown variables: The concentration of  $\alpha$ CaMKII in the spine, and the volume of that spine. Thus, fluorescence intensity measurements in a single color channel were not sufficient to quantify differences in protein concentration between spines and dendrites. We solved this problem by co-transfection with a freely diffusible dimeric RFP, which served as a marker of cytosolic volume. We then used a ratiometric approach (green/red fluorescence intensity ratio) to compare the concentration of  $\alpha$ CaMKII in spines of different size. The level of  $\alpha$ CaMKII overexpression was generally low in our experiments (~13% of endogenous  $\alpha$ CaMKII, **supplementary Fig. C2**).

A fluorescently labeled version of ChR2 would have resulted in staining of the cell membrane and thus interfered with our  $\alpha$ CaMKII measurements. To assess the expression level of ChR2 in individual cells, we combined unlabeled ChR2 and soluble RFP in a single plasmid with separate promoters, which resulted in very reliable co-

expression. Using particle-mediated gene transfer, we co-transfected hippocampal neurons with 2 vectors encoding 3 different proteins: ChR2 / RFP, and Dronpa- $\alpha$ CaMKII (**Fig. C1a**). In response to blue light illumination (200 ms, 470 nm LED), transfected cells produced large inward currents ( $1395 \text{ pA} \pm 115 \text{ pA}$  at peak and  $804 \text{ pA} \pm 89 \text{ pA}$  at steady-state,  $n = 21$ ). In current clamp mode, the same blue light stimulation induced robust spiking ( $5.4 \pm 0.5$  spikes, **Fig. C1c**).

We next examined whether the light stimulation technique could be used to induce long-term potentiation of Schaffer collateral synapses. We performed dual patch-clamp recordings of connected pairs of untransfected CA3 and transfected CA1 pyramidal cells (**Fig. C1b**). Our induction protocol consisted of repetitive pairing of single presynaptic action potentials in a single CA3 cell with brief postsynaptic bursts induced by 200 ms light pulses from a high-power blue LED (**Fig. C1c**). To compensate for the propagation delay from CA3 to CA1 (Zhang and Oertner, 2007), we started the light pulse with a delay of  $\Delta t = 6 \text{ ms}$  relative to the presynaptic current injection. After 20 pairings at 0.1 Hz in current clamp, excitatory postsynaptic currents (EPSCs) increased to  $274 \% \pm 76 \%$  (**Fig. C1d**). Previously, we and others have shown that light-induced spiking is accompanied by calcium influx through voltage-gated calcium channels and through ChR2 itself (Nagel et al., 2003; Zhang and Oertner, 2007). Therefore, it was important to test whether light-induced spiking could trigger synaptic plasticity in the absence of presynaptic activity. In control experiments in which repetitive blue light stimulation was not paired with presynaptic activation, postsynaptic response amplitudes remained unchanged ( $107 \% \pm 16 \%$ , **Fig. C1d**). We conclude that coincident stimulation was

needed to induce LTP on cells expressing ChR2 and  $\alpha$ CaMKII, analogous to the classical electrophysiological pairing protocol (Petersen et al., 1998; Debanne et al., 1999; Zhang and Oertner, 2007).

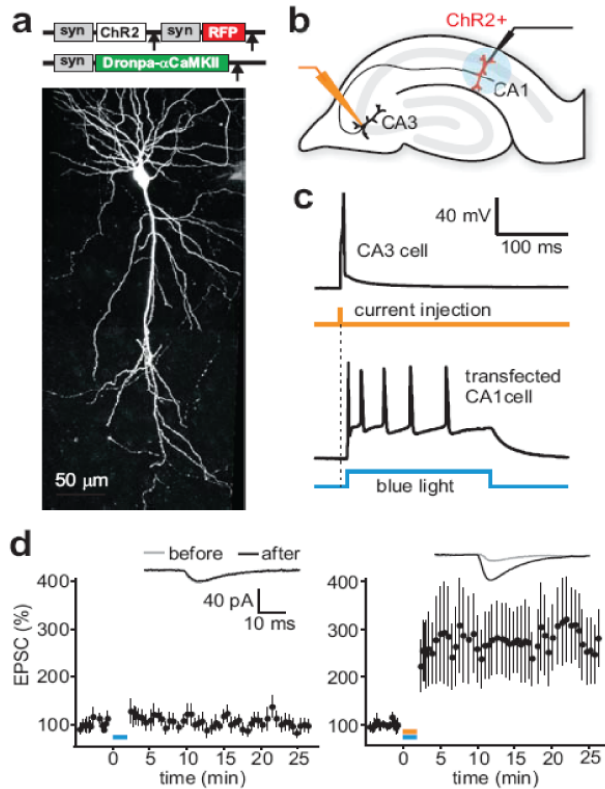


**Figure C1. LTP induction by pairing of single action potentials in CA3 cells with ChR2-mediated depolarization of synaptically connected CA1 cells.**

(a) CA1 pyramidal cell in organotypic slice culture expressing ChR2, RFP and Dronpa-CaMKII. Arrows indicate SV40 poly-A sequences.

(b) Paired recording configuration to assess light-induced plasticity in transfected CA1 pyramidal cell. Blue spot indicates illuminated area.

(c) LTP induction protocol. A single AP evoked by current injection into a patch-clamped CA3 pyramidal cell was paired with a short burst of 5 APs elicited by blue light illumination (200 ms) of a transfected CA1 pyramidal cell ( $\Delta t = 6$  ms). Pairing was repeated 20 times at 0.1 Hz.

(d) Light-induced bursting in postsynaptic cell (blue bar: 200 ms light pulses, 20 repetitions at 0.1 Hz) did not significantly change EPSC amplitudes in transfected CA1 pyramidal cells ( $107\% \pm 16\%$ ,  $n = 7$  pairs). Pairing stimulation as described in (c) induced  $274\% \pm 76\%$  potentiation ( $n = 7$  pairs). Insert: example traces before and after light stimulation. Error bars indicate SEM

### Spine volume changes induced by pairing of glutamate uncaging and blue light

Having established that postsynaptic depolarization by optical activation of ChR2 is sufficient for pairing-induced LTP, the next step was to replace the electrophysiological stimulation of CA3 axons by 2-photon glutamate uncaging at individual spines. For this purpose, we combined two Ti:Sapph lasers for simultaneous 2-photon uncaging and 2-photon imaging (**Fig. C2a**). Uncaging laser power (725 nm) was adjusted such that uncaging-evoked excitatory postsynaptic currents (uEPSCs) had amplitudes of  $15.2 \text{ pA} \pm 1.8 \text{ pA}$  (laser power,  $\sim 50 \text{ mW}$ , pulse duration, 0.5 ms), similar to spontaneous miniature EPSCs ( $\text{mEPSC} = 18 \text{ pA} \pm 3 \text{ pA}$ ,  $n = 7$  cells, data not shown). To induce LTP at

individual spines of transfected cells, we paired single glutamate uncaging pulses with 200 ms blue light pulses (20 pairings at 0.1 Hz,  $\Delta t = 0$ ). In a set of cells that were not used for morphometric analysis, we verified by patch clamp recording that this optical pairing protocol, but not glutamate uncaging *without* simultaneous ChR2 activation (20 pulses at 0.1 Hz), resulted in a lasting increase in uEPSC amplitude (**Fig. 2b**). To monitor spine morphology in 3D, we acquired stacks of 20 image planes at 5 min intervals. The integrated intensity of the spine head was used as a measure of spine volume. Stimulated spines responded with a rapid volume expansion by a factor of 2.4, on average (**Fig. 2c**). Spine volume partially decreased during the following 15 min, but most stimulated spines (11/16) remained enlarged 30-40 min after stimulation. In a separate set of control experiments, using identical pairing of blue light and uncaging laser pulses in the absence of MNI-glutamate, we did not detect any spine enlargement (**Fig. 2c**) and thus could rule out any unspecific effects induced by the uncaging laser pulse itself.

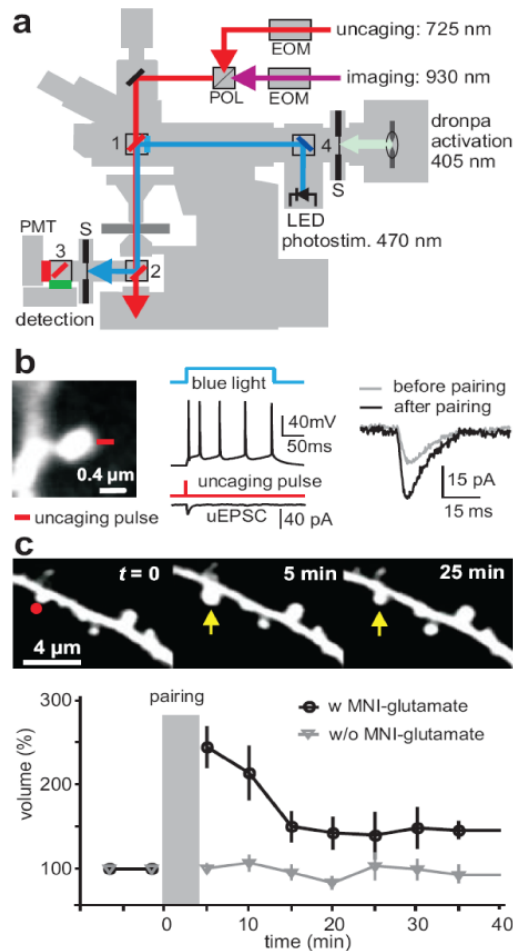


**Figure C2. Spine volume changes induced by pairing of glutamate uncaging and ChR2 activation.**

(a) Setup for simultaneous uncaging, imaging, and ChR2 stimulation.

(b) To induce plasticity at individual synapses, single uncaging pulses were paired with 200 ms blue light pulses 20 times at 0.1 Hz ( $\Delta t = 0$ ). uEPSCs are averages of 5 consecutive traces each.

(c) Spine volume change induced by optical pairing protocol in the presence of MNI-glutamate. Time course shows transient and permanent component (black circles,  $n = 16$  spines, 8 cells). No volume changes were induced in the absence of MNI-glutamate (gray triangles,  $n = 12$  spines, 5 cells).

### $\alpha$ CaMKII concentration in dendritic spines

By calculating the fluorescence intensity ratio between GFP- $\alpha$ CaMKII and RFP on a pixel-by-pixel basis ( $G/R$ ), we were able to compare the concentration of  $\alpha$ CaMKII in spines of different size (**Fig. C3a**). To pool spine data from cells with different relative expression levels of GFP- $\alpha$ CaMKII and RFP, we normalized the  $G/R$  ratio in the spine by  $G/R$  ratio in the dendrite ( $S/D$  ratio). The  $S/D$  ratio is a measure of  $\alpha$ CaMKII enrichment in spines independent of spine volume. Under baseline conditions,  $\alpha$ CaMKII in spines was enriched by a factor of 1.32 relative to the dendrite (**Fig. 3b**), suggesting that about 24% of total  $\alpha$ CaMKII in spines was bound to postsynaptic sites. To test for

potential measurement artifacts due to the different signal-to-noise ratio in spines and dendrites, we also determined  $S/D$  ratios of soluble EGFP/RFP.  $S/D$  ratios were normally distributed with a mean of 1.01, indicating that our ratiometric approach was indeed volume-independent.

An alternative method to distinguish bound and soluble fraction is fluorescence recovery after photobleaching (FRAP)(Shen and Meyer, 1999). For these experiments, we co-transfected cells with RFP and YFP- $\alpha$ CaMKII, which could be readily bleached using 2-photon excitation at 910 nm. After a brief laser pulse that bleached 70-80% of the fluorescent molecules in the spine, fluorescence in the red color channel recovered rapidly (median  $\tau = 0.28$  s,  $n = 80$ ) to its initial value, indicating free diffusion of the dimeric RFP (**Fig. C3c**). YFP- $\alpha$ CaMKII fluorescence, on the other hand, did not fully recover, indicating a fraction of  $\alpha$ CaMKII molecules that were bound to postsynaptic sites. To quantify the unrecoverable fraction, we fit a single exponential function to the normalized fluorescence recovery data  $F(t)$ :

$$F(t) = 1 - f_U - f_S e^{-\frac{t}{\tau}}$$

where  $f_U$  and  $f_S$  are the unrecoverable and soluble fraction of total  $\alpha$ CaMKII, respectively, and  $\tau$  is the recovery time constant. For wild-type YFP- $\alpha$ CaMKII, the unrecoverable fraction was  $21\% \pm 12\%$  (mean  $\pm$  SD). To test whether binding was dependent on the phosphorylation state of  $\alpha$ CaMKII, we generated a double mutant (TT305/6VA) where two inhibitory autophosphorylation sites were removed. The threshold for kinase activation and for LTP induction is known to be lowered in the TT305/6VA mutant (Hanson and Schulman, 1992; Elgersma et al., 2002; Thalhammer et

al., 2006). Indeed, cells transfected with mutant  $\alpha$ CaMKII had a significantly higher unrecoverable fraction of  $42\% \pm 28\%$  ( $p < 0.05$ ). Time constants of recovery, on the other hand, were not significantly different for WT and mutant  $\alpha$ CaMKII (median  $\tau_{WT} = 12.5$  s;  $\tau_{TTVA} = 14.3$  s), suggesting that the mobility of the soluble fraction was not influenced by the mutation. As expected, the  $S/D$  ratio and the unrecoverable fraction were correlated in individual spines, but individual measurements deviated from the expected relationship (curve in **Fig. C3d**). The deviation suggests that the assumption of a single, uniform population of bound  $\alpha$ CaMKII molecules was probably an oversimplification. More likely, subpopulations of bound  $\alpha$ CaMKII in the spine head turn over on multiple time scales (see N. Otmakhov et al., Soc. Neurosci. Abstr. 788.8, 2007). Based on these considerations, we decided to rely on ratio measurements rather than on FRAP to assess the effects of LTP on  $\alpha$ CaMKII binding.

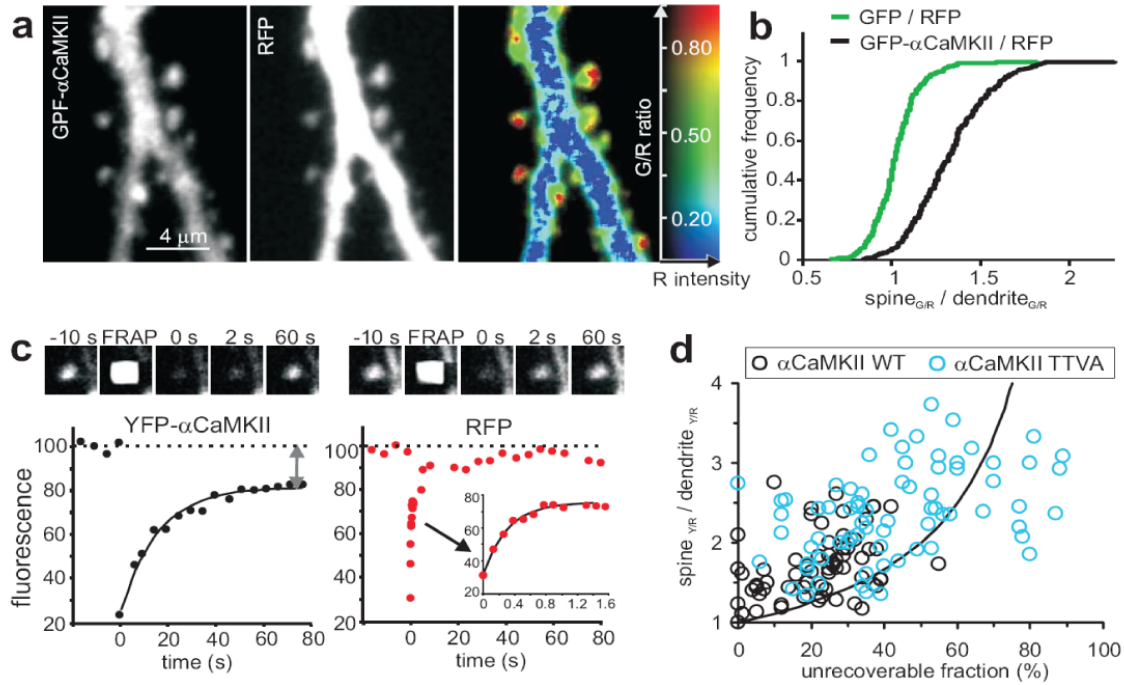


**Figure C3. Enrichment of  $\alpha$ CaMKII in spines.**

(a) CA1 pyramidal cell dendrite expressing GFP- $\alpha$ CaMKII and RFP.

Left: GFP- $\alpha$ CaMKII signal. Middle: Cytoplasmic volume (RFP). Right: Color-coded ratio of  $\alpha$ CaMKII/volume (G/R), indicating elevated  $\alpha$ CaMKII concentration in spines.

(b) Cumulative distribution of G/R ratio (protein concentration) in spines relative to parent dendrite (S/D ratio).

$\alpha$ CaMKII, but not GFP, is enriched in dendritic spines.

(c) FRAP analysis on a dendritic spine expressing YFP- $\alpha$ CaMKII and RFP. Black dots: YFP- $\alpha$ CaMKII fluorescence intensity in spine. Black line: single exponential fit. Note ~20% unrecoverable fraction. Red dots: RFP fluorescence. Note rapid (insert) and complete recovery of fluorescence.

(d) Correlation between FRAP and spine/dendrite (s/d) ratio measurements in individual spines. YFP- $\alpha$ CaMKII TT305/306VA mutant showed higher unrecoverable fraction and higher enrichment in spines compared to wild type  $\alpha$ CaMKII. Black line: predicted correlation  $f_u = 1 - 1/(s/d)$ .

## Spine enlargement precedes the input-specific accumulation of $\alpha$ CaMKII

$\alpha$ CaMKII translocation into spines after global chemical stimulation has been demonstrated previously (Shen and Meyer, 1999; Otmakhov et al., 2004; Bayer et al., 2006). Here, our question was whether  $\alpha$ CaMKII translocation is detectable, specific, and persistent following potentiation of a single synapse. A concern for optical concentration measurements of fluorescently labeled proteins is potential bleaching artifacts during time-lapse imaging and glutamate uncaging. To minimize this problem, we labeled



$\alpha$ CaMKII with the photoswitchable GFP Dronpa-Green, which can be reactivated after bleaching by brief UV illumination (Ando et al., 2004). From a series of control experiments, we estimated that ~95% of bleached Dronpa- $\alpha$ CaMKII was reactivated by low-power illumination at 405 nm (**supplementary Fig. C3**). We co-transfected CA1 pyramidal cells with Dronpa- $\alpha$ CaMKII, RFP, and unlabeled ChR2. Image stacks were obtained every 4 minutes, and Dronpa fluorescence was reactivated before each acquisition. We verified that UV illumination did not induce spiking of ChR2-transfected cells (**supplementary Fig. C3**). Following optical LTP induction, the majority of spines (18 / 23 experiments) responded with a rapid increase in spine head volume. Ten out of these 18 spines were still enlarged 30-40 min after stimulation (**Fig. C4a**, right example). Persistent spine enlargement has been linked previously to successful LTP induction at the spine synapse (Matsuzaki et al., 2004; Harvey and Svoboda, 2007). Therefore, we split our sample of stimulated spines in 2 different groups, spines that responded with a persistent volume increase to the pairing protocol and spines that did not (**Fig. C4b**). We also analyzed neighboring spines on the same dendrite that were not directly stimulated (average distance from the stimulated spine: 5.5  $\mu$ m). We then compared  $\alpha$ CaMKII enrichment (spine/dendrite) in the three groups (**Fig. C4c**). Only in the group of spines with persistent volume increases did we detect a significant increase in the concentration  $\alpha$ CaMKII at  $t = 13$  min after the onset of stimulation ( $p < 0.05$ , see also **supplementary Fig. C4**). Interestingly, all groups had the same  $\alpha$ CaMKII concentration before stimulation, indicating that the initial  $\alpha$ CaMKII level had no predictive value for the type of volume change (transient vs. persistent) induced by the pairing stimulation. In neighboring unstimulated spines, we did not detect an increase in  $\alpha$ CaMKII

concentration, indicating high spatial specificity of  $\alpha$ CaMKII enrichment. We noted that spine enlargement preceded the input-specific accumulation of  $\alpha$ CaMKII: Whereas spine volume reached its maximum immediately after stimulation,  $\alpha$ CaMKII concentration reached its peak ~10 min later. Using the spine/dendrite ratio before stimulation as a starting point, we calculated changes in the amount of bound and soluble  $\alpha$ CaMKII in stimulated and non-stimulated spines (**Fig. C4d**). This analysis revealed that in the spines with a persistent increase in volume, the *absolute amount* of bound  $\alpha$ CaMKII in the spine had approximately doubled 30-40 min after stimulation. The bound *fraction*, on the other hand, peaked transiently ~10 min after stimulation, but later returned to baseline (29% before stimulation, 33% 30-40 min after stimulation). These experiments suggests that paired stimulation moved 10 out of 23 spines to a new stable state, characterized by an increased amount of both soluble and bound  $\alpha$ CaMKII and a larger volume. No significant volume or  $\alpha$ CaMKII changes were detected in neighboring spines on the same dendrite.

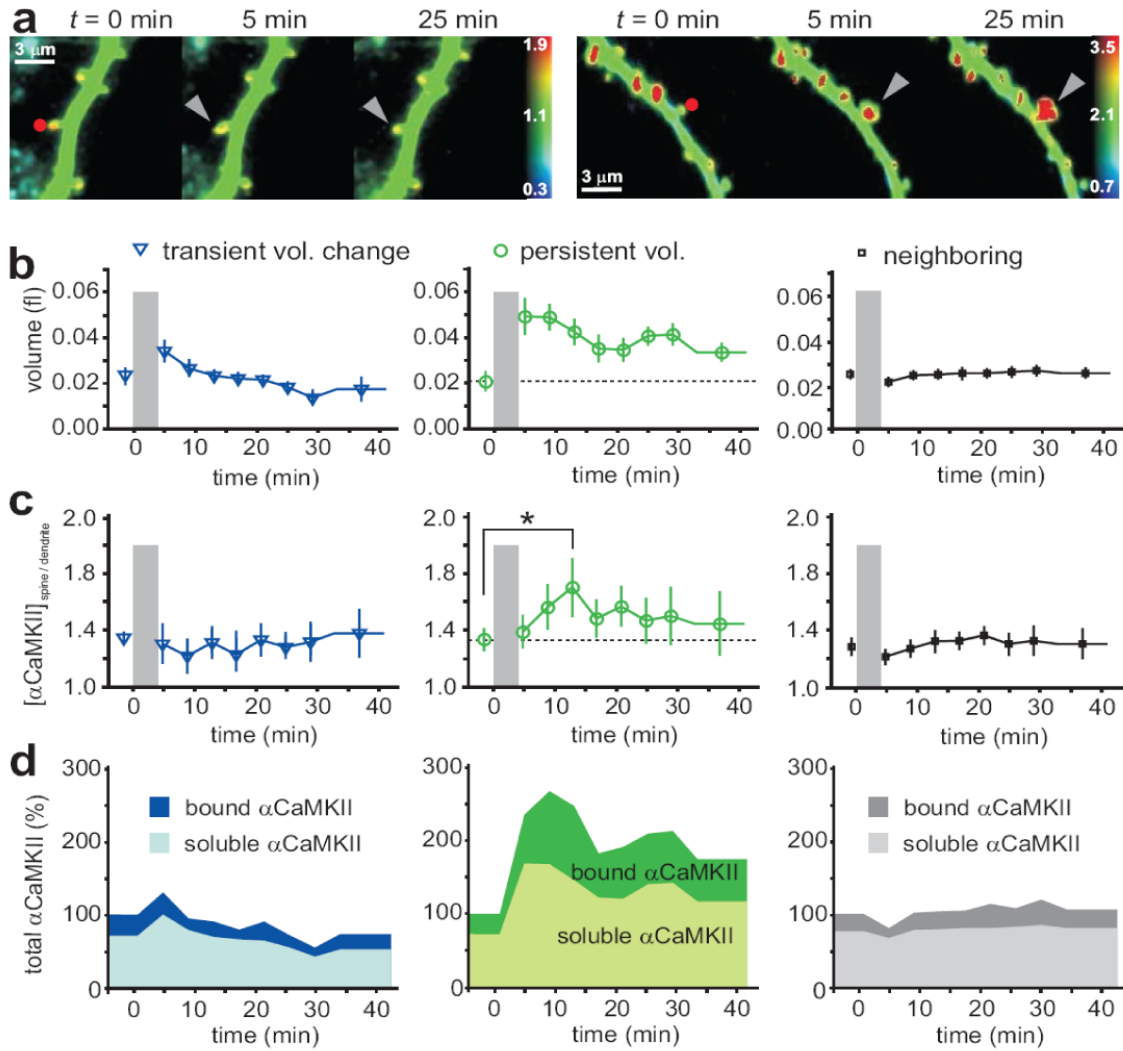


**Figure C4. Input-specific accumulation of  $\alpha$ CaMKII.**

(a) Maps of  $\alpha$ CaMKII concentration. Stimulated spines (red dot) showed either transient (left) or persistent increase in volume and  $\alpha$ CaMKII concentration (right).

(b) Spine volume changes in response to optical pairing protocol. Stimulated spines were sorted into 2 groups according to their volume 30-40 min after pairing (Transient spines: < 30% change,  $n = 13$ ; Persistent spines, >30% change,  $n = 10$ ). Right panel: neighboring, non-stimulated spines on the same dendrite show no significant volume change.

(c) CaMKII enrichment in spines:  $\alpha$ CaMKII concentration (G/R) in spine normalized by  $\alpha$ CaMKII concentration (G/R) in dendrite. Spines were sorted according to persistence of volume change as described in b. Significant  $\alpha$ CaMKII enrichment was detected in persistently enlarged spines at  $t = 13$  min (paired  $t$ -test, one-tailed,  $p < 0.05$ ), but not in the group that responded only with transient swelling. Neighboring, non-stimulated spines showed no significant change in  $\alpha$ CaMKII concentration.

(d) Soluble and bound fraction calculated from data shown in c and b. In the spines that responded with persistent volume change to paired stimulation (middle panel), the amount of both bound and soluble  $\alpha$ CaMKII was persistently increased by a factor of 2.0 and 1.6, respectively.

### **Induction of long-term plasticity by synaptic activation**

Glutamate uncaging is a convenient way to stimulate individual dendritic spines, but the glutamate concentration in the synaptic cleft depends on intensity and duration of the laser pulse (Harvey and Svoboda, 2007). If our observations following optical pairing (**Fig. C3, C4**) were indeed characteristic for LTP, similar changes would be expected following high frequency electrical activation of Schaffer collaterals; another well established LTP induction protocol. To identify synaptically stimulated spines, we used *post hoc* calcium imaging: Firstly, spiny dendrites of transfected CA1 pyramidal cells were imaged while stimulating Schaffer collateral axons at high frequency (3 x 1 s, 100 Hz). Following time-lapse imaging of a transfected cell for ~40 min, we patch-clamped the same cell to infuse a calcium sensitive dye (Fluo 4FF) and Alexa-Fluor 594. Although the plasticity-inducing tetanic stimulation was applied under blind conditions, we could re-activate the same set of synapses by applying short bursts (3 APs) to the stimulation electrode. In 4 experiments, we successfully identified synaptically stimulated spines by *post hoc*  $\text{Ca}^{2+}$  imaging (**supplementary Fig. C5**). Analysis of the volume-filling RFP fluorescence in the synaptically stimulated spines revealed that the LTP protocol induced a rapid volume increase with a large persistent component. The total amount of  $\alpha\text{CaMKII}$  also increased in the stimulated spines, peaking 5 min after stimulation. Analysis of the soluble and bound fraction in the tetanized spines revealed that 25-35 min after stimulation, the amount of bound  $\alpha\text{CaMKII}$  was increased by a factor of 2.0 (**supplementary Fig. C5**). In summary, the physiological and morphological consequences of high frequency stimulation were remarkably similar to the changes we observed after pairing of glutamate uncaging with postsynaptic depolarization by ChR2.

This indicates that persistent spine volume increase and synapse-specific binding of  $\alpha$ CaMKII are hallmarks of LTP in CA1 pyramidal neurons.

## DISCUSSION

Here we show that paired activation of a single synapse on a single cell leads to long-lasting enrichment of  $\alpha$ CaMKII at that synapse. Our study highlights several advantages of plasticity induction by optical pairing. Unlike chemical LTP and zero  $Mg^{2+}$  protocols (Fong et al., 2002; Otmakhov et al., 2004; Sharma et al., 2006), optical pairing does not lead to unspecific activation of the entire tissue. Therefore, activity-induced changes at individual synapses can be studied in an unperturbed cellular environment. The spatial resolution is clearly superior to local perfusion approaches, which have been used previously to probe the input specificity of LTP and CaMKII translocation (Engert and Bonhoeffer, 1997; Thalhammer et al., 2006). Degrading electrical access or cell health, which limits the duration of electrophysiological recordings, is not an issue in all-optical experiments. Most importantly, the intracellular milieu of the postsynaptic cell is not affected, permitting detection of subtle changes in protein concentration.

Two previous studies have established the tight correlation between lasting increases in spine volume and LTP of uncaging-evoked EPSPs (Matsuzaki et al., 2004; Harvey and Svoboda, 2007). Moreover, spine shrinkage was reported following the induction of long-term depression (Zhou et al., 2004). Here we report lasting spine volume increase following LTP induction by tetanic activation of Schaffer collaterals (**supplementary Fig. C5**) and in response to optical pairing (**Fig. C2 and C4**). To minimize photodamage

and bleaching in our pairing experiments, we used a relatively weak induction protocol (20 uncaging pulses at 0.1 Hz, 0.5 ms pulse duration, 3-5 postsynaptic APs) compared to previously used uncaging protocols (60 pulses at 1 Hz in zero  $Mg^{2+}$  solution (Matsuzaki et al., 2004); 30 pulses of 4 ms at 0.5 Hz,  $V_m = 0$  mV (Harvey and Svoboda, 2007)). As expected, our protocol induced lasting volume increases only in a subset of spines. This variability in the plasticity of CA3-CA1 connections was also apparent in our electrophysiological experiments using the same number and frequency of paired stimulations (**Fig. C1d**) and is consistent with previous studies (Petersen et al., 1998; Debanne et al., 1999; Zhang and Oertner, 2007). Since glutamate uncaging bypasses the presynaptic terminal, the differential sensitivity to optical pairing can be attributed to postsynaptic differences. We show that neither the initial spine volume nor the initial  $\alpha$ CaMKII concentration could be used to predict the response of a spine to pairing stimulation (**Fig. C4b,c**). Nevertheless, optical pairing provides the first non-invasive approach to investigate which biological parameters control the threshold for plasticity induction at individual synapses.

Translocation of  $\alpha$ CaMKII to postsynaptic sites has been previously reported after extracellular glutamate application or ‘chemical LTP’ (Shen and Meyer, 1999; Otmakhov et al., 2004; Merrill et al., 2005; Thalhammer et al., 2006). Here our goal was to investigate whether this enrichment is restricted to synapses that experience plasticity-inducing stimulation. We show that the concentration of  $\alpha$ CaMKII increased significantly only in those spines that underwent lasting volume changes (**Fig. C4**). High frequency synaptic stimulation (100 Hz, 1s) induced very similar increases in both soluble and

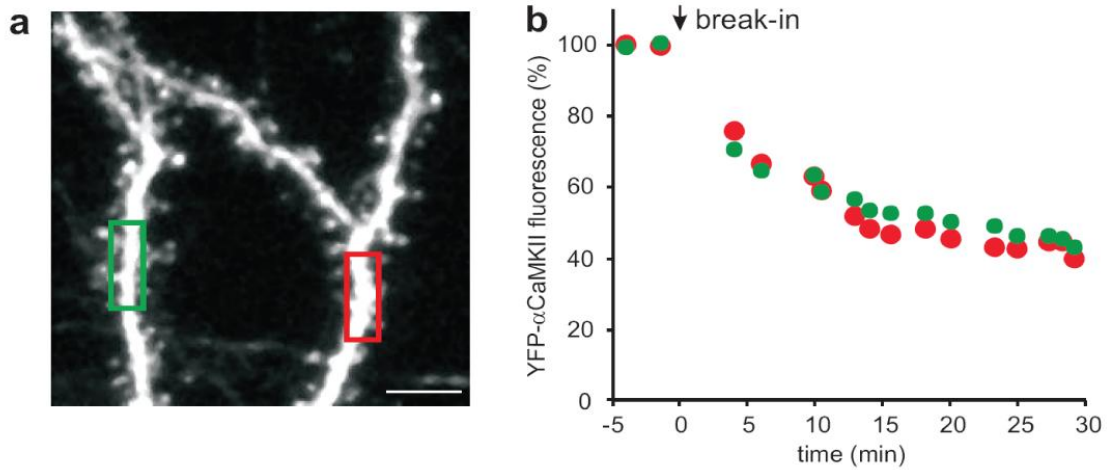
bound  $\alpha$ CaMKII (**supplementary Fig. C5**), indicating that  $\alpha$ CaMKII enrichment was not an artifact of uncaging stimulation. Spines that were not directly stimulated sometimes increased or decreased their volume spontaneously, but on average, no significant  $\alpha$ CaMKII loss or gain was detected. In a previous study, it has been shown that following plasticity induction at individual spines, the threshold for LTP induction is lowered in neighboring spines (Harvey and Svoboda, 2007). Although  $\alpha$ CaMKII can maintain its activation state for some time by autophosphorylation and is thus a potential candidate for a short-range communication system (Lisman and Zhabotinsky, 2001), we found no indication of functional crosstalk between neighboring spines on the level of  $\alpha$ CaMKII.

Given the time constant of  $\alpha$ CaMKII diffusion measured in our FRAP experiments ( $\tau = 12.5$  s), the  $\alpha$ CaMKII increase in the stimulated spines was surprisingly slow. In a recent study, a rapid increase in the diffusional resistance of the spine neck following paired stimulation was reported (Bloodgood and Sabatini, 2005), which could conceivably slow down diffusion of a large protein like CaMKII and thus limit the number of CaMKII molecules available for binding. A second possibility is the slow generation of additional binding sites for  $\alpha$ CaMKII by structural enlargement of the PSD in first 5-10 minutes following potentiation. Interestingly, a similarly protracted time course was reported for the AMPA receptor subunit GluR1 in a previous study, peaking 6 min after induction of chemical LTP (Kopec et al., 2006). The similar time course and the persistent, 2-fold increase in the amount of bound  $\alpha$ CaMKII we report here is consistent with a structural role of  $\alpha$ CaMKII in anchoring glutamate receptors to the postsynaptic density (Hayashi et al., 2000; Lisman and Zhabotinsky, 2001; Asrican et al., 2007). Under baseline

conditions, the *amount* of bound  $\alpha$ CaMKII correlates with spine size and synaptic strength, but the *ratio* between bound and soluble  $\alpha$ CaMKII does not (Asrican et al., 2007). This static picture can be understood in the light of our time resolved study, where we show that 30-40 min after the potentiation event, the equilibrium between bound and soluble  $\alpha$ CaMKII returned to values close to the baseline level, but the absolute amount of  $\alpha$ CaMKII in potentiated spines had doubled (**Fig. C4d, supplementary Fig. C5**). For the inhibition-deficient mutant TT305/6VA, we measured a significantly higher ratio of bound to soluble  $\alpha$ CaMKII (**Fig. C3d**), indicating that this ratio depends on the level of  $\alpha$ CaMKII activation in the spine. Recently, it has been demonstrated that LTP can be partially reversed by blocking CaMKII activity, providing evidence for its role in the maintenance of synaptic strength (Sanhueza et al., 2007). In summary, the insertion of additional AMPA receptors, which is the accepted structural correlate of LTP at Schaffer collateral synapses (Matsuzaki et al., 2004), seems to be linked with a lasting increase in spine volume and binding of additional  $\alpha$ CaMKII to postsynaptic sites. Here we show that these changes can be induced with single spine specificity, validating Hebb's postulate on the micrometer scale.



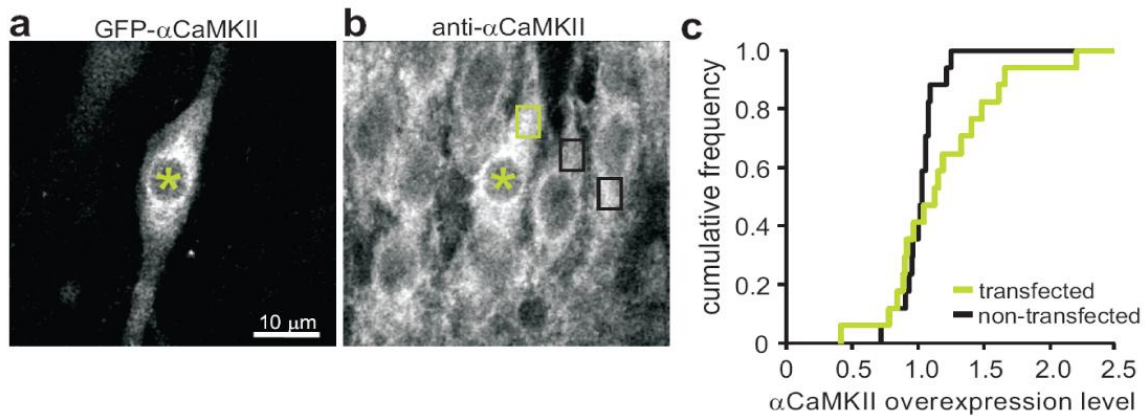
## SUPPLEMENTARY FIGURES



**Supplementary Figure C1. Example of CaMKII wash-out following whole-cell patch clamp.**

(a) Image of YFP-αCaMKII transfected cell before patch clamp. CA1 pyramidal cell, oblique dendrites. Scale bar: 5 μm.

(b) Decay of YFP-αCaMKII fluorescence in oblique dendrites after formation of the whole-cell configuration at  $t = 0$ .

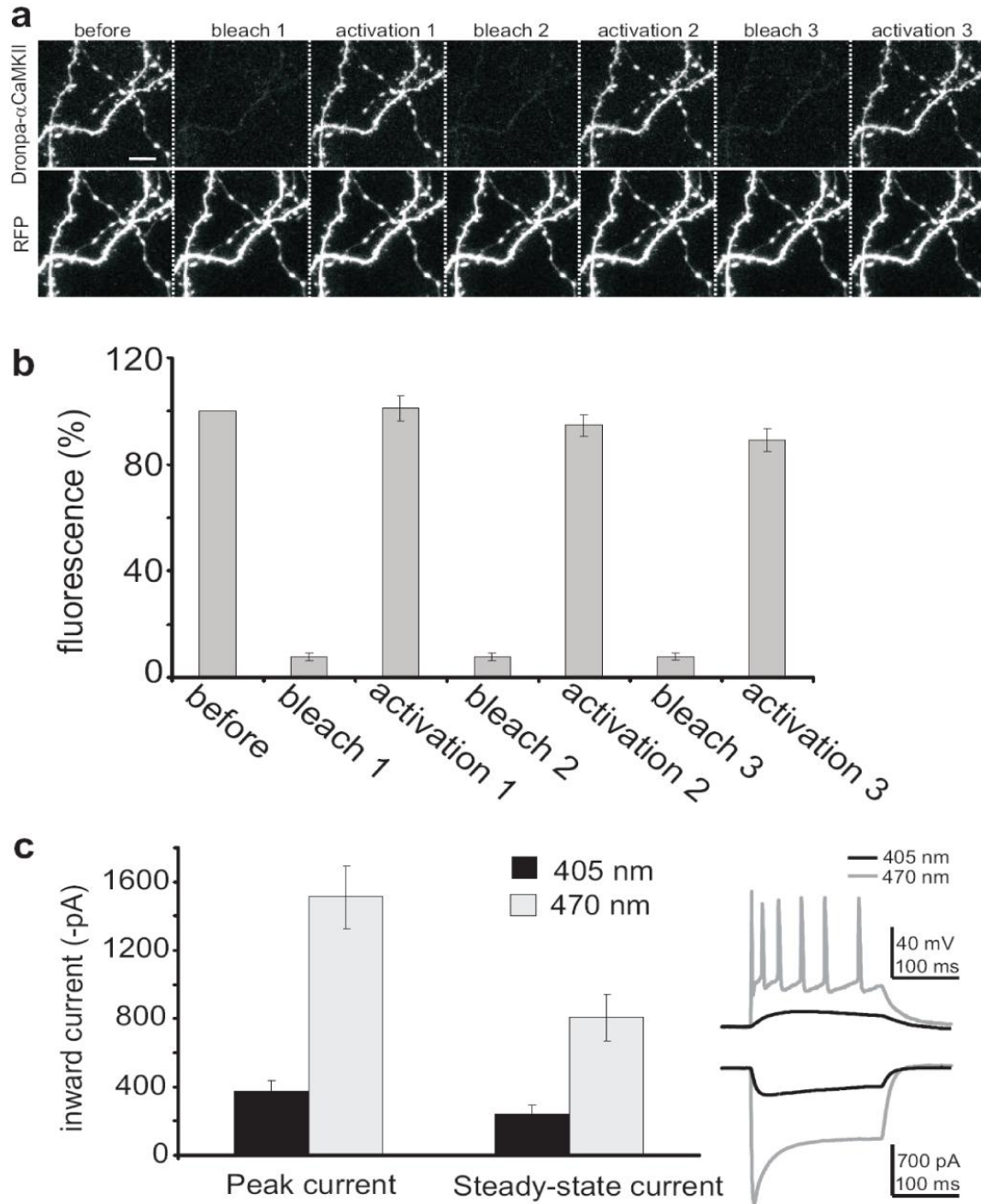


**Supplementary Figure C2. Estimating overexpression level of αCaMKII.**

(a) Fixed hippocampal slice culture with single neuron expressing GFP-αCaMKII.

(b) Same optical section showing immunofluorescence signal of anti-αCaMKII (red color channel). Transfected cell (asterisk) shows slightly elevated αCaMKII level in this example.

(c) Cumulative distribution of αCaMKII overexpression. Green curve: Overexpression level was calculated by taking the ratio of total immunofluorescence in a cytoplasmic region (endogenous plus recombinant αCaMKII) between transfected and non-transfected neurons.

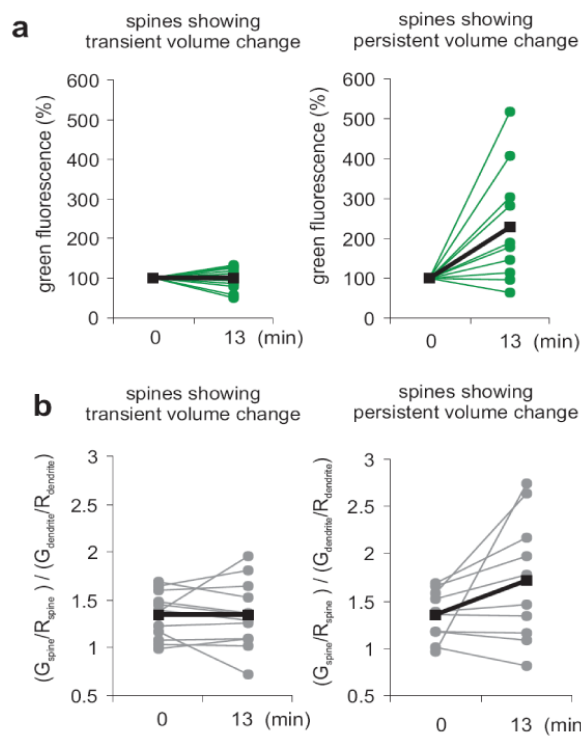


**Supplementary Figure C3. Reversible photoswitching of Dronpa- $\alpha$ CaMKII.**

(a) Simultaneous two-photon imaging of Dronpa- $\alpha$ CaMKII and RFP. Dronpa- $\alpha$ CaMKII fluorescence slowly bleaches at 500 nm, but can be reactivated by UV illumination (405 nm). Scale bar: 6  $\mu$ m.

(b) Quantification of Dronpa-CaMKII fluorescence recovery after full bleaching (1st recovery:  $101\% \pm 10\%$ , 2nd recovery:  $95\% \pm 9\%$ , 3rd recovery:  $89\% \pm 9\%$ ,  $n = 5$  cells).

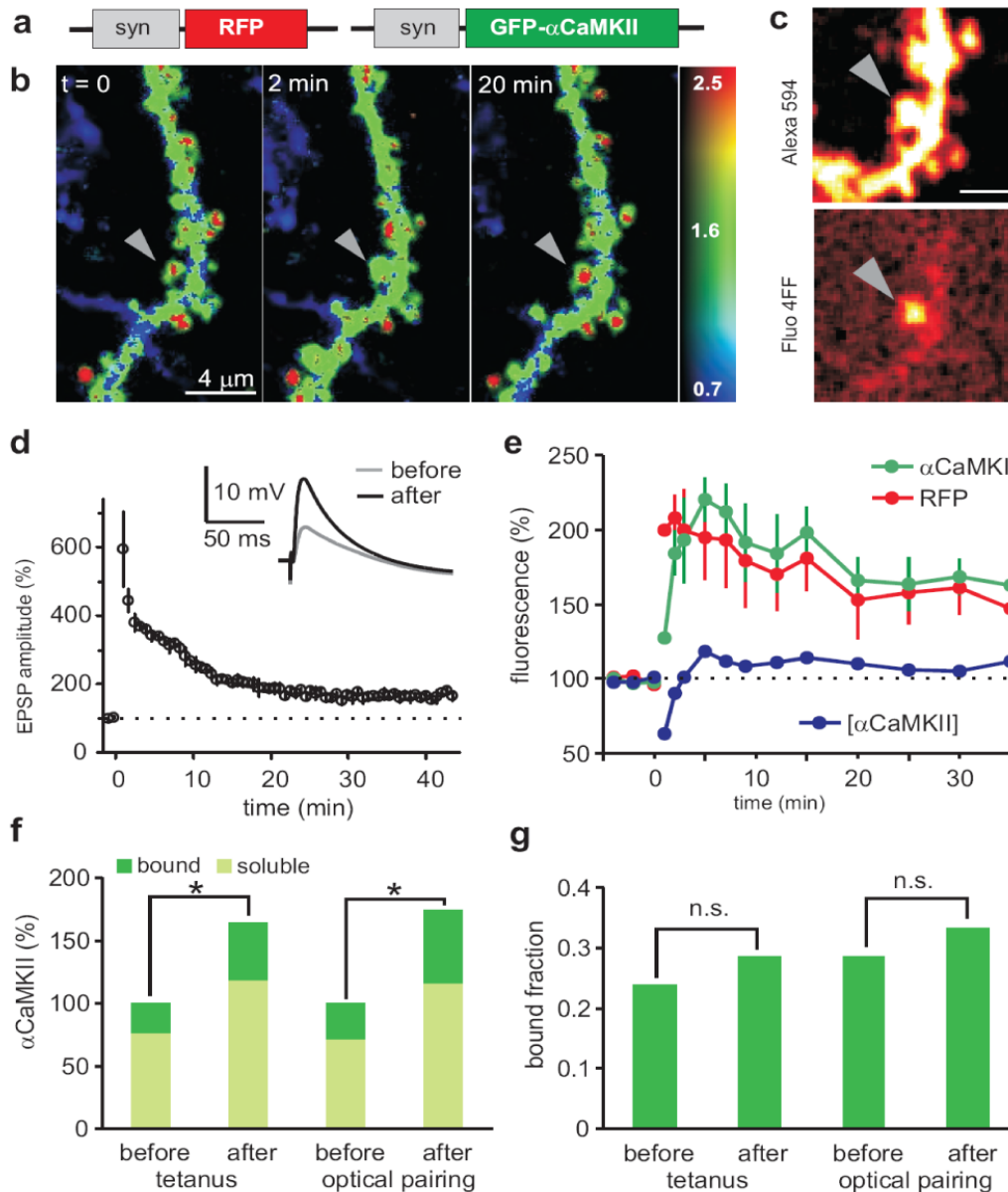
(c) Dronpa-reactivation (405 nm) caused small depolarizing current, but no spiking in ChR2-expressing cells.



**Supplementary Figure C4. Pairing-induced changes in  $\alpha$ CaMKII amount and CaMKII concentration.**

(a) Change in the total amount of Dronpa- $\alpha$ CaMKII (green fluorescence) in spines that showed a transient (left) or persistent change in volume (right) in response to optical pairing. Thick black lines: On average, the amount Dronpa- $\alpha$ CaMKII increased after stimulation to 101% and 230%, respectively.

(b) Concentration of Dronpa- $\alpha$ CaMKII (green / red fluorescence) in spines relative to the dendritic concentration. This measure (S/D ratio) is independent of spine volume changes. Average S/D ratio in spines with transient volume changes 1.34 (before pairing), 1.34 (13 min after pairing); spines with persistent volume changes 1.35 (before pairing), 1.72 (after pairing).



**Supplementary Figure C5. Input-specific accumulation of  $\alpha$ CaMKII induced by high frequency stimulation of Schaffer collaterals.**

(a) Schematic drawing of the two vectors used for double transfection by gene gun. Promoter denotes synapsin-I promoter.

(b) Ratio images of cells expressing YFP- $\alpha$ CaMKII and RFP before ( $t = 0$ ) and after (2 min, 20 min) repetitive stimulation of Schaffer collateral fibers at high frequency ( $3 \times 100$  Hz, 1 s, at 0.1 Hz). Warm colors indicate high CaMKII concentration. At  $t = 0$ , the high frequency protocol was applied. The spine marked by the arrow head was the stimulated spine, identified by post hoc calcium imaging.

(c) Post hoc identification of the stimulated spine using calcium imaging. Upper image: Alexa 594 fluorescence. Lower image: Fluo 4FF signal ( $\Delta f$ ) after synaptic stimulation at depolarized membrane potential (0 mV), indicating localized calcium influx at stimulated spine. Scale bar: 2  $\mu$ m.

(d) Tetanic stimulation induces LTP at Schaffer collateral synapses. Grey bar indicates high frequency stimulation ( $3 \times 1$  s, 100 Hz).

(e) Tetanic stimulation induces rapid spine volume increase (red curve) and delayed increase in total  $\alpha$ CaMKII (green curve) in the stimulated spines

(f) Tetanic stimulation leads to an increase in the total number of soluble and bound  $\alpha$ CaMKII molecules in the stimulated spines.

## **METHODS**

### **Plasmid construction**

ChR2-YFP, a gift from K. Deisseroth, was modified by inserting a stop codon (TAG) after amino acid 309 by PCR and inserted into a synapsin-I (syn) promoter vector (Kugler et al., 2001). The fragment of syn-ChR2-SV40-polyA was excised and inserted into a second expression vector containing syn-RFP (tdimer2, a dimeric red fluorescent protein from R.Y. Tsien), resulting in a single plasmid for neuron-specific co-expression of 2 proteins. GFP- $\alpha$ CaMKII (from T. Meyer) was subcloned into a separate syn promoter vector, and new  $\alpha$ CaMKII fusions were made by replacing GFP with YFP or Dronpa-Green (MBL, Naka-ku Nagoya, Japan). Mutant  $\alpha$ CaMKII (TTVA) was generated by site-directed mutagenesis (Thr<sup>305</sup>  $\rightarrow$  Val and Thr<sup>306</sup>  $\rightarrow$  Ala) using the QuickChange kit (Stratagene). All constructs were verified by DNA sequencing, amplified and purified using MaxiPrep Kits (Qiagen).

### **Slice culture and transfection**

Organotypic hippocampal slices were prepared as previously described. After 7 days in vitro, cultures were transfected with syn-ChR2-syn-RFP in combination with syn- $\alpha$ CaMKII fused to GFP, YFP, or Dronpa-Green, as previously described. All experiments were performed 2-3 weeks after transfection. At this time, total  $\alpha$ CaMKII in transfected pyramidal cells was increased by only ~12% relative to neighboring untransfected cells (**supplementary Fig. C2**).

### **Electrophysiology**

Hippocampal slice cultures were placed in the recording chamber of the microscope and superfused with artificial cerebrospinal fluid (ACSF) containing (in mM): 119 NaCl, 2.5 KCl, 4 CaCl<sub>2</sub>, 4 MgCl<sub>2</sub>, 26.2 NaHCO<sub>3</sub>, 1 NaH<sub>2</sub>PO<sub>4</sub>, 11 glucose. Single and dual whole-cell recordings were performed using Axopatch 200B and MultiClamp 700B amplifiers (Axon Instruments). Recording pipettes were filled with K-gluconate based intracellular solution containing (see section 4.A). LTP of unitary EPSCs was induced by repeatedly pairing (20 times, 0.1 Hz) presynaptic stimulation (2 nA, 5 ms) with a postsynaptic burst of 4-9 action potentials induced by blue light stimulation (200 ms). Glutamate uncaging

was performed as previously described. LTP of uncaging-evoked EPSCs was induced by repeatedly pairing (20 times, 0.1 Hz) uncaging of glutamate with blue light stimulation (200 ms) of the postsynaptic cell. For tetanic stimulation experiments, bipolar electrodes (FHC Inc., ME) were placed in *stratum radiatum* ~200  $\mu\text{m}$  lateral to the recording site, and 10  $\mu\text{M}$  bicuculline and 4  $\mu\text{M}$  2-chloroadenosine were added to the ACSF to facilitate LTP induction and avoid recurrent excitation. All recordings were performed at 30-32°C.

### Light stimulation

A blue LED (470 nm, Cairn Research Ltd.) was coupled into the epifluorescence pathway to deliver light pulses for ChR2 activation. Two PMTs below the condenser were used to detect red and green emission. During the blue light pulse, they were protected by a VS25 shutter (Vincent Associates).

### Spine volume measurements

Spine volume measurements were performed as previously described (section 4.A).

### Image analysis

Off-line analysis was performed using custom routines written in Matlab. We used the ratio of green/red fluorescence ( $G/R$ , or  $Y/R$  in case of YFP- $\alpha\text{CaMKII}$ ) as a measure of  $\alpha\text{CaMKII}$  concentration. We verified that no pixel in either channel was saturated. To display ratio images, we used a hue/saturation/brightness color model, where hue was determined by the  $G/R$  ratio of every pixel (using a rainbow color table), and brightness was set by the intensity in the red (volume) channel. For quantitative analysis, we calculated the  $G/R$  ratio in a region of interest after subtraction of background fluorescence and optical crosstalk. To compensate for differences in the relative expression levels of the two constructs in different cells, we normalized the  $G/R$  ratio in the spine by the  $G/R$  ratio in the dendrite to get the spine/dendrite ( $S/D$ ) ratio

$$S / D = \frac{G_{\text{spine}} / R_{\text{spine}}}{G_{\text{dendrite}} / R_{\text{dendrite}}} = \frac{[\text{CaMKII}]_{\text{spine}}}{[\text{CaMKII}]_{\text{dendrite}}} \quad (\text{Eq. 1})$$

To calculate the bound fraction from the  $S/D$  ratio, we assumed that the concentration difference between spine and dendrite was due to bound CaMKII in the spine:

$$[CaMKII]_{spine,bound} = [CaMKII]_{spine} - [CaMKII]_{dendrite} \quad (\text{Eq. 2})$$

$$[CaMKII]_{spine,bound} = [CaMKII]_{spine} - \frac{[CaMKII]_{spine}}{S/D} \quad (\text{Eq. 1 in 2})$$

or, expressed as a fraction of total  $[CaMKII]_{spine}$

$$[CaMKII]_{spine,bound} = 1 - \frac{1}{S/D} \quad (\text{Eq. 3})$$

Average values are given as mean  $\pm$  SEM if not indicated otherwise. Significance was defined as  $p < 0.05$  and determined using Student's  $t$  test (two-tailed) if not indicated otherwise.

## **5. GENERAL CONCLUSIONS AND OUTLOOK**

### **5.1 Microanatomy regulates synaptic function and plasticity**

We have shown that the differential subsynaptic distribution of an organelle can regulate the potential for synaptic plasticity at individual synapses. We provide evidence for the existence of defined subpopulations of synapses in regard to their potential for a specific form of synaptic plasticity.

#### **-Dynamic ER distribution as a major metaplasticity mechanism**

We found that the ER is preferentially localized to big spines containing strong synapses and locally regulates the potential for synaptic depression. LTP leads to an increase in volume of the spine containing the potentiated synapse (Matsuzaki et al., 2004; Harvey and Svoboda, 2007). Together these findings suggest that the ER actively moves into potentiated spines. Although this hypothesis remains to be tested, dynamic and regulated spine ER distribution could represent a powerful mechanism for synaptic metaplasticity.

The ER has been shown to be dynamic (Toresson and Grant, 2005). However, whether ER dynamics is regulated in an activity dependent way and whether LTP induction leads to ER dynamics is unknown. Delivery of ER to spines could be under the control of specific signaling molecules.

Spine ER has been shown to be tightly associated to the actin cytoskeleton (Capani et al., 2001). Proteins such as synaptopodin, which are closely associated with spine ER, also bind to actin (Deller et al., 2000; Asanuma et al., 2005). LTP leads to increased synaptopodin expression and synaptopodin concentration at synaptic sites (Yamazaki et al., 2001). Actin is a key cytoskeletal protein required for the induction of LTP (Kim and Lisman, 1999; Krucker et al., 2000) and stimuli inducing LTP have been demonstrated to induce actin polymerization and accumulation in the spine (Okamoto et al., 2004; Honkura et al., 2008). These cytoskeletal rearrangements could be associated with ER dynamics and regulate ER delivery during LTP inducing stimuli. Another candidate for the regulation of spine ER dynamics is Myosin Va. This protein has been shown to regulate spine ER distribution in the cerebellum (Dekker-Ohno et al., 1996). Myosin Va



is activated in a calcium dependent manner and could therefore be activated following LTP inducing stimuli (Homma et al., 2000). In the hippocampus Myosin Va has been involved in the delivery of AMPA receptors following the induction of LTP (Correia et al., 2008). This protein, in parallel of regulating receptor delivery, could play a major role in regulating spine ER delivery.

In contrast to LTP inducing stimuli, stimuli which induce synaptic depression could lead to ER loss from spines (Ng and Toresson, 2008). The possibility that subsynaptic ER dynamically follows the state of a synapse is intriguing and remains to be tested.

#### -mGluR dependent depression as a regulator for synaptic weight distribution

We found that the ER is preferentially localized to spines containing strong synapses. We consider these spines as a functionally distinct group of spines, containing a specialized machinery required for mGluR dependent synaptic depression. It is conceivable that strong synapses need a mechanism to limit their maximum strength or a mechanism which allows them to be weakened in response to new experience (Song et al., 2000; van Rossum et al., 2000; Holtmaat et al., 2006; Knott et al., 2006). The mechanism we describe could be the process regulating both requirements.

If mGluR dependent synaptic depression is the process regulating the upper limit a synapse can reach in its strength, blockade of postsynaptic mGluR→IP3 signaling would lead to a bimodal distribution of synaptic weights: strong synapses, which generate spikes with a higher probability compared to weak synapses, would get even stronger through hebbian mechanisms of synaptic potentiation (Song et al., 2000). This hypothesis could be tested by inducing synaptic potentiation in the presence of blockers of the mGluR→IP3 pathway; under these conditions LTP should be facilitated and, over a prolonged period of time, lead to a bimodal distribution in synaptic weights. Using electrophysiological approaches, it has been shown that pharmacological blockade of group I mGluRs or postsynaptic IP3 receptors leads to facilitated LTP (Nishiyama et al., 2000). Although the exact location of the involved receptors has not been assessed, it is

plausible that blockade of the depressing mGluR→IP3 pathway in ER containing spines is responsible for the increased potentiation.

In addition to setting an upper limit to synaptic strength, spine ER could also be required for weakening of strong synaptic connections in response to new experience (Holtmaat et al., 2006; Knott et al., 2006). We have shown that strong synapses, containing ER, in the absence of stabilizing stimuli (such as for example coincident activity), undergo mGluR dependent LTD. It is possible that the mechanism we describe is the basis for the loss of initially stable contacts in response to new experience.

#### -The ER as a general regulator of plasticity

We show that the ER regulates synaptic depression on the level of individual synapses. In previous studies, using electrophysiological approaches, it has been shown that calcium release from the ER also regulates the potential for synaptic potentiation: blockade of ER calcium release increases the amount of potentiation following an LTP inducing stimulus (Nishiyama et al., 2000). However, it is unknown, whether also this phenomenon is regulated at individual synapses. It is plausible that the ER localized to spines containing strong synapses, inhibits their potential to undergo synaptic potentiation. This negative regulation could involve the activation of the depressing mGluR→IP3 pathway (see previous section) or other pathways, such as calcium induced calcium release during the LTP stimulus (Nishiyama et al., 2000). It is conceivable that ER-containing spines are preferential sites for depression and ER-lacking spines preferential sites for potentiation. This hypothesis has to be tested but its eventual confirmation could shed light on the mechanism for the differential regulation of plasticity and stability at single synapses.

#### -Possible heterosynaptic spread of mGluR dependent LTD

We provide strong evidence that mGluR→IP3 mediated calcium release from the ER represents a key trigger for LTD. We show that these signals originate in the stimulated spine but can spread to the parent dendrite and possibly to neighboring synapses. The potential spread to neighboring synapses could represent a mechanism for the heterosynaptic spread of plasticity.

Several reports provided evidence that LTD can spread from activated to neighboring synapses, this heterosynaptic spread of LTD seems to be dependent on calcium release from the ER (Nishiyama et al., 2000; Daw et al., 2002). Inhibition of IP3 receptors has been shown to block heterosynaptic LTD (Nishiyama et al., 2000). Blockade of phosphatidylinositol 3 kinase (PI3K), an enzyme involved in the phosphorylation of phosphoinositide lipids (among others, PIP2, a precursor of IP3) leads to increased heterosynaptic LTD (Daw et al., 2002).

These studies point to a key regulatory role for phosphoinositide lipids and IP3 mediated signals in regulating heterosynaptic plasticity. The calcium release signals we observed could represent a powerful intersynaptic signaling mechanism to dynamically regulate and reciprocally tune synaptic weights on the same dendritic branch.

#### -ER calcium release as a homeostatic mechanism

We provide evidence that mGluR dependent calcium release from subsynaptic ER is a key trigger for the induction of synaptic depression. Previous studies have shown that ER calcium release depends on the filling state of the ER: high ER calcium content leads to more frequent calcium release compared to situations with low ER calcium content. ER calcium content is thought to be dependent on cell activity: the more active a cell, the more calcium flows into the cytoplasm through voltage gated channels in the cell membrane, the more calcium gets pumped into the ER (Berridge, 1998; Rae et al., 2000; Hong and Ross, 2007).

The depressing mechanism we describe could strongly be dependent on cell activity and ER calcium content and act as a homeostatic mechanism. In conditions where a cell is hyperactive, activation of mechanisms inducing synaptic depression would reduce the strength of synaptic inputs and therefore counterbalance cell hyperactivity. Increased mGluR dependent calcium release and synaptic depression would reduce cell firing through a selective reduction of synaptic strength at strong synapses.

#### -Possible modulation of mGluR→IP3 pathway

We show that only ER containing spines are capable of delayed, mGluR mediated calcium release. About 40% of the analyzed ER-containing spines showed this type of response. The high variability between spines and between trials on the same spine possibly reflects differences in the activation of signaling molecules involved in the mGluR→IP3 pathway or differences in ER calcium content. It has been shown that Homer proteins dramatically influence mGluR dependent signaling and plasticity (Kammermeier and Worley, 2007; Ronesi and Huber, 2008). Also G-proteins have been shown to be key factors regulating mGluR mediated signals (Kleppisch et al., 2001; Hartmann et al., 2004). Differences in the concentration of these or other factors could profoundly modulate the occurrence and frequency of delayed calcium transients, providing the basis for the modulation of the depressing mechanism at different levels.

#### -Spine ER and protein handling

We show that spine ER plays a crucial role in regulating spine calcium signals. In addition to this function, the ER could also play a major role in regulating synthesis, modification and delivery of proteins. Although extrasomatic ER is thought to be mostly smooth, the occurrence of rough ER in a subset of spines has been demonstrated (Pierce et al., 2000). This ER could regulate synapse-specific protein synthesis. Interestingly, mGluR dependent LTD has been shown to be dependent on local protein synthesis (Huber et al., 2000). The ER, in addition to trigger depression through calcium release, could play a major role in regulating the synapse-specific delivery of new proteins. Other forms of long term plasticity have been shown to be dependent on protein synthesis and it is an intriguing hypothesis that spine ER represents the structural basis for the specific delivery of new proteins to modified synapses.

## 5.2 Impact of spine neck on synaptic signals

We have shown that the coupling between spine head and parent dendrite can change in an activity dependent way. Strong insulation leads to electrical compartmentalization of dendritic spines. We therefore demonstrate how spine morphology dramatically affects the function of dendritic spines. We show that spine calcium signals are dependent on spine head depolarization and differential activation of voltage sensitive channels.

### -Spines can be electrical compartments

It is highly debated whether spines can be considered electrical compartments (Bourne and Harris, 2008; Spruston, 2008). A critical parameter determining the potential for electrical compartmentalization is the resistance of the spine neck. Different groups provided different estimates for spine neck resistances, laying between 4 and 1200 M $\Omega$  (Harris and Stevens, 1989; Svoboda et al., 1996; Bloodgood and Sabatini, 2005). Recently, studies using 2-photon uncaging of glutamate provided first evidence that spines can depolarize enough to allow activation of different classes of voltage dependent channels in response to stimulation (Ngo-Anh et al., 2005; Araya et al., 2007; Bloodgood and Sabatini, 2007b). However, it remains unclear if spine depolarization is sufficiently high to allow electrical compartmentalization in response to presynaptic release of single vesicles of glutamate.

Using electrical stimulation of presynaptic afferents and single spine calcium imaging as a reporter for NMDA receptor activation and spine head depolarization, we show that dendritic spines can be electrical compartments. In acute slices, after a depolarizing voltage pulse, the diffusional coupling between spines and their parent dendrite is low. Under these conditions spine head depolarization in response to single afferent stimulation is dramatically high and leads to unblocking of NMDA receptors and activation of voltage dependent channels. We show that *in vivo* a large fraction of spines are more isolated from their parent dendrite compared to the situation *in vitro*. These finding suggests that in the living animal a large fraction of spines can be considered electrical compartments.

#### -Spine neck plasticity as a metaplasticity mechanism

Using diffusional measurements between spine and parent dendrite, we have shown that spine neck resistance is highly plastic. We show that an increase in spine neck resistance leads to enhanced biochemical and electrical compartmentalization of synapses. This has important consequences for the regulation of the potential of a given synapse to undergo synaptic plasticity. Increased biochemical compartmentalization leads to a longer residence time of activated enzymes and second messengers in the stimulated spine (Bloodgood and Sabatini, 2005; Noguchi et al., 2005; Gray et al., 2006). Increased electrical compartmentalization leads to activation of more voltage dependent channels, stronger spine depolarization and consequently increased calcium influx into the spine. The amplitude of calcium signals has been shown to be correlated with the magnitude of change in synaptic strength (Nevian and Sakmann, 2006). Increased spine neck resistance could therefore drastically facilitate or even be a prerequisite for the induction of LTP.

#### -Spine neck plasticity and implications for synaptic crosstalk

We show that postsynaptic depolarization or cell spiking can lead to a dramatic increase in spine neck resistance. Pharmacological experiments showed that this increase is not dependent on activation of postsynaptic glutamate receptors but depends on postsynaptic calcium influx. It is conceivable that different stimuli which lead to postsynaptic calcium transients such as backpropagating action potentials, calcium release waves or dendritic spikes, lead to an increase in spine neck resistance at sites experiencing high calcium concentrations (Nakamura et al., 1999; Schiller and Schiller, 2001). These phenomena could lead to a clustering of spines with similar spine neck resistance. A change in spine neck resistance likely affects the potential for the induction of synaptic plasticity (see previous section). The eventual clustering of synapses with high spine neck resistances would represent a new metaplasticity mechanism for synaptic crosstalk and for reciprocal tuning of synaptic weights between neighbors. Although evidence for a clustering of spines with similar neck resistances or synaptic weights is missing, there is growing evidence for the existence of a high degree of crosstalk between neighboring synapses (Losonczy and Magee, 2006; Harvey and Svoboda, 2007; Losonczy et al., 2008). Spine

neck plasticity on the level of individual dendritic branches could be a main mechanism leading to reciprocal tuning of properties between neighboring synapses.

### 5.3 CaMKII accumulation is input specific

We show that single spine induction of LTP leads to spine enlargement and to the input-specific accumulation of the plasticity related protein CaMKII.

#### -New optical approach for the induction of LTP at identified synapses

We used a new optical approach to induce LTP at single synapses and monitor changes in protein concentration in individual spines. We combined single spine 2-photon glutamate uncaging with Channelrhodopsin-mediated depolarization of the postsynaptic cell. Channelrhodopsin, a light gated cation channel, can be activated by blue light and allows millisecond precise control of cell activity (Boyden et al., 2005). Pairing of glutamate uncaging and activation of Channelrhodopsin, allowed us to non-invasively mimic a conventional protocol for coincident activity. Two-photon imaging of fluorescently tagged proteins allowed us to measure protein dynamics with high spatial and temporal resolution.

The main advantage of our technique is that it is completely non-invasive. In contrast to other LTP protocols, where cell patching or alteration of the extracellular milieu is required, our protocol does not affect cell viability (Matsuzaki et al., 2004; Harvey and Svoboda, 2007). Our protocol, in principle, allows long-term imaging of potentiated synapses over several days or weeks.

#### -CaMKII accumulation is input specific

Using our optical approach to induce plasticity at single visualized synapses, we showed that CaMKII accumulates at stimulated spines with no change in concentration in neighboring spines. This result provides the first evidence that key enzymes regulating the induction of synaptic plasticity can be tagged to individual synapses. CaMKII seems to be a key molecule involved in the regulation of plasticity at synapses experiencing coincident activity. At present, we have no evidence for the possible involvement of CaMKII in regulating synaptic crosstalk (Harvey and Svoboda, 2007). We think that individual synapses represent the minimal computational units and can be independently modulated.



#### -The need for protein activity sensors

In recent years FRET sensors have been developed to assess the specific kinetics of activated second messengers ((Ting et al., 2001; Heim and Griesbeck, 2004; Okamoto et al., 2004; Pologruto et al., 2004; Yasuda et al., 2006; Harvey et al., 2008). Using fluorescently labeled CaMKII, we show that this protein can be specifically tagged to individual stimulated synapses. It would be of central importance to know how long and under which conditions the protein remains in its activated state. The spine neck represents a powerful barrier to biochemically isolate dendritic spines from their parent dendrite, allowing synapse specific activation of enzymes and second messengers (Bloodgood and Sabatini, 2005; Noguchi et al., 2005). The strength of this barrier depends on the kinetics of the activated enzymes: enzymes with a relatively slow inactivation kinetic are more prone to spread to the dendrite in their activated state compared to proteins with fast kinetics. It has been shown that Ras, a small GTPase, gets activated in individual spines and spreads to neighboring spines to regulate the potential for plasticity (Harvey et al., 2008). It is plausible that CaMKII only affects stimulated synapses because its activity has faster kinetics. It is also possible that the enzyme gets trapped to the stimulated spine by specific adaptor proteins (Gray et al., 2006).

#### 5.4 Concluding remarks

In the present dissertation we show that live imaging of single synapse represents a powerful tool for studying synaptic physiology. The understanding of how biochemical and electrical signaling at the level of single synapses or groups of synapses can regulate neuronal computation is of central importance. Single synapse imaging and stimulation uncovered new forms of synaptic plasticity and neuronal computation. In contrast to pure electrophysiological recordings, live imaging allows to visualize the subcellular specificity and the time course of signaling cascades and the structural modifications involved in synaptic plasticity. Live cell imaging and single synapse stimulation allowed us to describe the existence of defined subpopulations of synapses in regard to their potential for plasticity. It also allowed us to describe the existence of important metaplasticity mechanisms operating at the level of single dendritic spines.

## **6. APPENDIX:**

### **Two photon glutamate uncaging – practical considerations**

Two photon glutamate uncaging opens a new avenue for studying synaptic physiology at the level of single synapses or groups of synapses. This technique consists in the focal activation (uncaging) of glutamate from an inactive precursor molecule by a two photon laser. The uncaged glutamate mimics glutamate released by a presynaptic terminal and activates receptors on the postsynaptic cell.

#### **Optical table**

To allow simultaneous two photon uncaging and two photon imaging, two Ti-Sapphire lasers have to be combined and aligned. One laser is used for imaging (typical wavelength used: 800-980 nm), the other for uncaging (typical wavelength used: 720-730 nm). Electro-optical modulators (EOMs) allow precise and independent control of pulse duration and laser power. The lasers are combined using a polarizing beam-splitting cube. For rough laser alignment, removable pinholes or targets are placed after the beam-splitting cube. Mirrors in one or both laser lines allow spatial adjustments of the laser beam and superposition of the two lasers on the targets. For definitive alignment, excitation of small fluorescent structures in the focal plane has to be used. By using both lasers to image the same structure and by adjusting the laser lines in order to superimpose the two images independently given by the two lasers, fine alignment can be achieved.

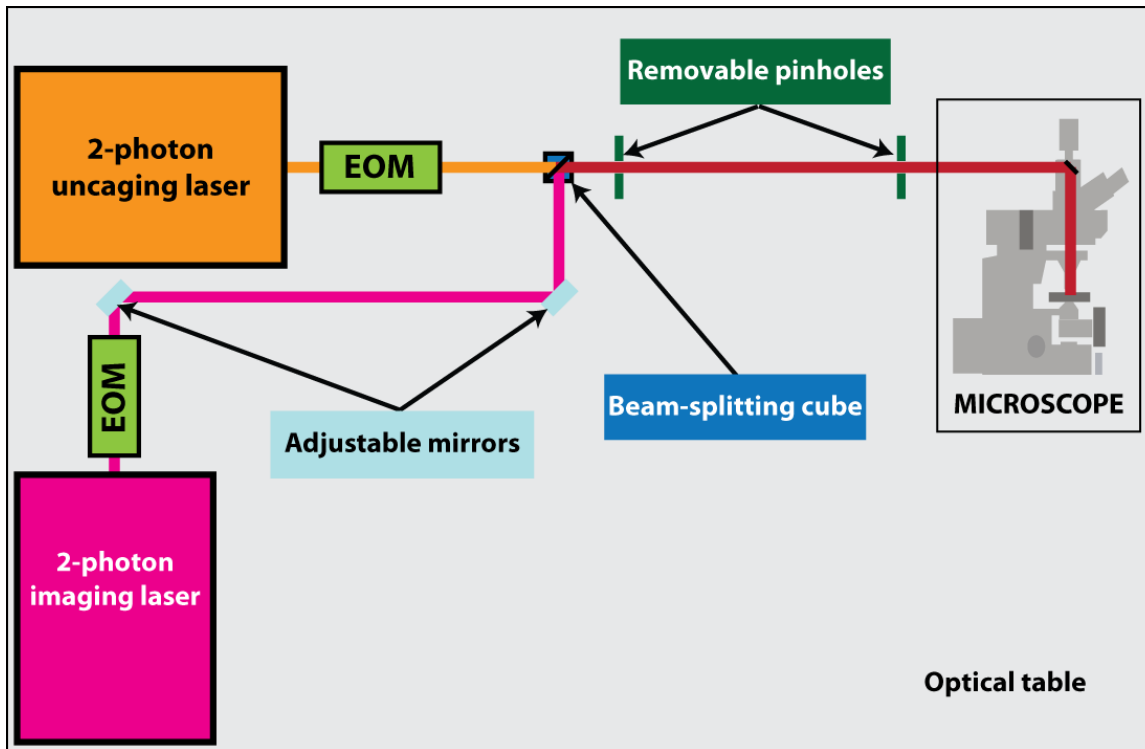


**Figure 6.1. Optical table for combined two-photon imaging and uncaging.**

*The outputs of two Ti:Sapphire lasers are combined with polarizing optics (beam-splitting cube). Electro-optical modulators (EOM) allow independent control of laser power and pulse duration. For laser alignment, removable pinholes or targets are inserted after the beam splitting cube. Adjustable mirrors allow control of laser beam spatial orientation.*

### Minimizing the uncaging volume

The use of a two-photon laser allows uncaging of glutamate in a relatively small volume. The focal volume where glutamate is uncaged is proportional to the size of the point spread function of the microscope (PSF,  $\sim 1 \mu\text{m}^3$ ). To best mimic glutamate released by a single synaptic vesicle (vesicle size:  $\sim 40 \text{ nm}$ ), the smallest possible uncaging volume has to be used. Minimizing the size of the PSF represents a key step for physiological uncaging. The size of the PSF can be minimized using relatively short wavelengths for uncaging (around  $720 \text{ nm}$ ), a high NA objective and overfilling the objectives back focal plane. Minimizing the size of the PSF also allows the use of lower average laser powers per uncaging event, minimizing photodamage and phototoxicity.

### Optimizing pulse duration

To mimic the nearly instantaneous release of glutamate from a presynaptic terminal, a relatively short uncaging pulse has to be used. However, shortening pulse duration leads to the need of higher laser power for uncaging. Similar to two-photon excitation, the amount of two photon uncaging events scales linearly with pulse duration and exponentially with pulse power. In order to reconcile short pulse duration with minimal photodamage and phototoxicity, pulse duration and laser power have to be carefully tuned. Optimal uncaging conditions (with 5 mM bath-applied caged glutamate) are achieved with pulse durations of 0.5-1 ms and average laser powers of 40-50 mW (measured in the back focal plane).

### Application of caged glutamate

Caged glutamate can be applied locally, through a pipette or bath-applied at a desired concentration. Because of the high cost of caged glutamate, local application has the advantage of being the cheaper solution, however, in contrast to bath-application, the concentration of the compound can not be precisely set. An optimal compound concentration for bath-application is 5mM. This concentration allows the use of relatively short and low-power laser pulses.

### Perfusion system

To minimize costs, a small total volume of ACSF with caged glutamate has to be used (5-6 ml). The solution can be bubbled and eventually heated in a small reservoir; the reservoir can be connected to the recording chamber through ultra-thin tubing, to minimize the needed amount of solution. The solution can be recycled and used for up to 20 hours. In order to keep the osmolarity constant during the experiment, the evaporated water has to be replaced. Calibration experiments can be performed to assess the evaporation rate and special syringe pumps can be used to replace the evaporated solution. With 6 ml total volume, heated to 32 °C, the evaporation rate is about 0.3 ml/hour.

### Calibrating the uncaging laser power

Although the laser power can be set to be constant in the back focal plane, the actual amount of photons reaching the sample depends on several factors. Differences in sample depth or refractory index of the slice lead to differences in the amount of absorbed and scattered photons on the way to the sample. These differences lead to variability in the amount of uncaged glutamate, even if the laser power in the back focal plane is kept constant. Because of these reasons, it is important to normalize and calibrate the laser power used for uncaging at the sample plane. A valuable method to standardize the laser power delivered at the focal plane consists in setting the power in order to bleach a constant fraction of a fluorophore in the plane of interest (Bloodgood and Sabatini, 2007b). If laser power is adjusted in order to bleach a constant fraction of fluorophore, differences in sample depth and refractory index between experiments have no influence on the amount of uncaged glutamate.

### Minimizing tissue damage

In two photon imaging and uncaging, photobleaching, phototoxicity and overheating effects have to be taken into account. The relatively long imaging windows used to characterize uncaging evoked responses and the uncaging pulse itself can lead to sample damage. Care has to be taken in order to minimize the laser power used for imaging, trials have to be spaced apart ( $\sim 0.03$  Hz for calcium imaging) and, if high frequency uncaging is required, the imaging laser has to be shuttered whenever possible.

### Limitations of the technique

Although two photon uncaging of glutamate represents an extremely powerful technique to unravel synaptic physiology, several limitations must be considered. Uncaging of glutamate circumvents the need of stimulating presynaptic afferents; the observed effects are purely postsynaptic. This fact can be advantageous if the investigator is interested in isolating and characterizing postsynaptic signals. However, it has to be kept in mind that half of the actual synapse is circumvented. All presynaptic effects and effects depending on reciprocal presynaptic-postsynaptic signaling are absent. In addition to that, postsynaptic responses purely depend on the amount of uncaged glutamate. Calibration

experiments need to be performed to reach physiological response amplitude and time course. Another limitation is that the volume where glutamate is uncaged is relatively large compared to the volume of a synaptic vesicle, this can result in differences in the microdomains where glutamate is active and stimulation of a different set of receptors. A key experiment, which remains to be performed, is the stimulation of the same synapse using glutamate uncaging and conventional electrical stimulation of presynaptic afferents.



## **7. REFERENCES**

- Abraham WC (2008) Metaplasticity: tuning synapses and networks for plasticity. *Nat Rev Neurosci* 9:387.
- Adesnik H, Nicoll RA, England PM (2005) Photoinactivation of native AMPA receptors reveals their real-time trafficking. *Neuron* 48:977-985.
- Amaral DG, Witter MP (1989) The three-dimensional organization of the hippocampal formation: a review of anatomical data. *Neuroscience* 31:571-591.
- Ando R, Mizuno H, Miyawaki A (2004) Regulated fast nucleocytoplasmic shuttling observed by reversible protein highlighting. *Science* 306:1370-1373.
- Araya R, Eiselthal KB, Yuste R (2006a) Dendritic spines linearize the summation of excitatory potentials. *Proc Natl Acad Sci U S A* 103:18799-18804.
- Araya R, Jiang J, Eiselthal KB, Yuste R (2006b) The spine neck filters membrane potentials. *Proc Natl Acad Sci U S A* 103:17961-17966.
- Araya R, Nikolenko V, Eiselthal KB, Yuste R (2007) Sodium channels amplify spine potentials. *Proc Natl Acad Sci U S A* 104:12347-12352.
- Asanuma K, Kim K, Oh J, Giardino L, Chabanis S, Faul C, Reiser J, Mundel P (2005) Synaptopodin regulates the actin-bundling activity of alpha-actinin in an isoform-specific manner. *J Clin Invest* 115:1188-1198.
- Asrican B, Lisman J, Otmakhov N (2007) Synaptic strength of individual spines correlates with bound  $Ca^{2+}$ -calmodulin-dependent kinase II. *J Neurosci* 27:14007-14011.
- Balschun D, Wolfer DP, Bertocchini F, Barone V, Conti A, Zuschratter W, Missiaen L, Lipp HP, Frey JU, Sorrentino V (1999) Deletion of the ryanodine receptor type 3 (RyR3) impairs forms of synaptic plasticity and spatial learning. *Embo J* 18:5264-5273.
- Banker G, Churchill L, Cotman CW (1974) Proteins of the postsynaptic density. *J Cell Biol* 63:456-465.
- Bayer KU, LeBel E, McDonald GL, O'Leary H, Schulman H, De Koninck P (2006) Transition from reversible to persistent binding of CaMKII to postsynaptic sites and NR2B. *J Neurosci* 26:1164-1174.
- Bear MF, Malenka RC (1994) Synaptic plasticity: LTP and LTD. *Current Opinion in Neurobiology* 4:389-399.
- Bear MF, Cooper LN, Ebner FF (1987) A physiological basis for a theory of synapse modification. *Science* 237:42-48.
- Bender VA, Bender KJ, Brasier DJ, Feldman DE (2006) Two coincidence detectors for spike timing-dependent plasticity in somatosensory cortex. *J Neurosci* 26:4166-4177.
- Berridge MJ (1998) Neuronal calcium signaling. *Neuron* 21:13-26.
- Bi G, Poo M (2001) Synaptic modification by correlated activity: Hebb's postulate revisited. *Annu Rev Neurosci* 24:139-166.
- Biess A, Korkotian E, Holcman D (2007) Diffusion in a dendritic spine: the role of geometry. *Phys Rev E Stat Nonlin Soft Matter Phys* 76:021922.
- Bliss TV, Collingridge GL (1993) A synaptic model of memory: long-term potentiation in the hippocampus. *Nature* 361:31-39.



- Bloodgood BL, Sabatini BL (2005) Neuronal activity regulates diffusion across the neck of dendritic spines. *Science* 310:866-869.
- Bloodgood BL, Sabatini BL (2007a) Regulation of synaptic signaling by postsynaptic, non-glutamate receptor ion channels. *J Physiol*.
- Bloodgood BL, Sabatini BL (2007b) Nonlinear Regulation of Unitary Synaptic Signals by CaV(2.3) Voltage-Sensitive Calcium Channels Located in Dendritic Spines. *Neuron* 53:249-260.
- Bloodgood BL, Sabatini BL (2007c) Ca(2+) signaling in dendritic spines. *Curr Opin Neurobiol*.
- Bortolotto ZA, Fitzjohn SM, Collingridge GL (1999) Roles of metabotropic glutamate receptors in LTP and LTD in the hippocampus. *Curr Opin Neurobiol* 9:299-304.
- Bourne J, Harris KM (2007) Do thin spines learn to be mushroom spines that remember? *Curr Opin Neurobiol* 17:381-386.
- Bourne JN, Harris KM (2008) Balancing structure and function at hippocampal dendritic spines. *Annu Rev Neurosci* 31:47-67.
- Boyden ES, Zhang F, Bamberg E, Nagel G, Deisseroth K (2005) Millisecond-timescale, genetically targeted optical control of neural activity. *Nat Neurosci* 8:1263-1268.
- Brocher S, Artola A, Singer W (1992) Intracellular injection of Ca<sup>2+</sup> chelators blocks induction of long-term depression in rat visual cortex. *Proc Natl Acad Sci U S A* 89:123-127.
- Burnashev N, Monyer H, Seeburg PH, Sakmann B (1992) Divalent ion permeability of AMPA receptor channels is dominated by the edited form of a single subunit. *Neuron* 8:189-198.
- Capani F, Martone ME, Deerinck TJ, Ellisman MH (2001) Selective localization of high concentrations of F-actin in subpopulations of dendritic spines in rat central nervous system: a three-dimensional electron microscopic study. *J Comp Neurol* 435:156-170.
- Carter AG, Sabatini BL (2004) State-dependent calcium signaling in dendritic spines of striatal medium spiny neurons. *Neuron* 44:483-493.
- Carter AG, Soler-Llavina GJ, Sabatini BL (2007) Timing and location of synaptic inputs determine modes of subthreshold integration in striatal medium spiny neurons. *J Neurosci* 27:8967-8977.
- Cash S, Yuste R (1999) Linear summation of excitatory inputs by CA1 pyramidal neurons. *Neuron* 22:383-394.
- Chen HX, Otmakhov N, Lisman J (1999) Requirements for LTP induction by pairing in hippocampal CA1 pyramidal cells. *J Neurophysiol* 82:526-532.
- Choi YM, Kim SH, Chung S, Uhm DY, Park MK (2006) Regional interaction of endoplasmic reticulum Ca<sup>2+</sup> signals between soma and dendrites through rapid luminal Ca<sup>2+</sup> diffusion. *J Neurosci* 26:12127-12136.
- Conti R, Lisman J (2003) The high variance of AMPA receptor- and NMDA receptor-mediated responses at single hippocampal synapses: evidence for multiquantal release. *Proc Natl Acad Sci U S A* 100:4885-4890.
- Cooney JR, Hurlburt JL, Selig DK, Harris KM, Fiala JC (2002) Endosomal compartments serve multiple hippocampal dendritic spines from a widespread rather than a local store of recycling membrane. *J Neurosci* 22:2215-2224.

- Correia SS, Bassani S, Brown TC, Lise MF, Backos DS, El-Husseini A, Passafaro M, Esteban JA (2008) Motor protein-dependent transport of AMPA receptors into spines during long-term potentiation. *Nat Neurosci* 11:457-466.
- Daw MI, Bortolotto ZA, Saulle E, Zaman S, Collingridge GL, Isaac JT (2002) Phosphatidylinositol 3 kinase regulates synapse specificity of hippocampal long-term depression. *Nat Neurosci* 5:835-836.
- Debanne D, Gahwiler BH, Thompson SM (1999) Heterogeneity of synaptic plasticity at unitary CA3-CA1 and CA3-CA3 connections in rat hippocampal slice cultures. *J Neurosci* 19:10664-10671.
- Dekker-Ohno K, Hayasaka S, Takagishi Y, Oda S, Wakasugi N, Mikoshiba K, Inouye M, Yamamura H (1996) Endoplasmic reticulum is missing in dendritic spines of Purkinje cells of the ataxic mutant rat. *Brain Res* 714:226-230.
- Deller T, Merten T, Roth SU, Mundel P, Frotscher M (2000) Actin-associated protein synaptopodin in the rat hippocampal formation: localization in the spine neck and close association with the spine apparatus of principal neurons. *J Comp Neurol* 418:164-181.
- Deller T, Bas Orth C, Vlachos A, Merten T, Del Turco D, Dehn D, Mundel P, Frotscher M (2006) Plasticity of synaptopodin and the spine apparatus organelle in the rat fascia dentata following entorhinal cortex lesion. *J Comp Neurol* 499:471-484.
- Deller T, Korte M, Chabanis S, Drakew A, Schwegler H, Stefani GG, Zuniga A, Schwarz K, Bonhoeffer T, Zeller R, Frotscher M, Mundel P (2003) Synaptopodin-deficient mice lack a spine apparatus and show deficits in synaptic plasticity. *Proc Natl Acad Sci U S A* 100:10494-10499.
- Dumas TC (2005) Developmental regulation of cognitive abilities: modified composition of a molecular switch turns on associative learning. *Prog Neurobiol* 76:189-211.
- Elgersma Y, Fedorov NB, Ikonen S, Choi ES, Elgersma M, Carvalho OM, Giese KP, Silva AJ (2002) Inhibitory autophosphorylation of CaMKII controls PSD association, plasticity, and learning. *Neuron* 36:493-505.
- Emptage N, Bliss TV, Fine A (1999) Single synaptic events evoke NMDA receptor-mediated release of calcium from internal stores in hippocampal dendritic spines. *Neuron* 22:115-124.
- Emptage NJ, Reid CA, Fine A, Bliss TV (2003) Optical quantal analysis reveals a presynaptic component of LTP at hippocampal schaffer-associational synapses. *Neuron* 38:797-804.
- Engert F, Bonhoeffer T (1997) Synapse specificity of long-term potentiation breaks down at short distances. *Nature* 388:279-284.
- Erondu NE, Kennedy MB (1985) Regional distribution of type II Ca<sup>2+</sup>/calmodulin-dependent protein kinase in rat brain. *J Neurosci* 5:3270-3277.
- Fagni L, Chavis P, Ango F, Bockaert J (2000) Complex interactions between mGluRs, intracellular Ca<sup>2+</sup> stores and ion channels in neurons. *TINS* 23:80-88.
- Finch EA, Augustine GJ (1998) Local calcium signalling by inositol-1,4,5-trisphosphate in Purkinje cell dendrites. *Nature* 396:753-756.
- Foehring RC, Mermelstein PG, Song WJ, Ulrich S, Surmeier DJ (2000) Unique properties of R-type calcium currents in neocortical and neostriatal neurons. *J Neurophysiol* 84:2225-2236.

- Fong DK, Rao A, Crump FT, Craig AM (2002) Rapid synaptic remodeling by protein kinase C: reciprocal translocation of NMDA receptors and calcium/calmodulin-dependent kinase II. *J Neurosci* 22:2153-2164.
- Futatsugi A, Kato K, Ogura H, Li ST, Nagata E, Kuwajima G, Tanaka K, Itohara S, Mikoshiba K (1999) Facilitation of NMDAR-independent LTP and spatial learning in mutant mice lacking ryanodine receptor type 3. *Neuron* 24:701-713.
- Gasparini S, Magee JC (2006) State-dependent dendritic computation in hippocampal CA1 pyramidal neurons. *J Neurosci* 26:2088-2100.
- Geiger JR, Melcher T, Koh DS, Sakmann B, Seeburg PH, Jonas P, Monyer H (1995) Relative abundance of subunit mRNAs determines gating and Ca<sup>2+</sup> permeability of AMPA receptors in principal neurons and interneurons in rat CNS. *Neuron* 15:193-204.
- Giese KP, Fedorov NB, Filipkowski RK, Silva AJ (1998) Autophosphorylation at Thr286 of the alpha calcium-calmodulin kinase II in LTP and learning. *Science* 279:870-873.
- Golding NL, Kath WL, Spruston N (2001) Dichotomy of action-potential backpropagation in CA1 pyramidal neuron dendrites. *J Neurophysiol* 86:2998-3010.
- Gray EG (1959a) Electron microscopy of synaptic contacts on dendrite spines of the cerebral cortex. *Nature* 183:1592-1593.
- Gray EG (1959b) Axo-somatic and axo-dendritic synapses of the cerebral cortex: an electron microscope study. *J Anat* 93:420-433.
- Gray NW, Weimer RM, Bureau I, Svoboda K (2006) Rapid redistribution of synaptic PSD-95 in the neocortex in vivo. *PLoS Biol* 4:e370.
- Grutzendler J, Kasthuri N, Gan WB (2002) Long-term dendritic spine stability in the adult cortex. *Nature* 420:812-816.
- Hanson PI, Schulman H (1992) Inhibitory autophosphorylation of multifunctional Ca<sup>2+</sup>/calmodulin-dependent protein kinase analyzed by site-directed mutagenesis. *J Biol Chem* 267:17216-17224.
- Harris KM, Stevens JK (1989) Dendritic spines of CA 1 pyramidal cells in the rat hippocampus: serial electron microscopy with reference to their biophysical characteristics. *J Neurosci* 9:2982-2997.
- Hartmann J, Blum R, Kovalchuk Y, Adelsberger H, Kuner R, Durand GM, Miyata M, Kano M, Offermanns S, Konnerth A (2004) Distinct roles of Gα<sub>q</sub> and Gα<sub>i1</sub> for Purkinje cell signaling and motor behavior. *J Neurosci* 24:5119-5130.
- Harvey CD, Svoboda K (2007) Locally dynamic synaptic learning rules in pyramidal neuron dendrites. *Nature* 450:1195-1200.
- Harvey CD, Yasuda R, Zhong H, Svoboda K (2008) The Spread of Ras Activity Triggered by Activation of a Single Dendritic Spine. *Science*.
- Hayashi Y, Shi SH, Esteban JA, Piccini A, Poncer JC, Malinow R (2000) Driving AMPA receptors into synapses by LTP and CaMKII: requirement for GluR1 and PDZ domain interaction. *Science* 287:2262-2267.
- Heim N, Griesbeck O (2004) Genetically encoded indicators of cellular calcium dynamics based on troponin C and green fluorescent protein. *J Biol Chem*.

- Hines ML, Carnevale NT (1997) The NEURON simulation environment. *Neural Computation* 9:1179-1209.
- Holtmaat A, Wilbrecht L, Knott GW, Welker E, Svoboda K (2006) Experience-dependent and cell-type-specific spine growth in the neocortex. *Nature* 441:979-983.
- Homma K, Saito J, Ikebe R, Ikebe M (2000) Ca(2+)-dependent regulation of the motor activity of myosin V. *J Biol Chem* 275:34766-34771.
- Hong M, Ross WN (2007) Priming of intracellular calcium stores in rat CA1 pyramidal neurons. *J Physiol* 584:75-87.
- Honkura N, Matsuzaki M, Noguchi J, Ellis-Davies GC, Kasai H (2008) The Subspine Organization of Actin Fibers Regulates the Structure and Plasticity of Dendritic Spines. *Neuron* 57:719-729.
- Huang ZJ, Di Cristo G, Ango F (2007) Development of GABA innervation in the cerebral and cerebellar cortices. *Nat Rev Neurosci* 8:673-686.
- Huber KM, Kayser MS, Bear MF (2000) Role for rapid dendritic protein synthesis in hippocampal mGluR-dependent long-term depression. *Science* 288:1254-1257.
- Jahr CE, Stevens CF (1990) Voltage dependence of NMDA-activated macroscopic conductances predicted by single-channel kinetics. *J Neurosci* 10:3178-3182.
- Kammermeier PJ, Worley PF (2007) Homer 1a uncouples metabotropic glutamate receptor 5 from postsynaptic effectors. *Proc Natl Acad Sci U S A* 104:6055-6060.
- Kampa BM, Letzkus JJ, Stuart GJ (2006) Requirement of dendritic calcium spikes for induction of spike-timing-dependent synaptic plasticity. *J Physiol* 574:283-290.
- Kepecs A, van Rossum MC, Song S, Tegner J (2002) Spike-timing-dependent plasticity: common themes and divergent vistas. *Biol Cybern* 87:446-458.
- Kim CH, Lisman JE (1999) A role of actin filament in synaptic transmission and long-term potentiation. *J Neurosci* 19:4314-4324.
- Kirov SA, Sorra KE, Harris KM (1999) Slices have more synapses than perfusion-fixed hippocampus from both young and mature rats. *J Neurosci* 19:2876-2886.
- Kleppisch T, Voigt V, Allmann R, Offermanns S (2001) G(alpha)q-deficient mice lack metabotropic glutamate receptor-dependent long-term depression but show normal long-term potentiation in the hippocampal CA1 region. *J Neurosci* 21:4943-4948.
- Knott GW, Holtmaat A, Wilbrecht L, Welker E, Svoboda K (2006) Spine growth precedes synapse formation in the adult neocortex in vivo. *Nat Neurosci* 9:1117-1124.
- Koch C (1999) *Biophysics of Computation*. New York: Oxford Univ. Press.
- Koch C, Poggio T (1985) The biophysical properties of spines as a basis for their electrical function: a comment on Kawato & Tsukahara (1983). *Journal of Theoretical Biology* 113:225-229.
- Koch C, Zador A (1993) The function of dendritic spines: devices subserving biochemical rather than electrical compartmentalization. *J Neurosci* 13:413-422.
- Koester HJ, Sakmann B (1998) Calcium dynamics in single spines during coincident pre- and postsynaptic activity depend on relative timing of back-propagating action potentials and subthreshold excitatory postsynaptic potentials. *Proc Natl Acad Sci USA* 95:9596-9601.

- Koester HJ, Johnston D (2005) Target cell-dependent normalization of transmitter release at neocortical synapses. *Science* 308:863-866.
- Kopec CD, Li B, Wei W, Boehm J, Malinow R (2006) Glutamate receptor exocytosis and spine enlargement during chemically induced long-term potentiation. *J Neurosci* 26:2000-2009.
- Kovalchuk Y, Eilers J, Lisman J, Konnerth A (2000) NMDA receptor-mediated subthreshold  $\text{Ca}^{2+}$  signals in spines of hippocampal neurons. *J Neurosci* 20:1791-1799.
- Krucker T, Siggins GR, Halpain S (2000) Dynamic actin filaments are required for stable long-term potentiation (LTP) in area CA1 of the hippocampus. *Proc Natl Acad Sci U S A* 97:6856-6861.
- Kugler S, Meyn L, Holzmüller H, Gerhardt E, Isenmann S, Schulz JB, Bahr M (2001) Neuron-specific expression of therapeutic proteins: evaluation of different cellular promoters in recombinant adenoviral vectors. *Mol Cell Neurosci* 17:78-96.
- Larkum ME, Watanabe S, Nakamura T, Lasser-Ross N, Ross WN (2003) Synaptically activated  $\text{Ca}^{2+}$  waves in layer 2/3 and layer 5 rat neocortical pyramidal neurons. *J Physiol* 549:471-488.
- Li Z, Okamoto K, Hayashi Y, Sheng M (2004) The importance of dendritic mitochondria in the morphogenesis and plasticity of spines and synapses. *Cell* 119:873-887.
- Lisman JE, Zhabotinsky AM (2001) A model of synaptic memory: a CaMKII/PP1 switch that potentiates transmission by organizing an AMPA receptor anchoring assembly. *Neuron* 31:191-201.
- Lledo PM, Hjelmstad GO, Mukherji S, Soderling TR, Malenka RC, Nicoll RA (1995) Calcium/calmodulin-dependent kinase II and long-term potentiation enhance synaptic transmission by the same mechanism. *Proc Natl Acad Sci U S A* 92:11175-11179.
- Losonczy A, Magee JC (2006) Integrative properties of radial oblique dendrites in hippocampal CA1 pyramidal neurons. *Neuron* 50:291-307.
- Losonczy A, Makara JK, Magee JC (2008) Compartmentalized dendritic plasticity and input feature storage in neurons. *Nature* 452:436-441.
- Madden DR (2002) The structure and function of glutamate receptor ion channels. *Nat Rev Neurosci* 3:91-101.
- Magee J, Hoffman D, Colbert C, Johnston D (1998) Electrical and calcium signaling in dendrites of hippocampal pyramidal neurons. *Annu Rev Physiol* 60:327-346.
- Mainen ZF, Malinow R, Svoboda K (1999) Synaptic calcium transients in single spines indicate that NMDA receptors are not saturated. *Nature* 399:151-155.
- Mainen ZF, Jia Z, Roder J, Malinow R (1998) Use-dependent AMPA receptor block in mice lacking GluR2 suggests postsynaptic site for LTP expression. *Nat Neurosci* 1:579-586.
- Majewska A, Tashiro A, Yuste R (2000) Regulation of spine calcium dynamics by rapid spine motility. *J Neurosci* 20:8262-8268.
- Malenka RC, Nicoll RA (1999) Long-term potentiation--a decade of progress? *Science* 285:1870-1874.
- Malenka RC, Bear MF (2004) LTP and LTD: an embarrassment of riches. *Neuron* 44:5-21.

- Malinow R, Schulman H, Tsien RW (1989) Inhibition of postsynaptic PKC or CaMKII blocks induction but not expression of LTP. *Science* 245:862-866.
- Matsuzaki M, Honkura N, Ellis-Davies GC, Kasai H (2004) Structural basis of long-term potentiation in single dendritic spines. *Nature* 429:761-766.
- Matsuzaki M, Ellis-Davies GC, Nemoto T, Miyashita Y, Iino M, Kasai H (2001) Dendritic spine geometry is critical for AMPA receptor expression in hippocampal CA1 pyramidal neurons. *Nat Neurosci* 4:1086-1092.
- Merrill MA, Chen Y, Strack S, Hell JW (2005) Activity-driven postsynaptic translocation of CaMKII. *Trends Pharmacol Sci* 26:645-653.
- Michailova A, DelPrincipe F, Egger M, Niggli E (2002) Spatiotemporal features of Ca<sup>2+</sup> buffering and diffusion in atrial cardiac myocytes with inhibited sarcoplasmic reticulum. *Biophysical Journal* 83:3134-3151.
- Milani H, Uemura UU, Oliveira RM, Lepri ER, Xavier GF (1998) Loss of CA1 cells following global ischaemia correlates with spatial deficits in the circular platform task. *J Neurosci Methods* 80:19-27.
- Miller SG, Kennedy MB (1985) Distinct forebrain and cerebellar isozymes of type II Ca<sup>2+</sup>/calmodulin-dependent protein kinase associate differently with the postsynaptic density fraction. *J Biol Chem* 260:9039-9046.
- Miyata M, Finch EA, Khiroug L, Hashimoto K, Hayasaka S, Oda SI, Inouye M, Takagishi Y, Augustine GJ, Kano M (2000) Local calcium release in dendritic spines required for long-term synaptic depression. *Neuron* 28:233-244.
- Mullasseril P, Dosemeci A, Lisman JE, Griffith LC (2007) A structural mechanism for maintaining the 'on-state' of the CaMKII memory switch in the post-synaptic density. *J Neurochem* 103:357-364.
- Muller W, Connor JA (1991) Dendritic spines as individual neuronal compartments for synaptic Ca<sup>2+</sup> responses. *Nature* 354:73-76.
- Nagel G, Szellas T, Huhn W, Kateriya S, Adeishvili N, Berthold P, Ollig D, Hegemann P, Bamberg E (2003) Channelrhodopsin-2, a directly light-gated cation-selective membrane channel. *Proc Natl Acad Sci U S A* 100:13940-13945.
- Nakamura T, Barbara JG, Nakamura K, Ross WN (1999) Synergistic release of Ca<sup>2+</sup> from IP<sub>3</sub>-sensitive stores evoked by synaptic activation of mGluRs paired with backpropagating action potentials. *Neuron* 24:727-737.
- Neves G, Cooke SF, Bliss TV (2008) Synaptic plasticity, memory and the hippocampus: a neural network approach to causality. *Nat Rev Neurosci* 9:65-75.
- Nevian T, Sakmann B (2004) Single spine Ca<sup>2+</sup> signals evoked by coincident EPSPs and backpropagating action potentials in spiny stellate cells of layer 4 in the juvenile rat somatosensory barrel cortex. *J Neurosci* 24:1689-1699.
- Nevian T, Sakmann B (2006) Spine Ca<sup>2+</sup> signaling in spike-timing-dependent plasticity. *J Neurosci* 26:11001-11013.
- Ng AN, Toresson H (2008) Gamma-secretase and metalloproteinase activity regulate the distribution of endoplasmic reticulum to hippocampal neuron dendritic spines. *Faseb J* 22:2832-2842.
- Ngo-Anh TJ, Bloodgood BL, Lin M, Sabatini BL, Maylie J, Adelman JP (2005) SK channels and NMDA receptors form a Ca<sup>2+</sup>-mediated feedback loop in dendritic spines. *Nat Neurosci* 8:642-649.

- Nimchinsky EA, Yasuda R, Oertner TG, Svoboda K (2004) The number of glutamate receptors opened by synaptic stimulation in single hippocampal spines. *J Neurosci* 24:2054-2064.
- Nishiyama M, Hong K, Mikoshiba K, Poo MM, Kato K (2000) Calcium stores regulate the polarity and input specificity of synaptic modification. *Nature* 408:584-588.
- Noguchi J, Matsuzaki M, Ellis-Davies GC, Kasai H (2005) Spine-neck geometry determines NMDA receptor-dependent  $\text{Ca}^{2+}$  signaling in dendrites. *Neuron* 46:609-622.
- Nosyreva ED, Huber KM (2005) Developmental switch in synaptic mechanisms of hippocampal metabotropic glutamate receptor-dependent long-term depression. *J Neurosci* 25:2992-3001.
- Nowak L, Bregestovski P, Ascher P, Herbet A, Prochiantz A (1984) Magnesium gates glutamate-activated channels in mouse central neurones. *Nature* 307:462-465.
- Nusser Z, Lujan R, Laube G, Roberts JD, Molnar E, Somogyi P (1998) Cell type and pathway dependence of synaptic AMPA receptor number and variability in the hippocampus. *Neuron* 21:545-559.
- O'Connor DH, Wittenberg GM, Wang SS (2005) Dissection of bidirectional synaptic plasticity into saturable unidirectional processes. *J Neurophysiol* 94:1565-1573.
- Okamoto K, Nagai T, Miyawaki A, Hayashi Y (2004) Rapid and persistent modulation of actin dynamics regulates postsynaptic reorganization underlying bidirectional plasticity. *Nat Neurosci* 7:1104-1112.
- Oliet SH, Malenka RC, Nicoll RA (1997) Two distinct forms of long-term depression coexist in CA1 hippocampal pyramidal cells. *Neuron* 18:969-982.
- Ostroff LE, Fiala JC, Allwardt B, Harris KM (2002) Polyribosomes redistribute from dendritic shafts into spines with enlarged synapses during LTP in developing rat hippocampal slices. *Neuron* 35:535-545.
- Otmakhov N, Tao-Cheng JH, Carpenter S, Asrican B, Dosemeci A, Reese TS, Lisman J (2004) Persistent accumulation of calcium/calmodulin-dependent protein kinase II in dendritic spines after induction of NMDA receptor-dependent chemical long-term potentiation. *J Neurosci* 24:9324-9331.
- Park M, Salgado JM, Ostroff L, Helton TD, Robinson CG, Harris KM, Ehlers MD (2006) Plasticity-induced growth of dendritic spines by exocytic trafficking from recycling endosomes. *Neuron* 52:817-830.
- Petersen CC, Malenka RC, Nicoll RA, Hopfield JJ (1998) All-or-none potentiation at CA3-CA1 synapses. *Proc Natl Acad Sci U S A* 95:4732-4737.
- Pierce JP, van Leyen K, McCarthy JB (2000) Translocation machinery for synthesis of integral membrane and secretory proteins in dendritic spines. *Nat Neurosci* 3:311-313.
- Pologruto TA, Sabatini BL, Svoboda K (2003) ScanImage: Flexible software for operating laser scanning microscopes. *Biomed Eng Online* 2:13.
- Pologruto TA, Yasuda R, Svoboda K (2004) Monitoring neural activity and  $[\text{Ca}^{2+}]$  with genetically encoded  $\text{Ca}^{2+}$  indicators. *J Neurosci* 24:9572-9579.
- Polsky A, Mel BW, Schiller J (2004) Computational subunits in thin dendrites of pyramidal cells. *Nat Neurosci* 7:621-627.
- Power JM, Sah P (2002) Nuclear calcium signaling evoked by cholinergic stimulation in hippocampal CA1 pyramidal neurons. *J Neurosci* 22:3454-3462.

- Rae MG, Martin DJ, Collingridge GL, Irving AJ (2000) Role of Ca<sup>2+</sup> stores in metabotropic L-glutamate receptor-mediated supralinear Ca<sup>2+</sup> signaling in rat hippocampal neurons. *J Neurosci* 20:8628-8636.
- Rammes G, Swandulla D, Collingridge GL, Hartmann S, Parsons CG (1996) Interactions of 2,3-benzodiazepines and cyclothiazide at AMPA receptors: patch clamp recordings in cultured neurones and area CA1 in hippocampal slices. *Br J Pharmacol* 117:1209-1221.
- Reed JM, Squire LR (1997) Impaired recognition memory in patients with lesions limited to the hippocampal formation. *Behav Neurosci* 111:667-675.
- Rempel-Clower NL, Zola SM, Squire LR, Amaral DG (1996) Three cases of enduring memory impairment after bilateral damage limited to the hippocampal formation. *J Neurosci* 16:5233-5255.
- Reyes M, Stanton PK (1996) Induction of hippocampal long-term depression requires release of Ca<sup>2+</sup> from separate presynaptic and postsynaptic intracellular stores. *J Neurosci* 16:5951-5960.
- Rodriguez-Moreno A, Paulsen O (2008) Spike timing-dependent long-term depression requires presynaptic NMDA receptors. *Nat Neurosci* 11:744-745.
- Ronesi JA, Huber KM (2008) Homer interactions are necessary for metabotropic glutamate receptor-induced long-term depression and translational activation. *J Neurosci* 28:543-547.
- Rose CR, Konnerth A (2001) Stores not just for storage. intracellular calcium release and synaptic plasticity. *Neuron* 31:519-522.
- Sabatini BL, Maravall M, Svoboda K (2001) Ca(2+) signaling in dendritic spines. *Neuron* 31:349-356.
- Sabatini BL, Oertner TG, Svoboda K (2002) The life cycle of Ca(2+) ions in dendritic spines. *Neuron* 33:439-452.
- Sala C, Roussignol G, Meldolesi J, Fagni L (2005) Key role of the postsynaptic density scaffold proteins Shank and Homer in the functional architecture of Ca<sup>2+</sup> homeostasis at dendritic spines in hippocampal neurons. *J Neurosci* 25:4587-4592.
- Sala C, Piech V, Wilson NR, Passafaro M, Liu G, Sheng M (2001) Regulation of dendritic spine morphology and synaptic function by Shank and Homer. *Neuron* 31:115-130.
- Sanhueza M, McIntyre CC, Lisman JE (2007) Reversal of synaptic memory by Ca<sup>2+</sup>/calmodulin-dependent protein kinase II inhibitor. *J Neurosci* 27:5190-5199.
- Schikorski T, Stevens CF (1997) Quantitative ultrastructural analysis of hippocampal excitatory synapses. *J Neurosci* 17:5858-5867.
- Schiller J, Schiller Y (2001) NMDA receptor-mediated dendritic spikes and coincident signal amplification. *Curr Opin Neurobiol* 11:343-348.
- Schiller J, Major G, Koester HJ, Schiller Y (2000) NMDA spikes in basal dendrites of cortical pyramidal neurons. *Nature* 404:285-289.
- Segev I, Rall W (1988) Computational study of an excitable dendritic spine. *J Neurophysiol* 60:499-523.
- Sharma K, Fong DK, Craig AM (2006) Postsynaptic protein mobility in dendritic spines: long-term regulation by synaptic NMDA receptor activation. *Mol Cell Neurosci* 31:702-712.



- Sharp AH, McPherson PS, Dawson TM, Aoki C, Campbell KP, Snyder SH (1993) Differential immunohistochemical localization of inositol 1,4,5-trisphosphate- and ryanodine-sensitive  $\text{Ca}^{2+}$  release channels in rat brain. *J Neurosci* 13:3051-3063.
- Shen K, Meyer T (1999) Dynamic control of CaMKII translocation and localization in hippocampal neurons by NMDA receptor stimulation. *Science* 284:162-166.
- Shen K, Teruel MN, Connor JH, Shenolikar S, Meyer T (2000) Molecular memory by reversible translocation of calcium/calmodulin-dependent protein kinase II. *Nat Neurosci* 3:881-886.
- Sheng M, Cummings J, Roldan LA, Jan YN, Jan LY (1994) Changing subunit composition of heteromeric NMDA receptors during development of rat cortex. *Nature* 368:144-147.
- Shigemoto R, Kinoshita A, Wada E, Nomura S, Ohishi H, Takada M, Flor PJ, Neki A, Abe T, Nakanishi S, Mizuno N (1997) Differential presynaptic localization of metabotropic glutamate receptor subtypes in the rat hippocampus. *J Neurosci* 17:7503-7522.
- Shimuta M, Yoshikawa M, Fukaya M, Watanabe M, Takeshima H, Manabe T (2001) Postsynaptic modulation of AMPA receptor-mediated synaptic responses and LTP by the type 3 ryanodine receptor. *Mol Cell Neurosci* 17:921-930.
- Sjostrom PJ, Rancz EA, Roth A, Hausser M (2008) Dendritic excitability and synaptic plasticity. *Physiol Rev* 88:769-840.
- Snyder EM, Philpot BD, Huber KM, Dong X, Fallon JR, Bear MF (2001) Internalization of ionotropic glutamate receptors in response to mGluR activation. *Nat Neurosci* 4:1079-1085.
- Sobczyk A, Svoboda K (2007) Activity-dependent plasticity of the NMDA-receptor fractional  $\text{Ca}^{2+}$  current. *Neuron* 53:17-24.
- Sobczyk A, Scheuss V, Svoboda K (2005) NMDA receptor subunit-dependent  $[\text{Ca}^{2+}]$  signaling in individual hippocampal dendritic spines. *J Neurosci* 25:6037-6046.
- Soderling TR, Derkach VA (2000) Postsynaptic protein phosphorylation and LTP. *TINS* 23:75-80.
- Song S, Miller KD, Abbott LF (2000) Competitive Hebbian learning through spike-timing-dependent synaptic plasticity. *Nat Neurosci* 3:919-926.
- Spruston N (2008) Pyramidal neurons: dendritic structure and synaptic integration. *Nat Rev Neurosci* 9:206-221.
- Stoppini L, Buchs PA, Muller D (1991) A simple method for organotypic cultures of nervous tissue. *J Neurosci Meth* 37:173-182.
- Svoboda K (2004) Do spines and dendrites distribute dye evenly? *Trends in Neuroscience* 27:445-446.
- Svoboda K, Mainen ZF (1999) Synaptic  $[\text{Ca}^{2+}]$ : intracellular stores spill their guts. *Neuron* 22:427-430.
- Svoboda K, Tank DW, Denk W (1996) Direct measurement of coupling between dendritic spines and shafts. *Science* 272:716-719.
- Tanaka J, Horiike Y, Matsuzaki M, Miyazaki T, Ellis-Davies GC, Kasai H (2008) Protein synthesis and neurotrophin-dependent structural plasticity of single dendritic spines. *Science* 319:1683-1687.

- Terasaki M, Slater NT, Fein A, Schmidek A, Reese TS (1994) Continuous network of endoplasmic reticulum in cerebellar Purkinje neurons. *Proc Natl Acad Sci U S A* 91:7510-7514.
- Thalhammer A, Rudhard Y, Tigaret CM, Volynski KE, Rusakov DA, Schoepfer R (2006) CaMKII translocation requires local NMDA receptor-mediated  $\text{Ca}^{2+}$  signaling. *Embo J* 25:5873-5883.
- Ting AY, Kain KH, Klemke RL, Tsien RY (2001) Genetically encoded fluorescent reporters of protein tyrosine kinase activities in living cells. 98:15003-15008.
- Toni N, Buchs PA, Nikonenko I, Bron CR, Muller D (1999) LTP promotes formation of multiple spine synapses between a single axon terminal and a dendrite. *Nature* 402:421-425.
- Toresson H, Grant SG (2005) Dynamic distribution of endoplasmic reticulum in hippocampal neuron dendritic spines. *Eur J Neurosci* 22:1793-1798.
- Torok TL (2007) Electrogenic  $\text{Na}^{+}/\text{Ca}^{2+}$ -exchange of nerve and muscle cells. *Prog Neurobiol* 82:287-347.
- Tsuriel S, Geva R, Zamorano P, Dresbach T, Boeckers T, Gundelfinger ED, Garner CC, Ziv NE (2006) Local sharing as a predominant determinant of synaptic matrix molecular dynamics. *PLoS Biol* 4:e271.
- van Rossum MC, Bi GQ, Turrigiano GG (2000) Stable Hebbian learning from spike timing-dependent plasticity. *J Neurosci* 20:8812-8821.
- Verkhratsky A (2005) Physiology and pathophysiology of the calcium store in the endoplasmic reticulum of neurons. *Physiol Rev* 85:201-279.
- Ward B, McGuinness L, Akerman CJ, Fine A, Bliss TV, Emptage NJ (2006) State-dependent mechanisms of LTP expression revealed by optical quantal analysis. *Neuron* 52:649-661.
- Yamazaki M, Matsuo R, Fukazawa Y, Ozawa F, Inokuchi K (2001) Regulated expression of an actin-associated protein, synaptopodin, during long-term potentiation. *J Neurochem* 79:192-199.
- Yasuda R, Sabatini BL, Svoboda K (2003) Plasticity of calcium channels in dendritic spines. *Nat Neurosci* 6:948-955.
- Yasuda R, Harvey CD, Zhong H, Sobczyk A, van Aelst L, Svoboda K (2006) Supersensitive Ras activation in dendrites and spines revealed by two-photon fluorescence lifetime imaging. *Nat Neurosci* 9:283-291.
- Yasuda R, Nimchinsky EA, Scheuss V, Pologruto TA, Oertner TG, Sabatini BL, Svoboda K (2004) Imaging calcium concentration dynamics in small neuronal compartments. *Science's STKE*:p15.
- Yuste R, Majewska A, Cash SS, Denk W (1999) Mechanisms of calcium influx into Hippocampal spines: Heterogeneity among spines, coincidence detection by NMDA receptors, and optical quantal analysis. *J Neurosci* 19:1976-1987.
- Zhang XL, Zhou ZY, Winterer J, Muller W, Stanton PK (2006) NMDA-dependent, but not group I metabotropic glutamate receptor-dependent, long-term depression at Schaffer collateral-CA1 synapses is associated with long-term reduction of release from the rapidly recycling presynaptic vesicle pool. *J Neurosci* 26:10270-10280.
- Zhang YP, Oertner TG (2007) Optical induction of synaptic plasticity using a light-sensitive channel. *Nat Meth* 4:139-141.

- Zhang YP, Holbro N, Oertner TG (2008) Optical induction of plasticity at single synapses reveals input-specific accumulation of alphaCaMKII. *Proc Natl Acad Sci U S A* 105:12039-12044.
- Zhou Q, Homma KJ, Poo MM (2004) Shrinkage of dendritic spines associated with long-term depression of hippocampal synapses. *Neuron* 44:749-757.

## **8. Abbreviations**

ACSF artificial cerebrospinal fluid

AMPA  $\alpha$ -amino-3-hydroxy-5-methylisoxazole-4- propionic acid

CA: Cornus Ammoni

CaMKII: calcium/calmodulin-dependent protein kinase II

ChR2: channelrhodopsin-2

DG: dentate gyrus

EPSCs: excitatory postsynaptic currents

ER: endoplasmic reticulum

GFP: green fluorescent protein

IP3: inositol-triphosphate

IP3R: inositol-triphosphate receptor

LTD: long-term depression

LTP: long-term potentiation

mGluR: metabotropic glutamate receptor

NMDA: N-methyl-D-aspartate

PBS: phosphate buffered saline

PSD: postsynaptic density

RFP: red fluorescent protein

RyR: ryanodine receptor



## **9. Acknowledgements:**

I would like to thank Thomas Oertner for giving me an exciting project, for his guidance, support and for the nice discussions during all these years.

Thanks to Silvia Arber and Bernhard Bettler for scientific advice, critical discussions and helpful comments.

Thanks to Åsa Muller-Grunditz and Yang Ping Zhang for the nice lab atmosphere and the wonderful collaborations.

Thanks a lot to Daniela Gerosa for the extremely nice cultures and for all the nice discussions about science and Ticino.

Thanks to all present and past members of the Oertner lab for all suggestions, comments and for the nice working atmosphere.

I would like to specially thank my parents and my 3 brothers for great support during the last 25 - 28 years.

Special thanks to Lucia and family for enormous support, encouragement and ideas.

Very special thanks to Anja and Igor for their encouragement!

*This thesis is dedicated to my family, Lucia and family, Nadia and Enrico.*



## **10. Curriculum Vitae**

### **Personal profile**

Name: Niklaus Holbro  
Date of birth: 13. April 1980  
Place of birth: Basel  
Address: via Sottochiesa 12C, 6616 Losone, Switzerland  
Phone: +41 78 720 54 33  
e-mail: [niklaus.holbro@fmi.ch](mailto:niklaus.holbro@fmi.ch)

### **Education**

**2004 - present:** University of Basel (Switzerland); PhD in neurobiology at the Friedrich Miescher Institute

**1999 - 2004:** University of Basel (Switzerland); Master of Science (Biology)

**1995 - 1999:** High school Ascona (Switzerland); Matura type C (mathematical)

### **Publications**

Holbro N, Grunditz Å, Oertner TG. **Synaptic depression at individual synapses is governed by spine microanatomy.** Manuscript submitted.

Grunditz Å\*, Holbro N\*, Tian L, Zuo Y, Oertner TG. **Spine neck plasticity controls postsynaptic calcium signals through electrical compartmentalization.** Journal of Neuroscience, in press

**\*: equal contribution**

Zhang YP, Holbro N, Oertner TG. **Optical induction of plasticity at single synapses reveals input-specific accumulation of alphaCaMKII.** Proc Natl Acad Sci U S A. 2008 Aug 19;105(33):12039-44.

Bello B, Holbro N, Reichert H. **Polycomb group genes are required for neural stem cell survival in postembryonic neurogenesis of Drosophila.** Development. 2007 Mar;134(6):1091-9



## **Presentations**

Holbro N, Grunditz Å, Oertner TG. **Assessing the role of the endoplasmic reticulum in dendritic spines.** 45.10/J5. San Diego (USA), Society for Neuroscience Meeting 2007

Holbro N, Grunditz Å, Oertner TG. **Assessing the role of the ER in dendritic spines of pyramidal cells.** 046.10. Vienna (Austria), Forum of European Neuroscience 2008

Oertner TG, Holbro N, Grunditz Å. **Spine neck plasticity controls spine head depolarization.** 046.15. Vienna (Austria), Forum of European Neuroscience 2008

## **Awards**

2008: 1<sup>st</sup> prize poster award Bench to Bedside Symposium (Basel, Switzerland)

1999: Award for 3<sup>rd</sup> best Matura